Large- and Small-scale Dynamics in Turbulent Rayleigh-Bénard Convection

Penger Tong

Department of Physics

Hong Kong University of Science & Technology

2013 Spring Progress in Mathematical and Computational Studies on Science and Engineering Problems

May 6-8, 2013, National Taiwan University

OUTLINE:

1. Rayleigh-Bénard convection near the onset (historical)
2. Turbulent Rayleigh-Bénard convection in an upright cylinder
3. Dynamic features of turbulent Rayleigh-Bénard convection
4. Turbulent Rayleigh-Bénard convection in a horizontal cylinder
   - 4.1 Scalings in turbulent convection
   - 4.2 Dynamic phases (flow modes) of large-scale circulation
5. Summary

Collaborators:
Xiao-zhou He (HKUST), Hao Song (HKUST), K.-Q. Xia (CUHK), Emily Ching (CUHK), G.-W. He (IMCAS), E. Villermaux (Universite de Provence, France), and E. Brown (UC, Merced)

Work supported by the Hong Kong Research Grants Council

1. Rayleigh-Bénard convection near the onset

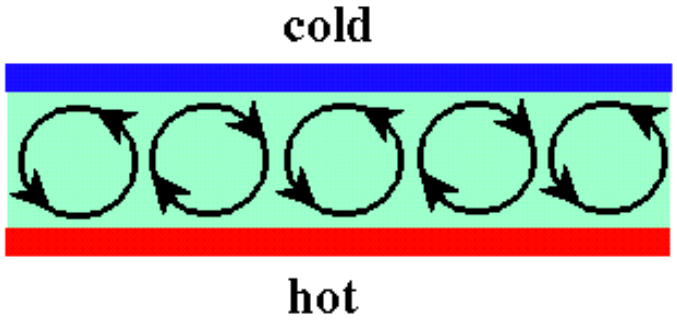

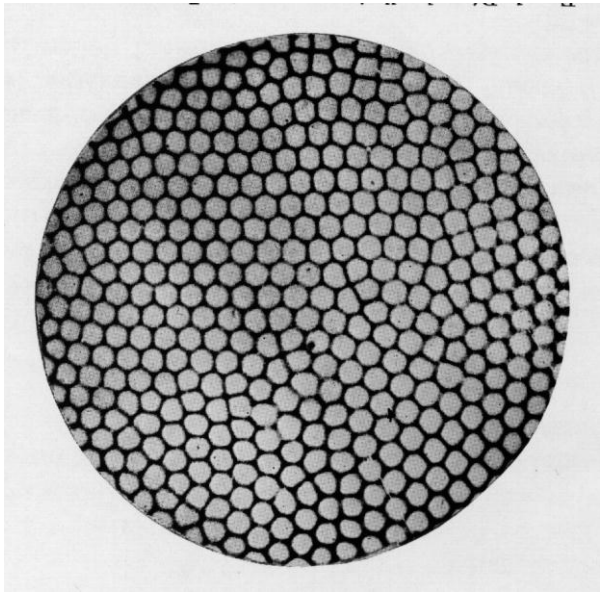

Henri Benard (PhD thesis, 1900) conducted the first systematic study of convection patterns in a shallow layer heated from below.

PHILOSOPHICAL MAGAZINE

AND

JOURNAL OF SCIENCE.

[SIXTH SERIES]

DECEMBER 1916.

LIX. *On Convection Currents in a Horizontal Layer of Fluid, when the Higher Temperature is on the Under Side.*

By Lord RAYLEIGH, *O.M., F.R.S.**

THE present is an attempt to examine how far the interesting results obtained by Bénard † in his careful and skilful experiments can be explained theoretically. Bénard worked with very thin layers, only about 1 mm. deep, standing on a levelled metallic plate which was maintained at a uniform temperature. The upper surface was usually free, and being in contact with the air was at a lower temperature. Various liquids were employed—some, indeed, which would be solids under ordinary conditions.

Lord Rayleigh

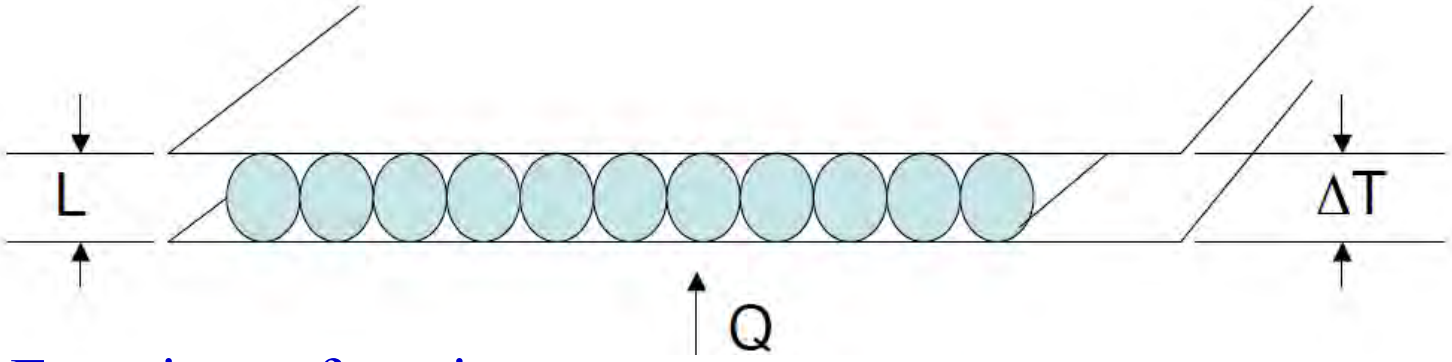

Equations of motion

$$(\partial_t + \mathbf{u}\cdot\nabla)\mathbf{u} = -\frac{1}{\rho}\nabla p + \nu\nabla^2\mathbf{u} + g\alpha T\mathbf{z}$$

$$(\partial_t + \mathbf{u}\cdot\nabla)T = \kappa\nabla^2 T$$

$$\nabla\cdot\mathbf{u} = 0$$

Dimensionless form

$$(\partial_t + \mathbf{u}\cdot\nabla)\mathbf{u} = -\nabla p + (\mathrm{Pr}/\mathrm{Ra})^{1/2}\nabla^2\mathbf{u} + \theta\mathbf{z}$$

$$(\partial_t + \mathbf{u}\cdot\nabla)\theta = (\mathrm{Pr}\,Ra)^{-1/2}\nabla^2\theta$$

$$\nabla\cdot\mathbf{u} = 0$$

$$Ra = \frac{\alpha g\Delta T H^3}{\nu\kappa}$$

$$\mathrm{Pr} = \frac{\nu}{\kappa}$$

Stability analysis of the onset of convection for a quiescent fluid layer in which heat is transported by diffusion

Rayleigh's results for the slip boundary conditions at both the top and bottom surfaces:

$$Ra_c = \frac{27}{4}\pi^4 \qquad k_c = \frac{\pi}{\sqrt{2}}$$

Sir Harold's (1891 – 1989) results for no-slip boundary conditions at both the top and bottom surfaces:

$$Ra_c = 1708 \qquad k_c = 3.117$$

Convection patterns just above the onset (weak nonlinear analysis):

$$\varepsilon = \frac{\Delta T - \Delta T_c}{\Delta T_c} = \frac{\Delta T}{\Delta T_c} - 1$$

- nature of the bifurcation (supercritical vs. subcritical)
- wavenumber selection
- spatio-temporal chaos

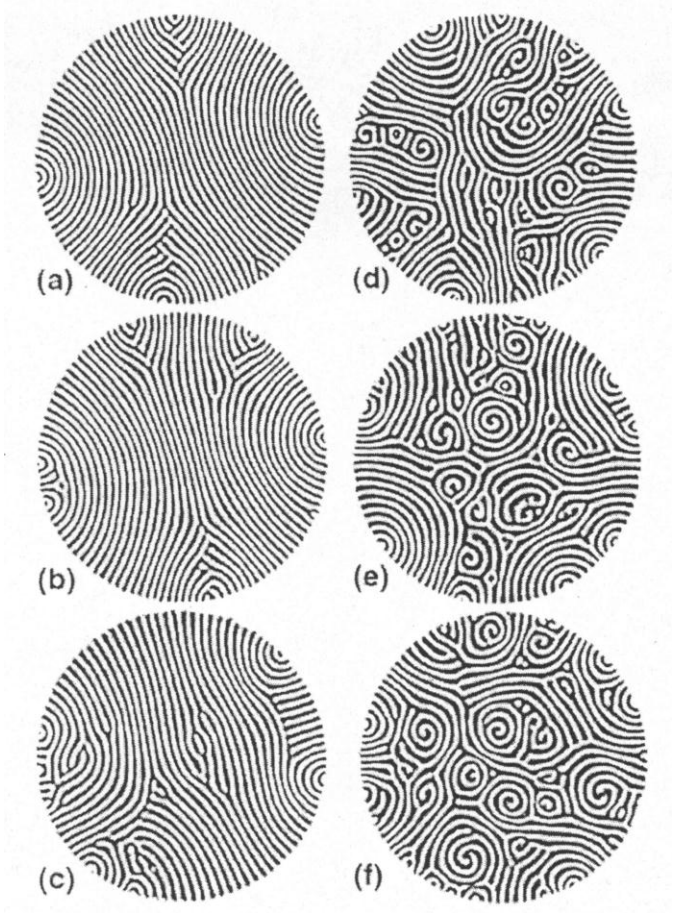

convection rolls near the onset of R-B convection, Guenter Ahlers et al., Phys. Rev. E 1993.

2. Turbulent Rayleigh-Bénard convection (Ra >10^8) in an upright cylinder

Convection experiments using low temperature helium gas at University of Chicago

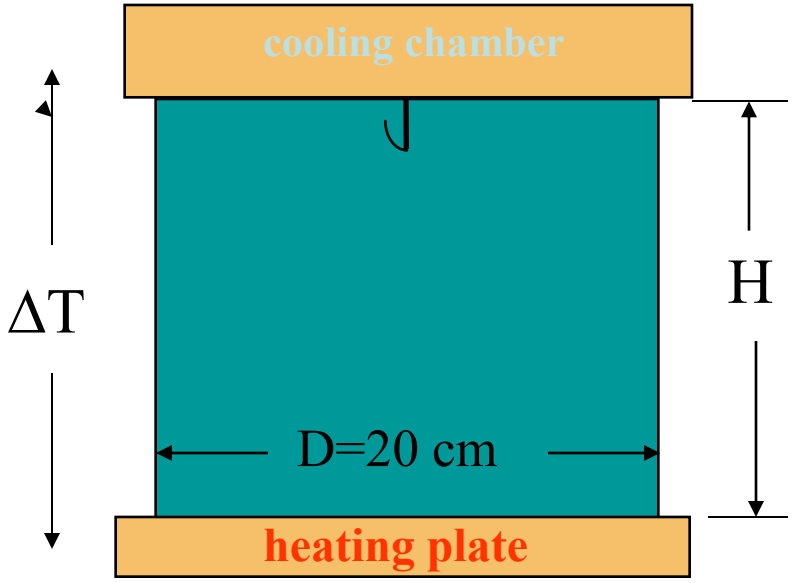

$$Ra = \frac{\alpha g \Delta T H^3}{\nu \kappa} = 10^7 - 10^{14},$$

$$\mathrm{Pr} = \frac{\nu}{\kappa} \approx 0.7,$$

$$\Gamma = \frac{D}{H} = 0.5,\ 1$$

Scaling results from the Chicago group (JFM, 1989)

Scaling of hard thermal turbulence in Rayleigh–Bénard convection

By BERNARD CASTAING†, GEMUNU GUNARATNE‡, FRANÇOIS HESLOT§, LEO KADANOFF‡, ALBERT LIBCHABER‡, STEFAN THOMAE‖, XIAO-ZHONG WU‡, STÉPHANE ZALESKI¶ AND GIANLUIGI ZANETTI‡

Quantity	Amplitude Experiment	Name	Index Experimental value	Theoretical values Present paper	Classical
Nu	0.23 ± 0.03	β	0.282 ± 0.006	$\frac{2}{7}$	$\frac{1}{3}$
Δ_c/Δ	0.36 ± 0.04	γ	-0.147 ± 0.005	$-\frac{1}{7}$	$-\frac{1}{9}$
$\omega_p L^2/\kappa$	0.36 ± 0.01	δ	0.491 ± 0.002	$\frac{1}{2}$	$\frac{2}{3}$
$u_c L/\nu$	$1.05\,Pr^{-\frac{2}{3}}$	ϵ	0.43	$\frac{3}{7}$	$\frac{4}{9}$
$\langle T(z)\rangle/\Delta$	varies	s	varies	0	$\frac{1}{3}$

TABLE 1. Summary of index values. The origin of the data and the theoretical predictions are given in the text. The fits are all in the form quantity = Amplitude $\times Ra^{\text{index}}$ except for the temperature which scales as a power of the distance from the bottom plate (see also §1.2).

Low temperature helium gas, Pr = 0.7, Niemela et al. Nature 2000

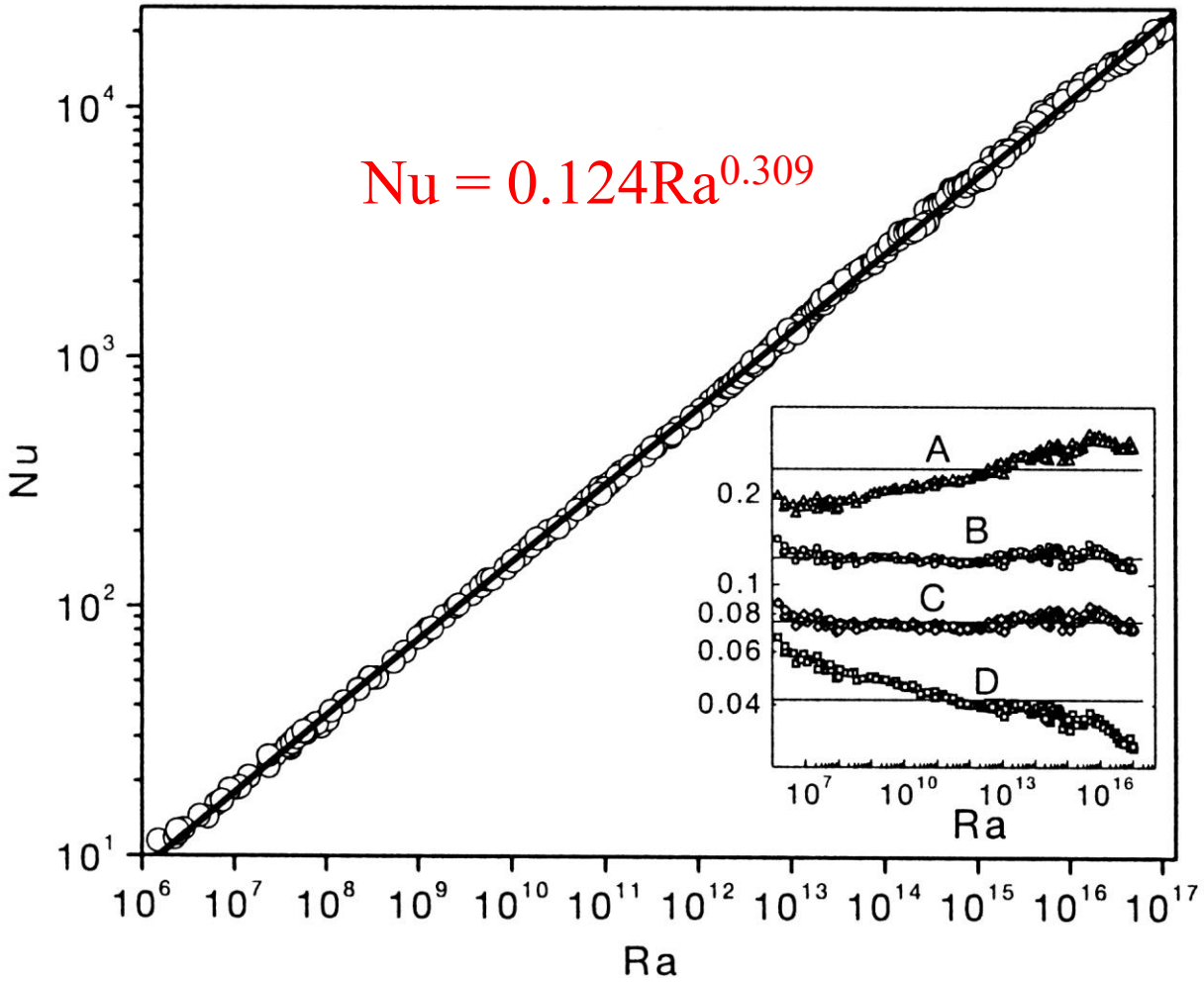

convection in the ocean Ra~10^{20}, near Sun Ra~10^{23}

Turbulent Rayleigh-Bénard convection in water

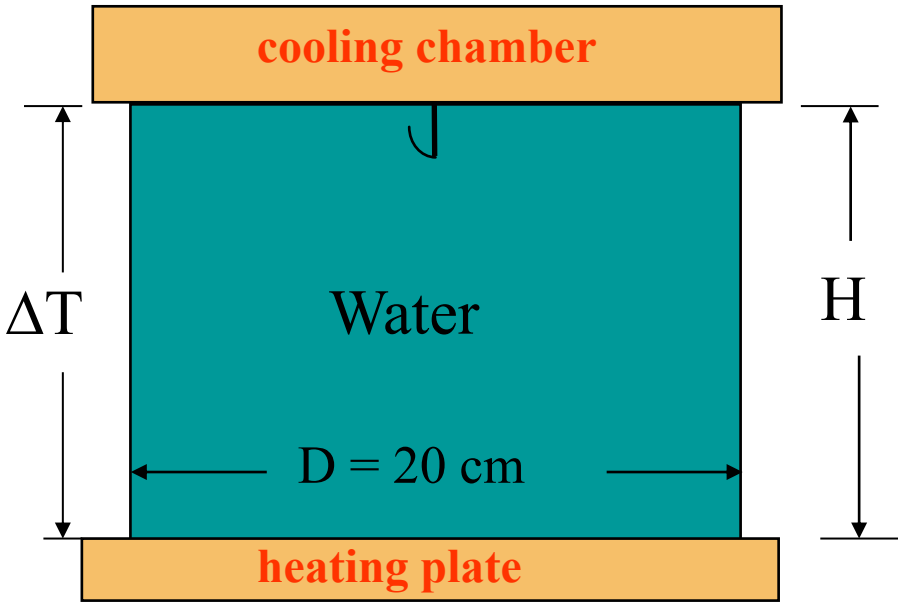

$$\Gamma = \frac{D}{H} = 0.5, 1$$

$$\mathrm{Pr} = \frac{\nu}{\kappa} \approx 5.4$$

$$Ra = \frac{\alpha g H^3 \Delta T}{\nu \kappa} = 10^8 - 10^{10}$$

- Global measurements: Nu (Ra,Pr), Re (Ra,Pr), flow visualization

- Local measurements: local temperature T(**r**,t), velocity **v**(**r**,t), local convective heat flux **j**(**r**,t) and local thermal dissipation rate ϵ_T(**r**,t)

Rayleigh-Bénard convection in a upright cylinder

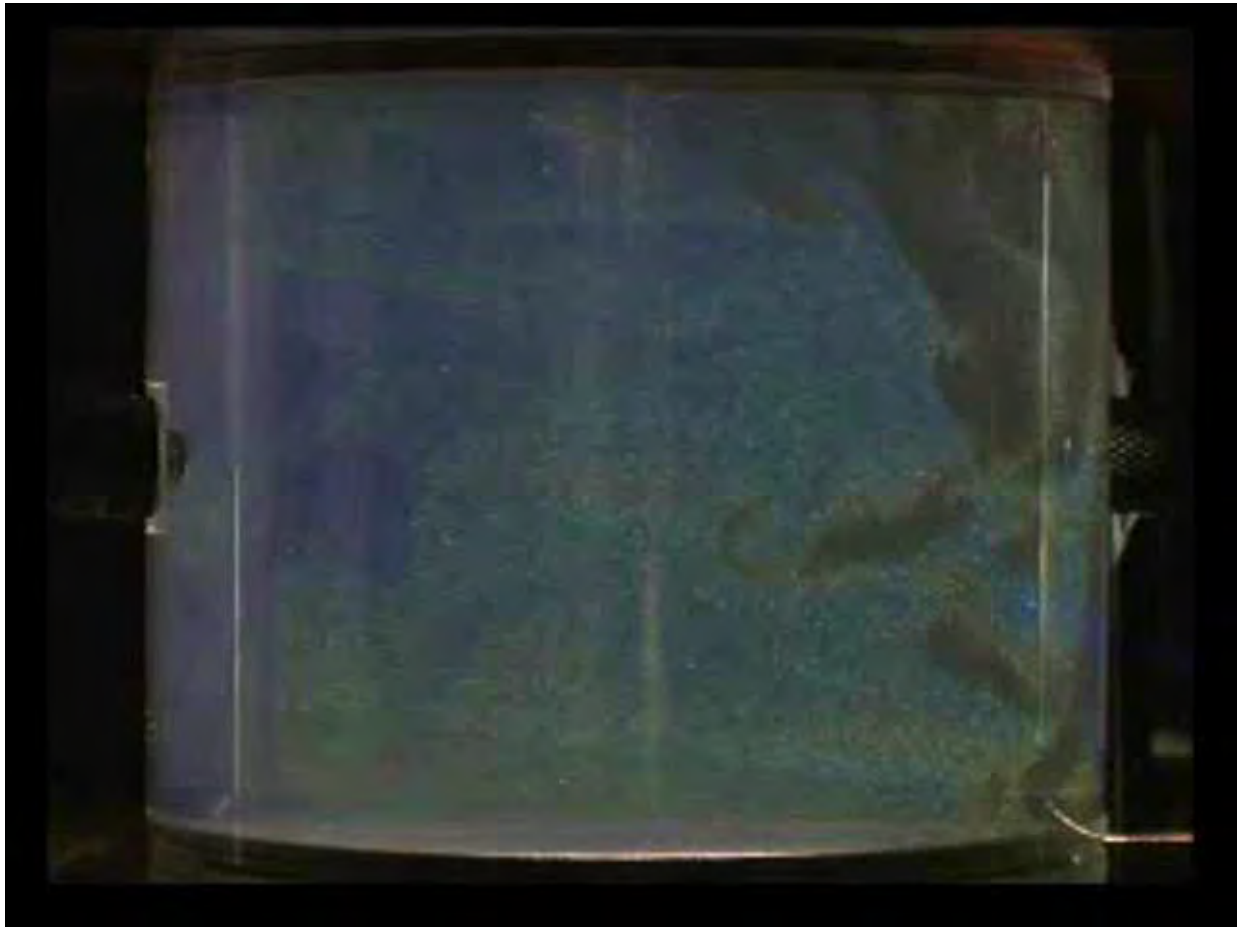

$H = 10$ cm, $\Gamma = D/H = 1$, $Ra = 3.7 \times 10^8$, $Pr \approx 5$ (water).

Experimental efforts in my group focus on:

- Visualization and measurement of the velocity field: velocity fluctuations at the cell center (Phys. Rev. Lett. 1992, 1995), velocity boundary layer (Phys. Rev. Lett. 1996), large-scale flow structures (Phys. Rev. E 2001, 2005).
- Heat transport over rough surfaces (Phys. Rev. Lett. 1996, 1998, J. Fluid Mech. 2000).
- Coherent temperature and velocity oscillations (Phys. Rev. E 2000, Phys. Rev. Lett. 2001, Phys. Rev. E 2002, 2004, Phys. Rev. Lett. 2011).
- Spatial distribution and scaling of the local convective heat flux (Phys. Rev. Lett. 2003, Phys. Rev. E 2004, Phys. Rev. Lett. 2008).
- Thermal dissipation field and its statistics (Phys. Rev. Lett. 2007, Phys. Rev. E 2009, J. Turb., 2010, Phys. Fluids 2011).
- Effects of cell geometry on turbulent convection (Europhys. Lett., 2010).
- Space-time relation in convective turbulence (Phys. Rev. E 2010, 2011).
- Anomalous scaling and intermittency of passive temperature fluctuations (Phys. Rev. E 2013).

3. Dynamic features of turbulent RB convection

(i) Temperature difference ΔT across the fluid layer is concentrated on two thin boundary layers of thickness δ near the upper and lower conducting surfaces. This is the smallest length scale in turbulent thermal convection.

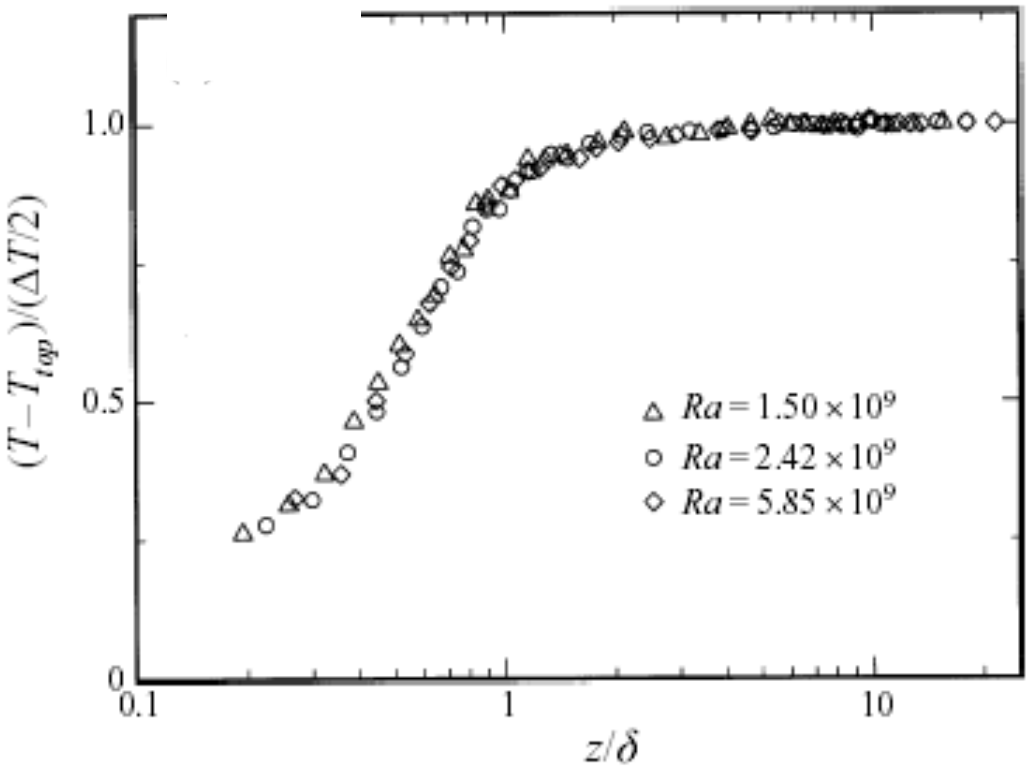

(ii) Thermal boundary layers are highly dynamic structures, from which thermal plumes erupt irregularly to the bulk region.

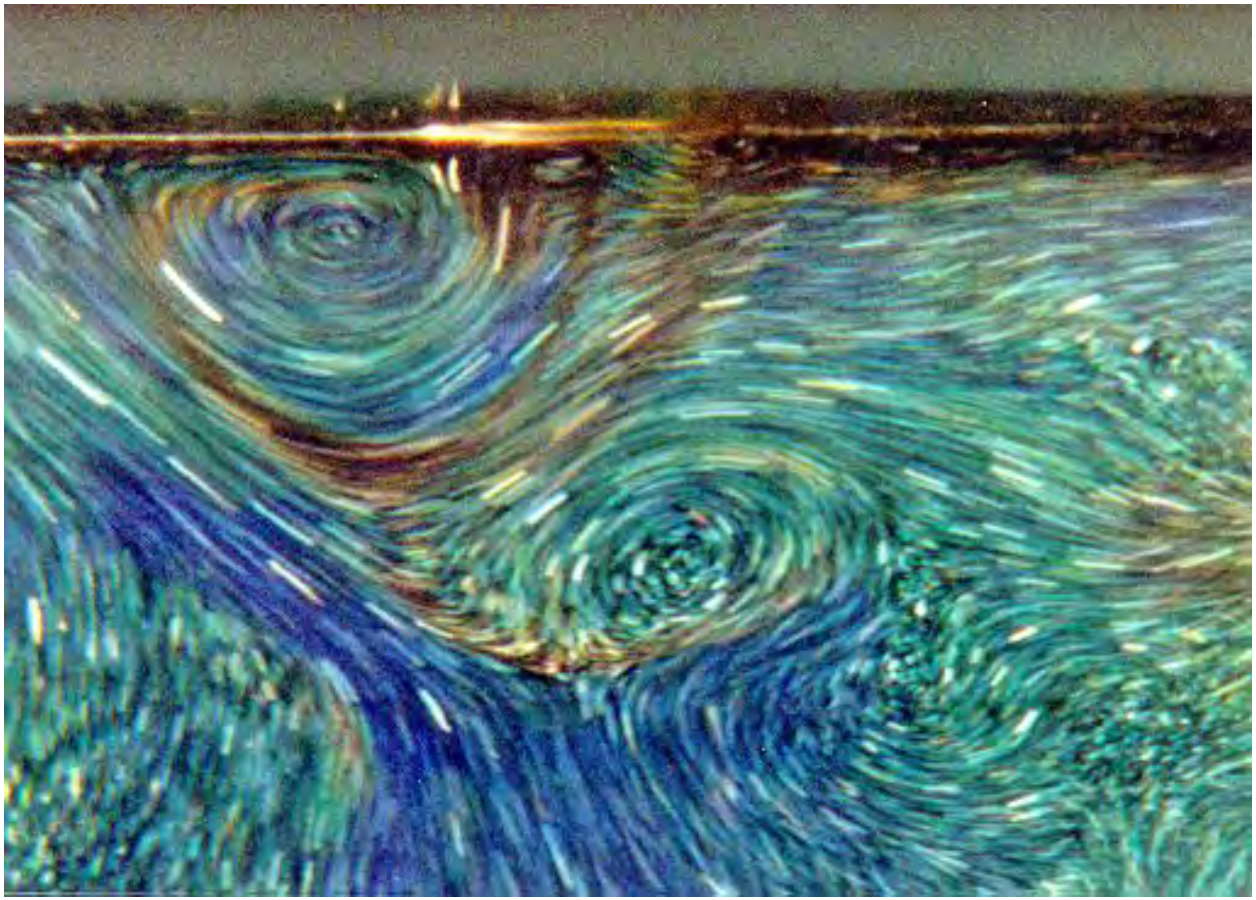

6.5 cm × 4.0 cm, Ra = 2.6×10^9

(iii) Spatial distribution of thermal plumes is neither homogeneous nor isotropic; thermal plumes organize themselves in a closed cell.

shadowgraph showing the spatial distribution of thermal plumes in an aspect-ratio-one cylindrical cell (from Xia's group).

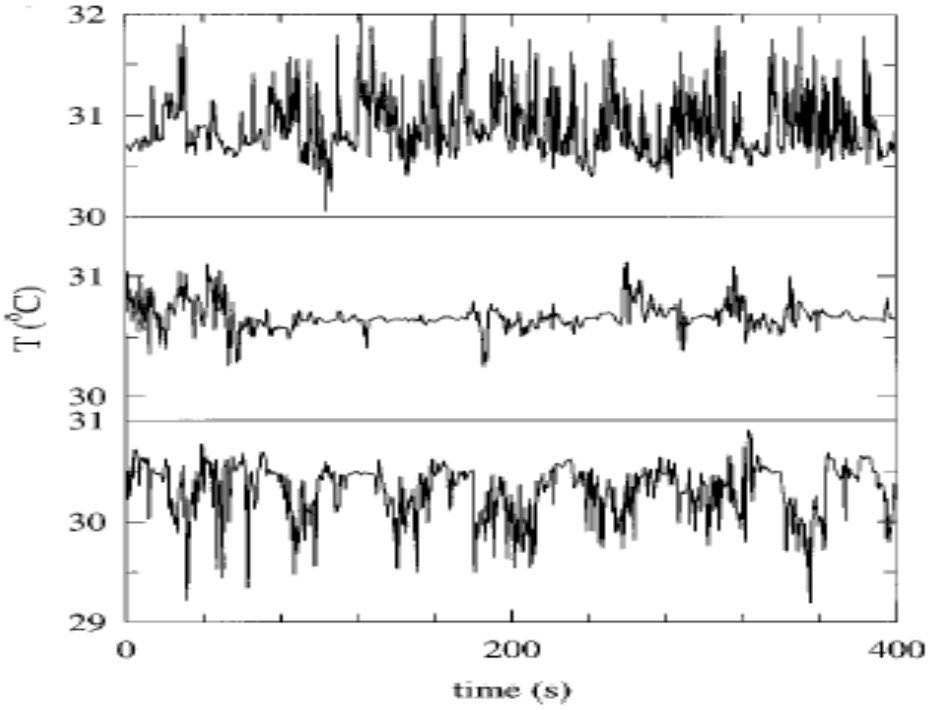

left sidewall

center

right sidewall

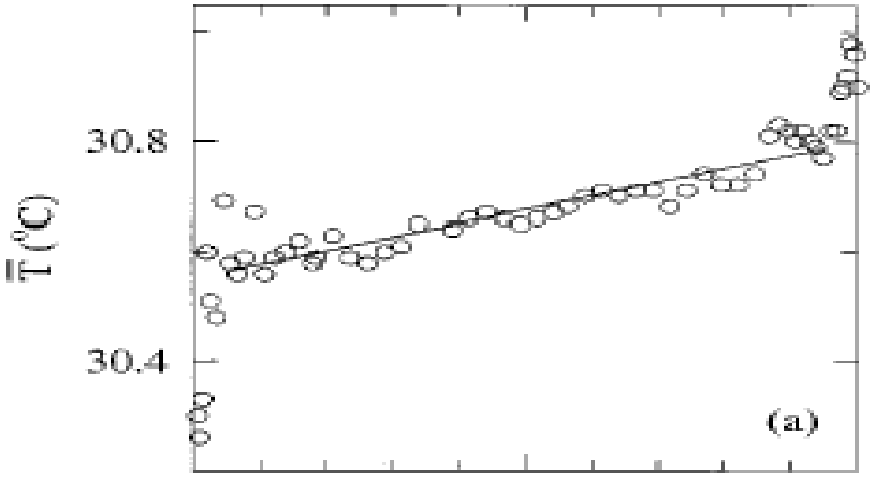

$\Delta T = 18^0 C$

Ra = 3.3×10^9

(iv) The warm and cold plumes near the sidewall exert buoyancy forces on the fluid and generate a large-scale circulation across the height of the cell. The central region is "sheared" by the rising and falling plumes, producing a constant mean velocity gradient in the region.

20cm × 14cm, top 2/3 cell, Ra = 2.6×10^9

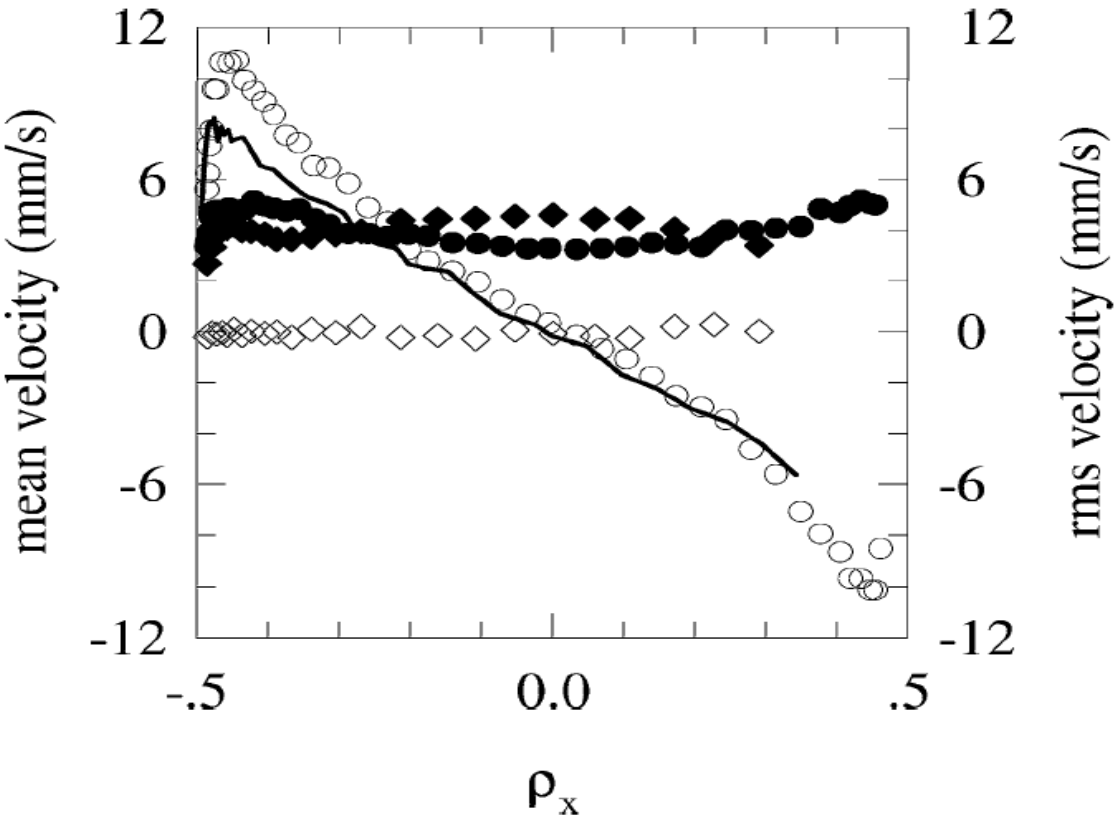

LDV measurements of three velocity components and their rms values in the plane of the large-scale circulation at Ra = 3.7×10^9 (Γ=1 cell).

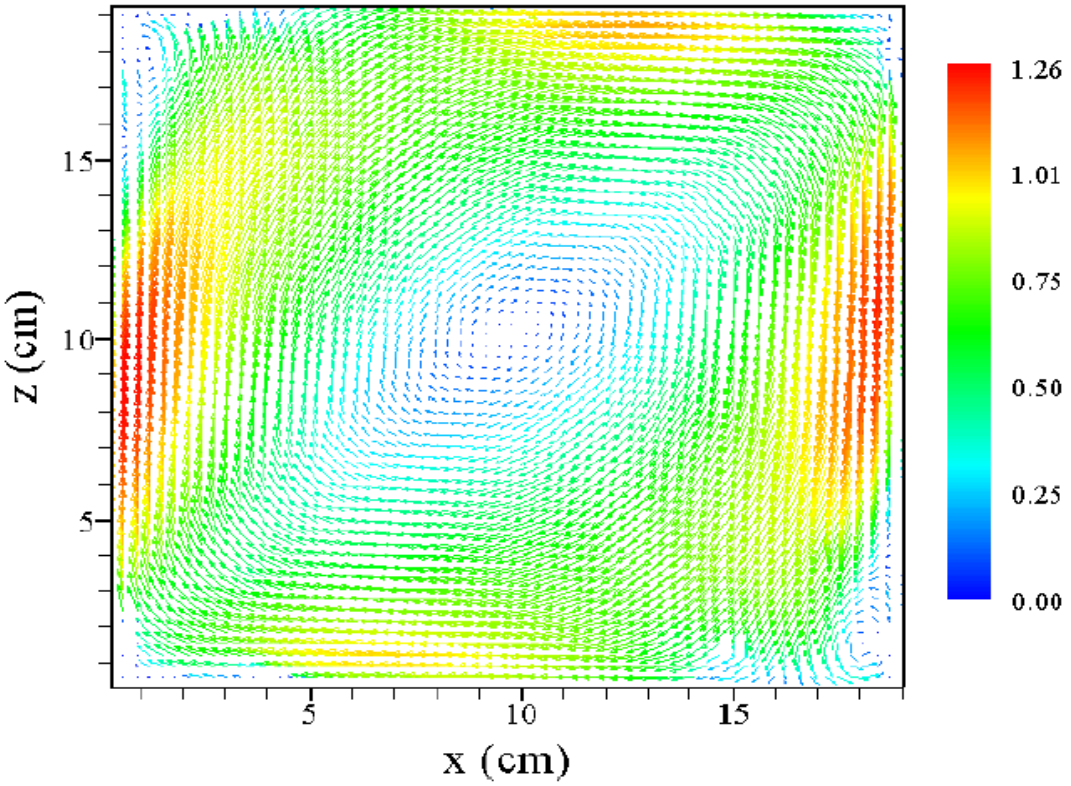

Time-averaged (2.2 frames/s, 2×10^4 frames, 2.5 hrs) velocity (cm/s) vector map in the plane of large-scale circulation (LSC) at Ra = 7.0×10^9. Acceleration is important and is related directly to the local thermal forcing.

(v) In the Γ=1 cell, the thermal plumes are excited alternately between the upper and lower boundary layers. This produces temperature and velocity oscillations in the cell with a local frequency $f_0 \approx U/(2H)$.

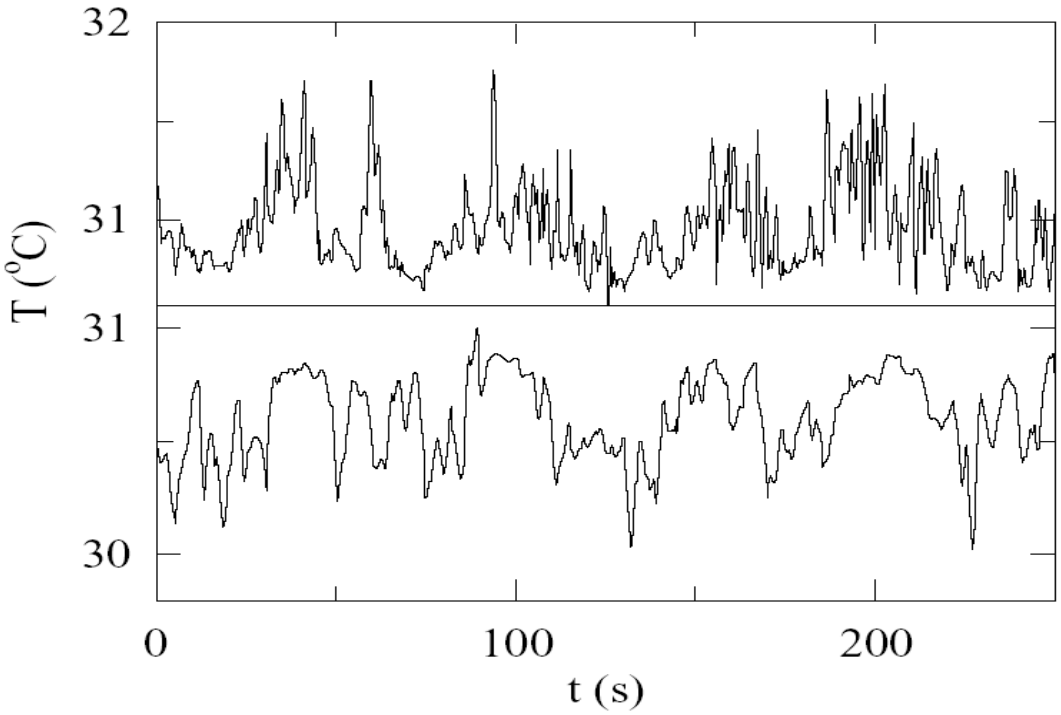

right sidewall

left sidewall

$Ra = 3.2 \times 10^9$

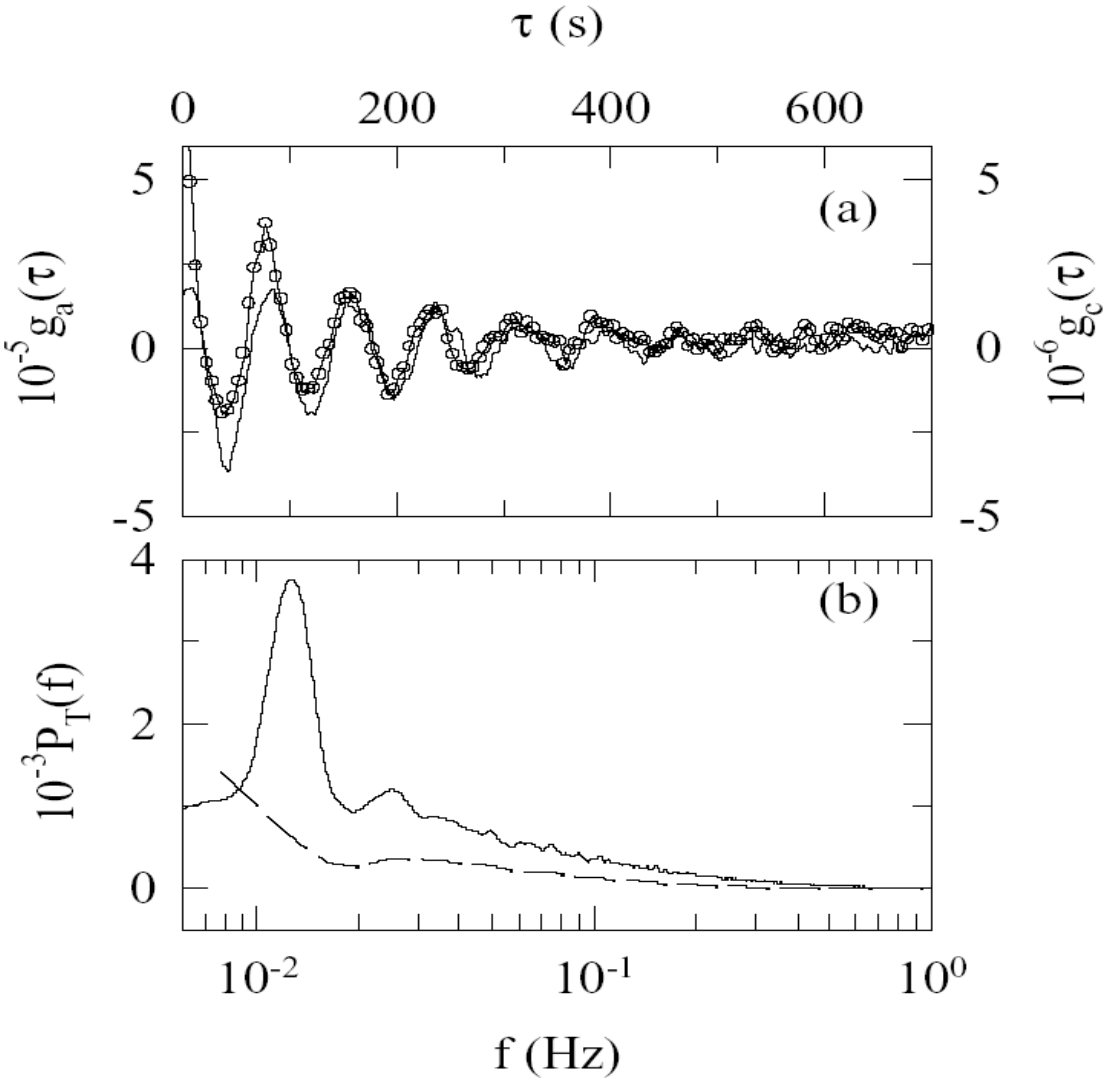

$Ra = 1.4\times10^{9}$, $f_0 = 0.0117$ Hz

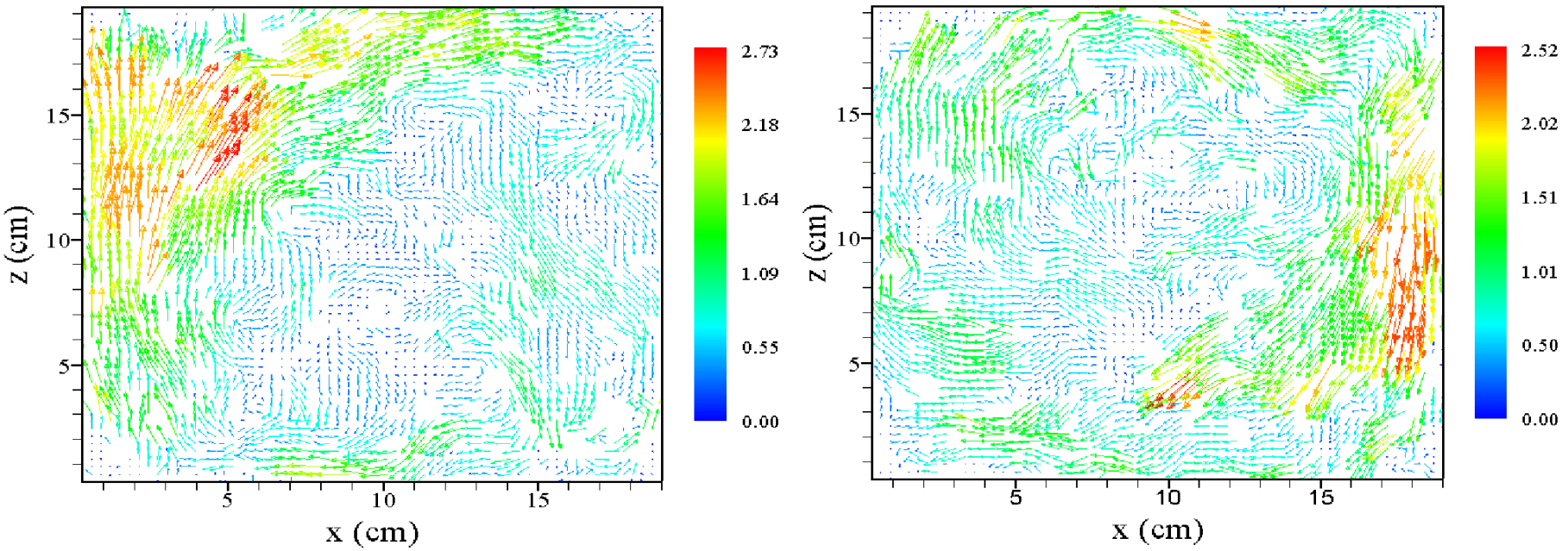

instantaneous velocity (cm/s) vector maps in the plane of LSC with a time delay $\Delta t = 31$ s and at $Ra = 7.0\times10^9$.

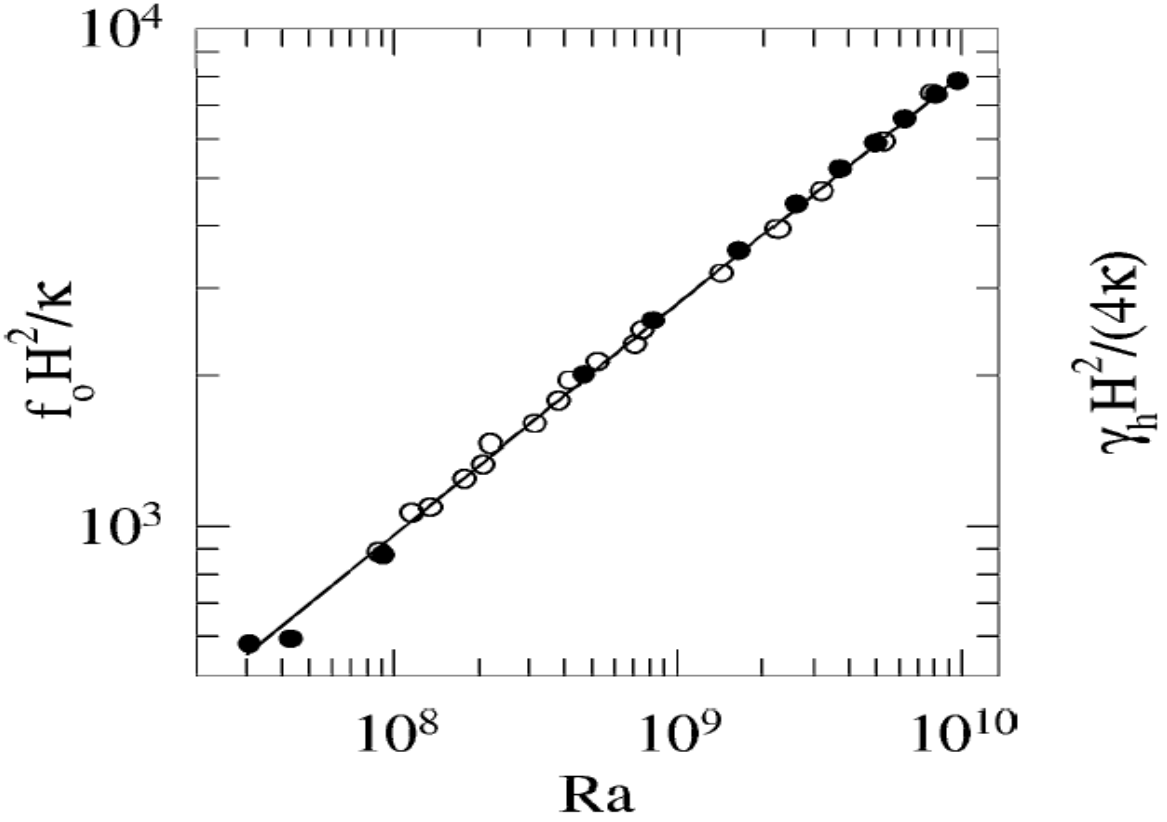

$f_0 = U/(2H) \neq U/(4H)$

$U = \gamma_h H/2$

• velocity

◯ frequency

— $0.20Ra^{0.46}$

(vi) Dynamics of thermal plumes in a closed convection cell is a self-organizing process in that the plume separation and the large-scale circulation help each other and they are no longer independent any more.

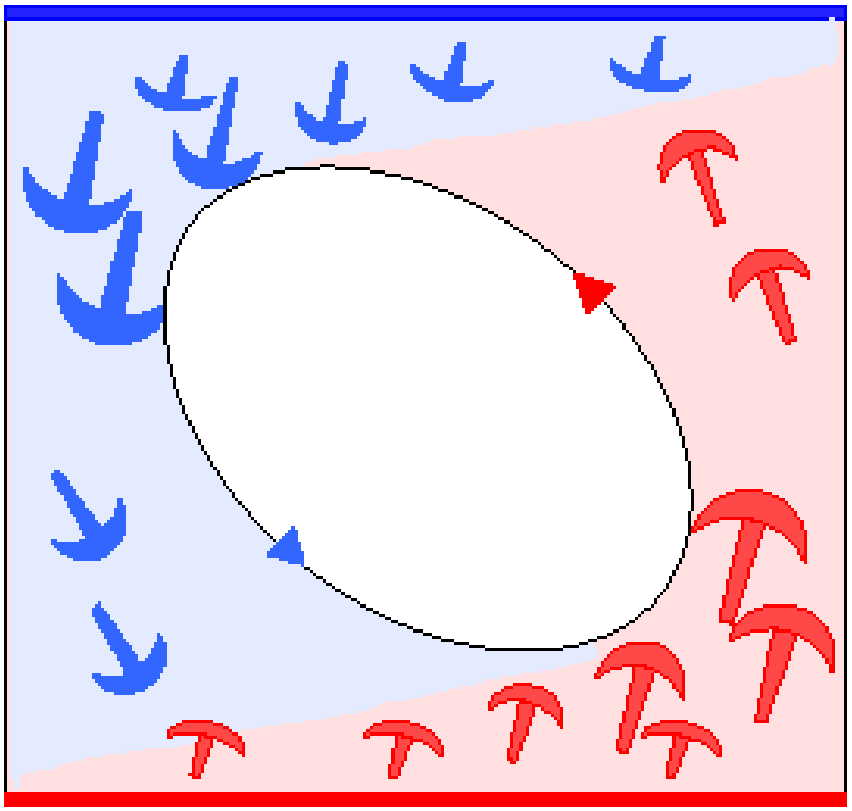

A simple (time-averaged) cartoon

Why is turbulent Rayleigh-Bénard convection so interesting?

- It is a model system with simple boundary conditions to study a range of interesting problems of turbulence, such as turbulent heat transport, boundary layer dynamics, large-scale flow structures and dynamics, and coherent oscillations. What causes the self-organization of the thermal plumes in a closed cell? maximum heat transport? minimum dissipation? or some kind of instabilities?

- It has rich dynamics and is a "playground" for experimentalists and theorists with interests in non-equilibrium dynamics and non-linear physics.

- As an "exactly solvable model system," it provides a platform for interactions between theory, simulation and experiment to test different ideas and computational modeling.

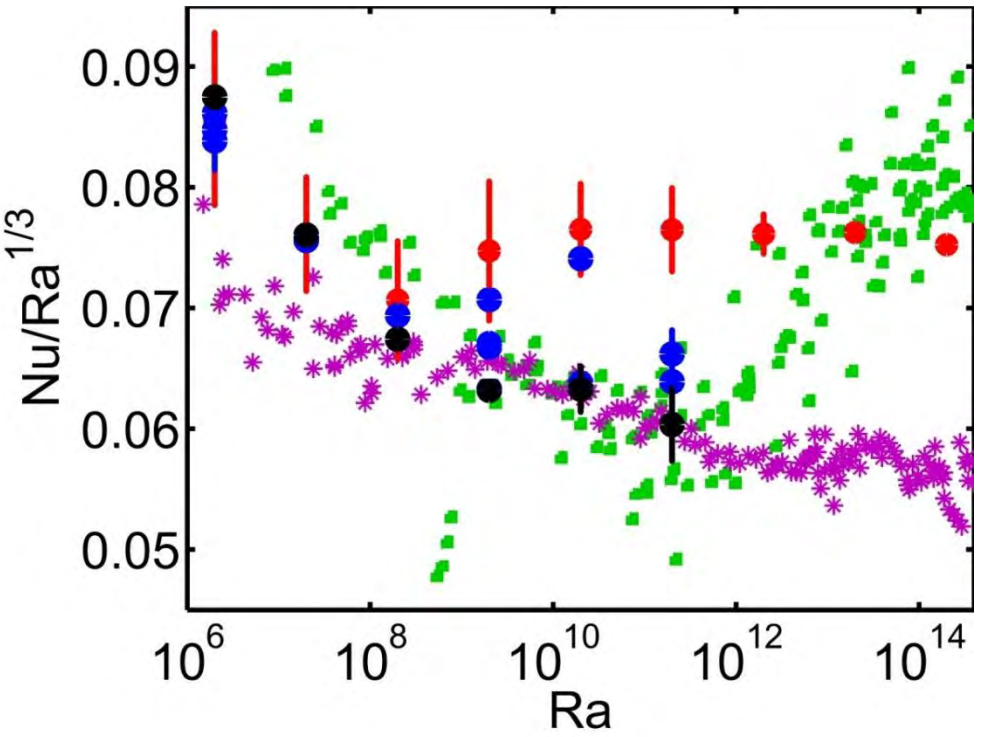

Why is turbulent Rayleigh-Bénard convection so interesting?

- It is relevant to a large number of practical problems, ranging from the thermal convection processes in buildings and metal production to natural convection at geophysical and astrophysical scales.

Large-scale astro/geo-physical convection in the outer layer of Sun, Earth's mantle, atmosphere and ocean

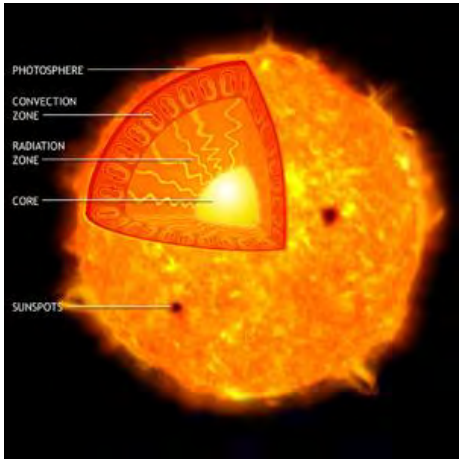

image from: http://chandra.harvard.edu

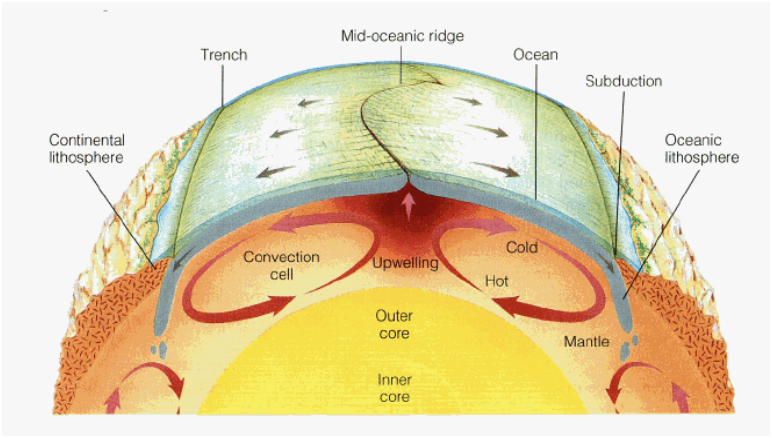

image from: http://bprc.osu.edu

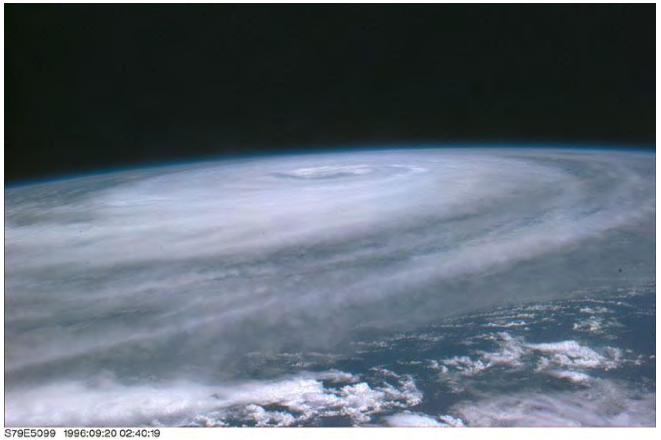

image from NASA

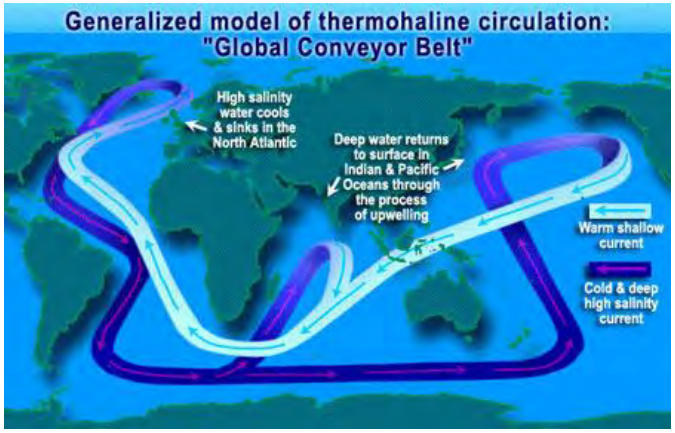

image from NASA

4. Turbulent Rayleigh-Bénard convection in a horizontal cylinder

- To what extend are the results obtained in small-Γ cells applicable to large-scale convection problems? This is an important question because one wants to understand which aspects of convection are universal and which depend on the details of spatial geometry.
- Such an understanding is needed for a large number of practical problems ranging from the thermal convection processes in buildings and metal production to natural convection occurred at geo- and astro-physical scales
- Two ways to test: (a) scale up the cell or (b) change the cell geometry

(a) Scale up the cell

2.2 m tall high-pressure SF_6 vessel (upright cylinder) built at the Max Planck Institute in Gottingen, Germany (Bodenschatz's lab)

1 m tall water tank (upright cylinder) built at the Chinese University of Hong Kong (Ke-Qing Xia's lab).

(b) change the cell geometry

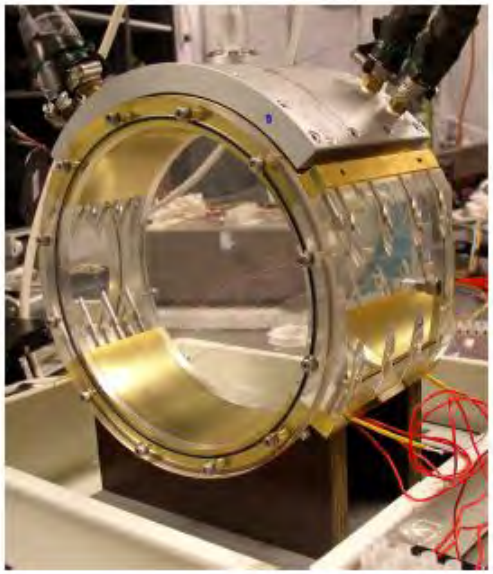

Top and bottom 1/3 of the circular sidewall are conducting plates. Sandwiched in the middle are two pieces of thermal insulating (curved) plate made of Plexiglas.

"Rayleigh-Bénard convection" in a horizontal cylinder

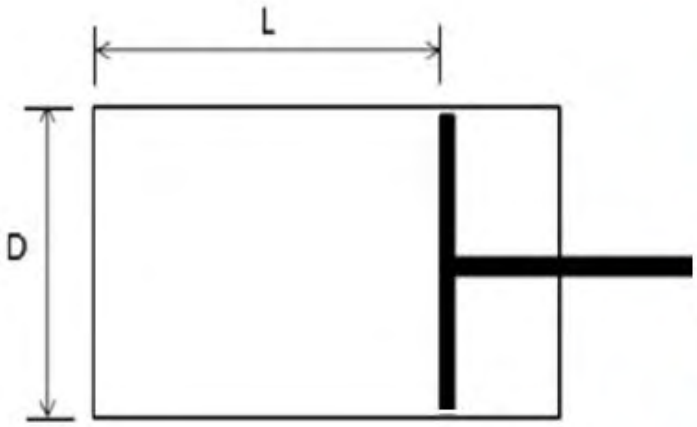

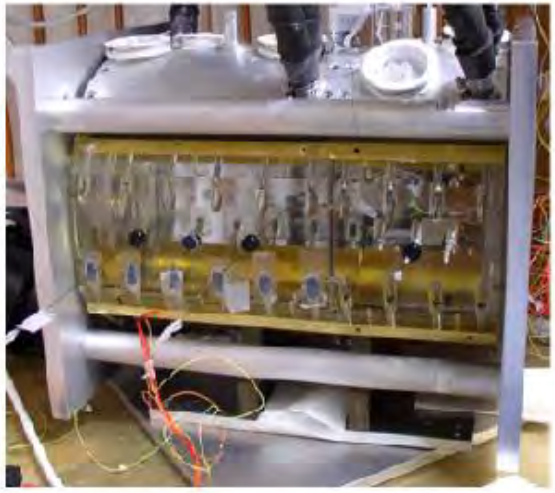

Experimental control parameters:

$$Ra = \frac{\alpha g \Delta T D^3}{\nu \kappa} : \quad 5\times10^8 - 1\times10^{10} \qquad \mathbf{Pr} = \frac{\nu}{\kappa} \approx 5.4$$

Geometric parameters:

cell diameter D = 18.8 cm (fixed)

cylinder length L: 2 - 31.8 cm

Γ = L/D: 0.1 – 1.7

System responses:

$$Nu(Ra) = \frac{\text{total heat flux}}{\text{conductive heat flux}} \qquad Re(Ra) = \frac{UD}{\nu}$$

$\Gamma = 0.5$ cell

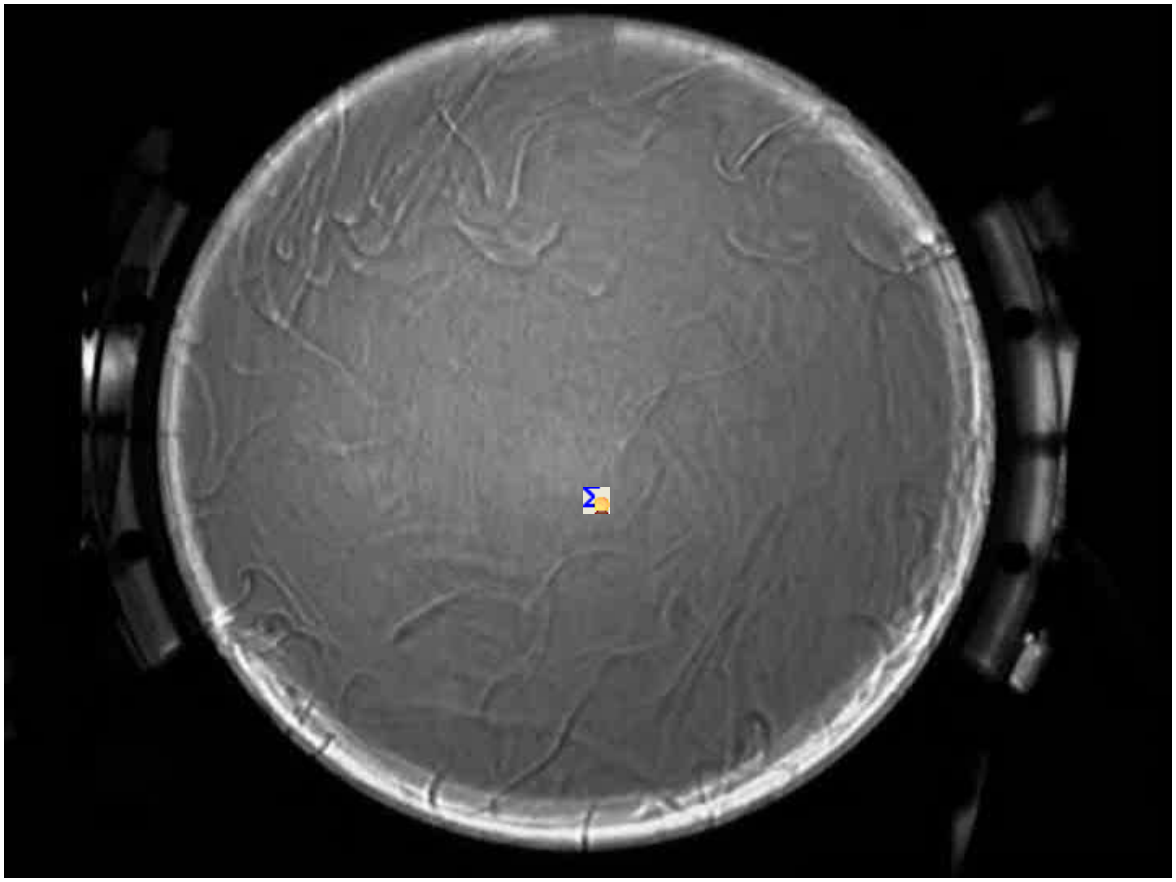

Shadowgraph movie showing the large-scale flow and spatial distribution of thermal plumes in a horizontal cylindrical cell.

Ra = 4.0×10^9, Pr = 74.5 (silicon oil with η = 10 cP)

4.1 Scalings in turbulent convection

(i) Scaling of the Nusselt number

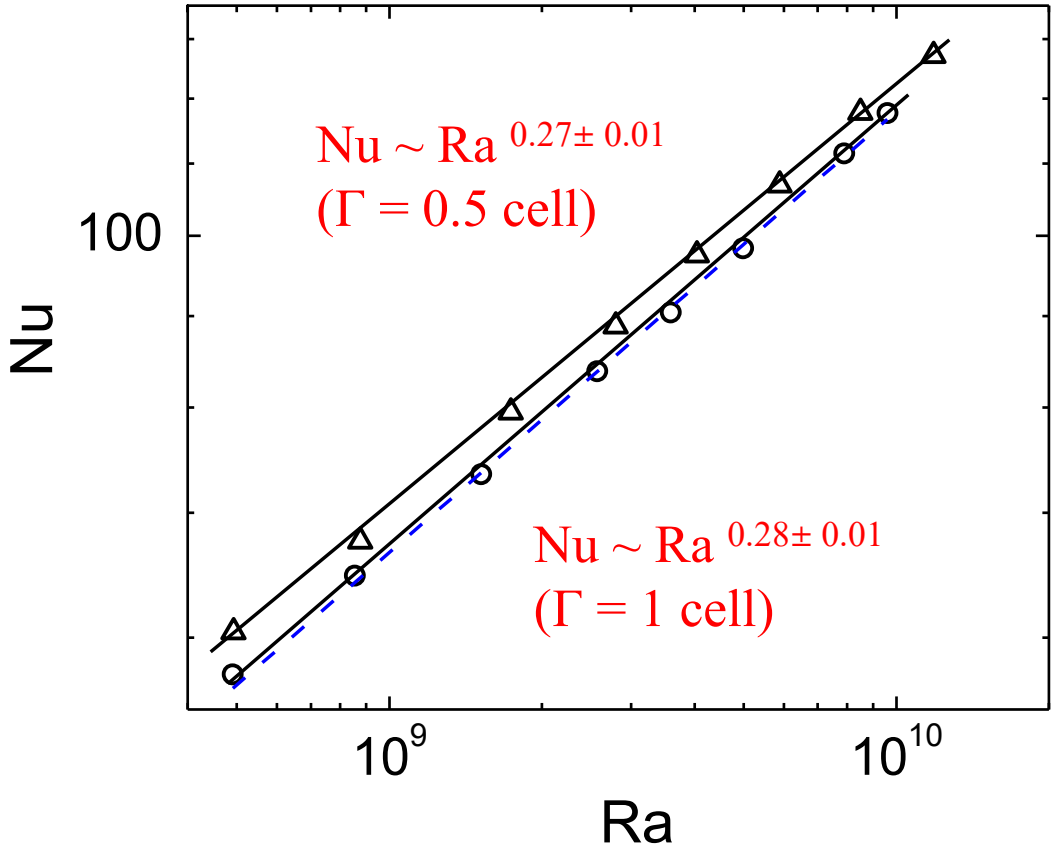

Upright cylinder: $Nu = 0.19\,Ra^{0.28}$ (in water) (Xia & Lui, PRL, 1997)

$Nu = 0.23\,Ra^{0.282}$ (in helium gas) (Castaing et al., JFM, 1989)

(ii) Scaling of the Reynolds number Re = ⟨V⟩D/ν

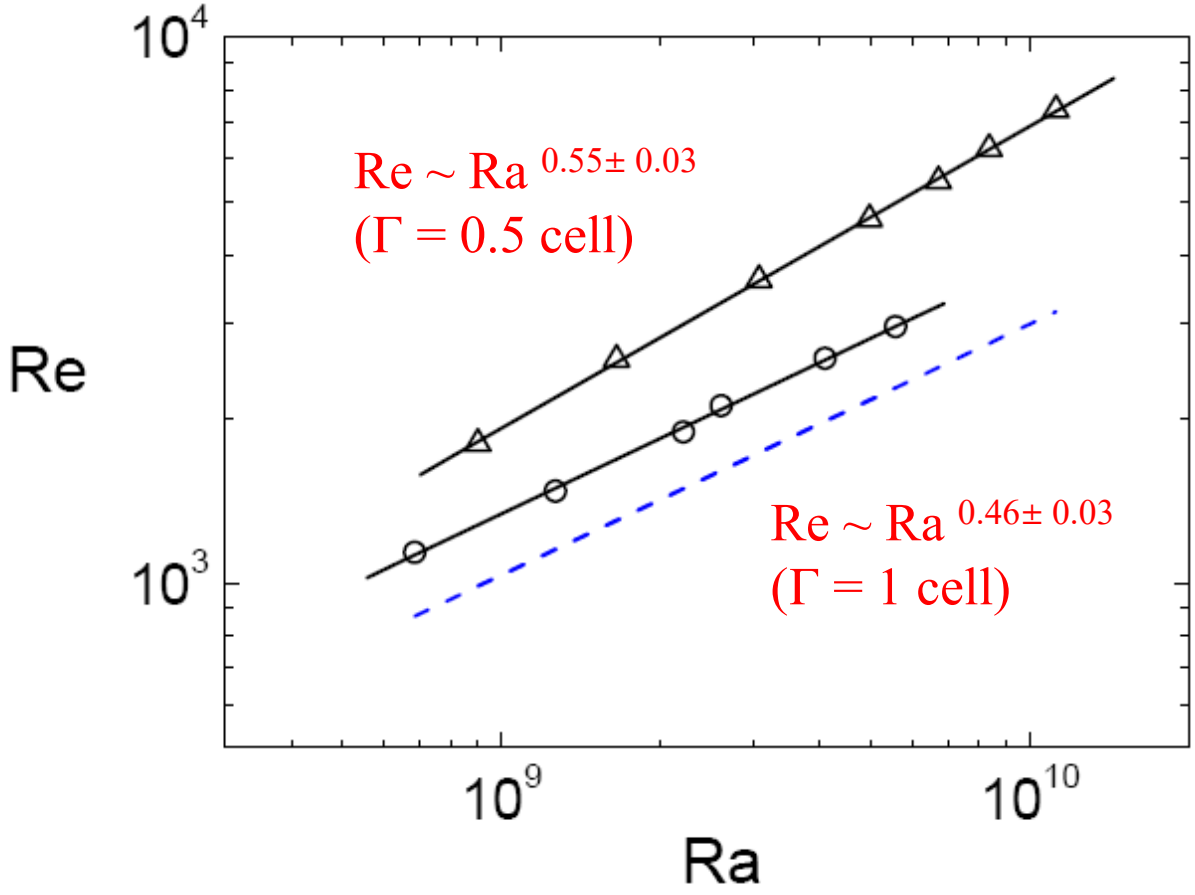

Upright cylinder: $Re = 0.075\, Ra^{0.46}$ (in water)

(Qiu & Tong, Phys. Rev. E, 2002)

(iii) Scaling of local temperature fluctuations

Temperature histograms at the center of $\Gamma = 1$ cell

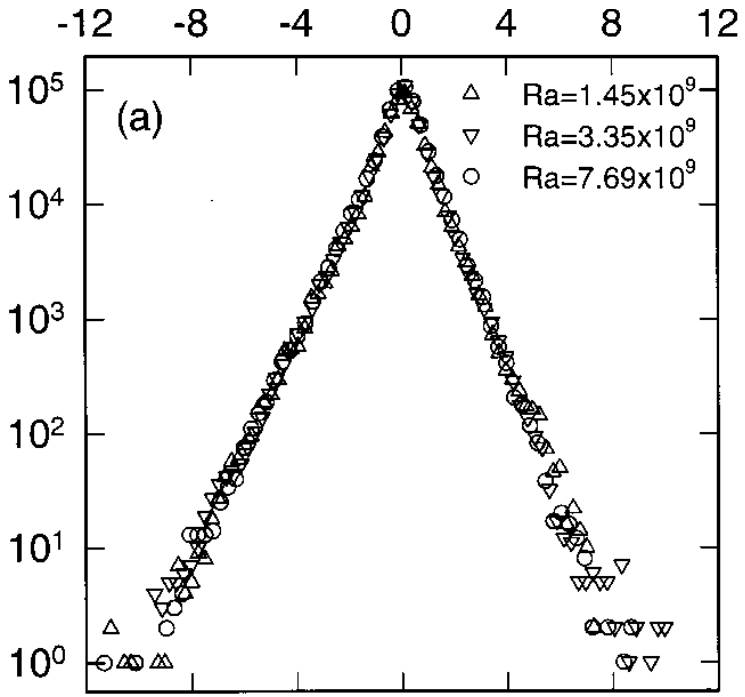

Upright cylinder

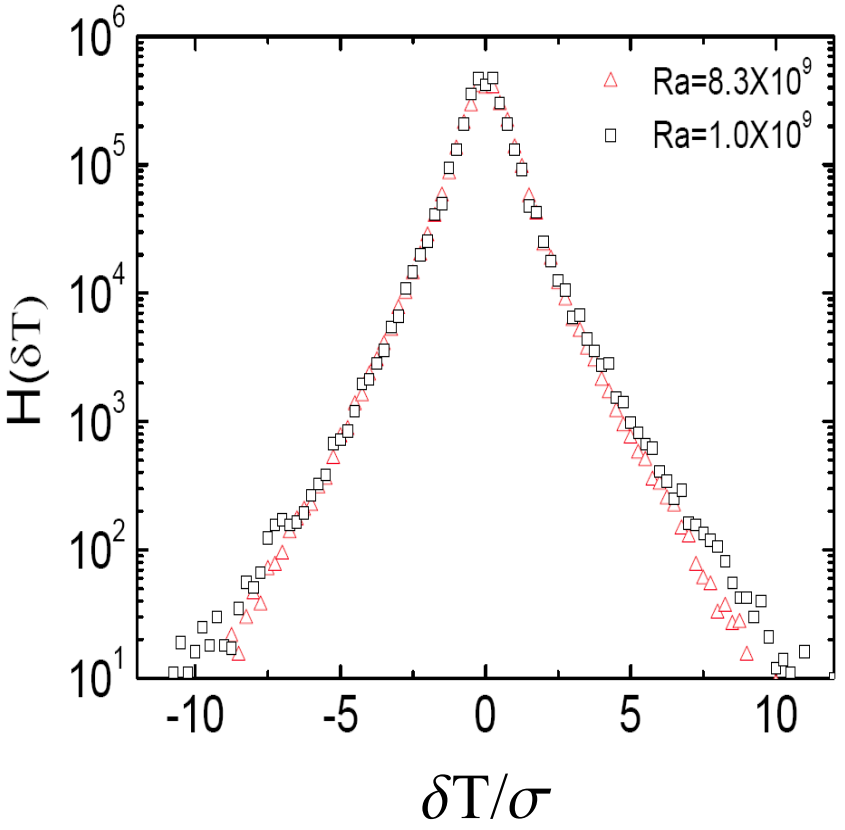

Horizontal cylinder

(Du & Tong, Phys. Rev. E, 2001)

Scaling of the normalized temperature rms

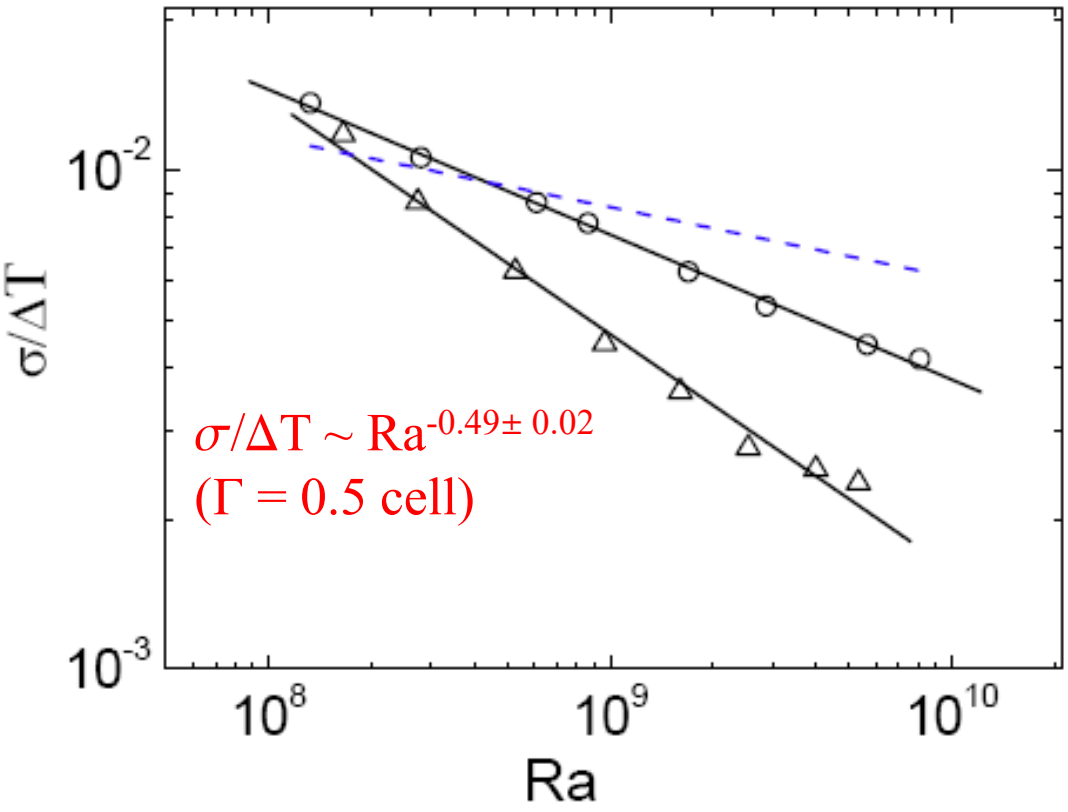

$$\sigma^2 = \frac{1}{n}\sum_{i=1}^{n}(T_i - \langle T \rangle)^2$$

$\sigma/\Delta T \sim Ra^{-0.29\pm 0.01}$
($\Gamma = 1$ cell)

Upright cylinder: $\sigma/\Delta T = 0.153\, Ra^{-0.14}$ (in water) (Du & Tong, PRE, 2001)

$\sigma/\Delta T = 0.36\, Ra^{-0.147}$ (in helium gas) (Castaing et al., JFM, 1989)

Square cell: $\sigma/\Delta T \sim Ra^{-0.48}$ (in water) (Daya & Ecke, PRL, 2001)

4.2 Dynamic phases (flow modes) of large-scale circulation (LSC)

Normalized oscillation period t_0/τ_t by LSC turnover time τ_t

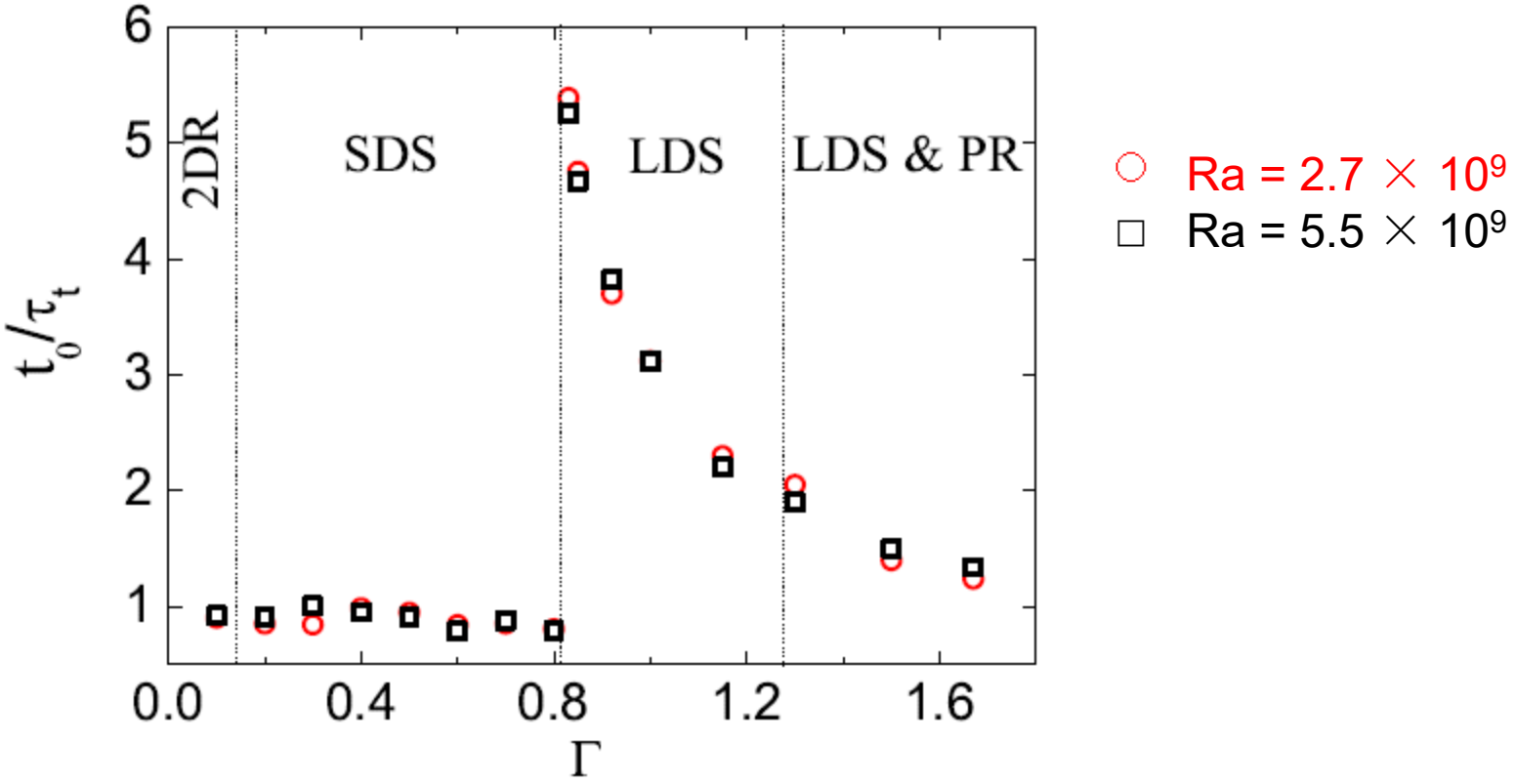

(1) All phases show coherent oscillations in the velocity and temperature measurements and the oscillation period t_0 varies with the aspect ratio Γ.

(i) Two-dimensional rotation (2DR): $\Gamma \leq 0.16$

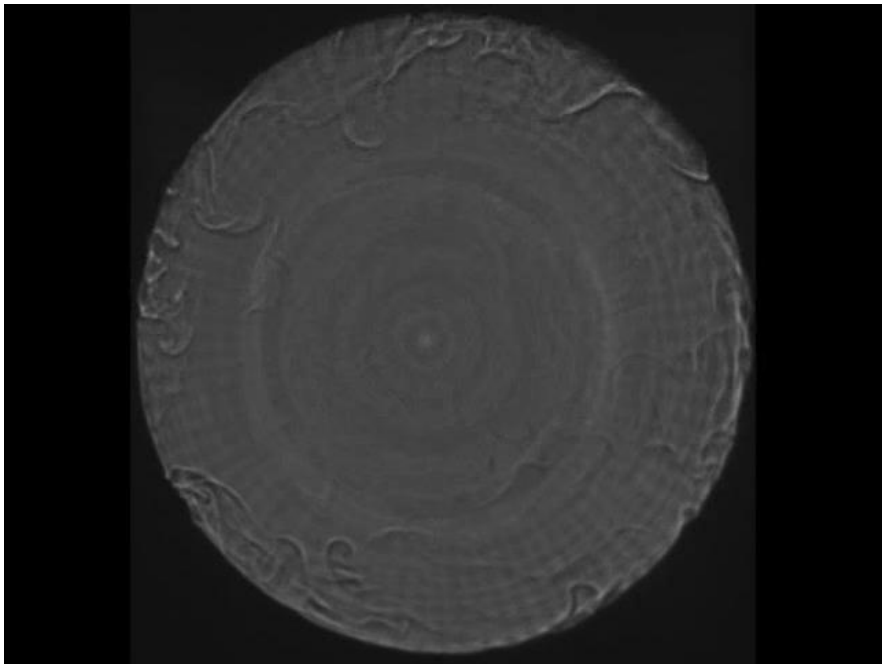

4×movie, $\Gamma = 0.16$, $Ra = 3.4 \times 10^9$ and $Pr = 4.3$ (water).

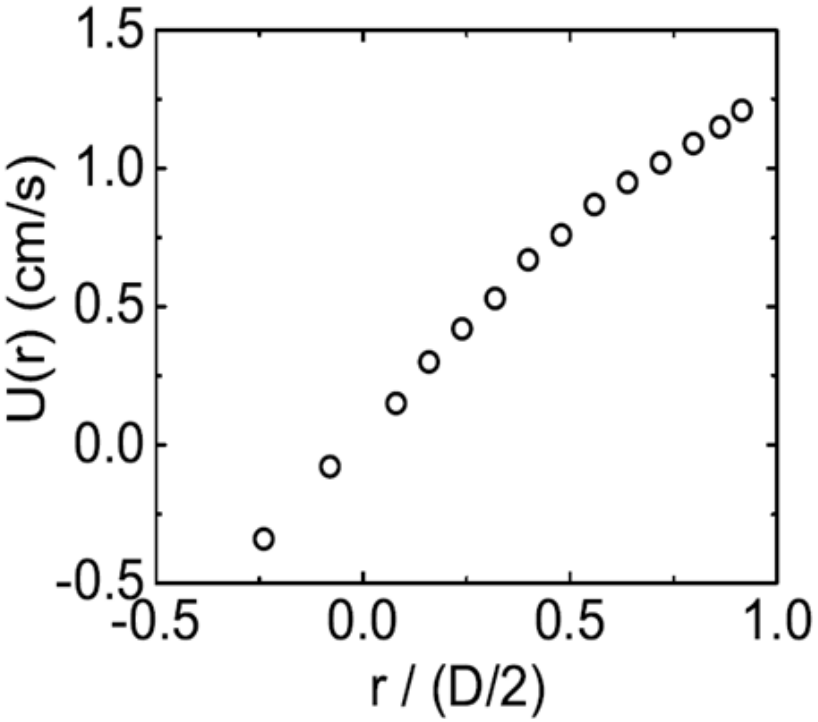

Vertical velocity profile

Flow is highly confined in a thin disk-like cell with a quasi-2D LSC in the circular plane of the cell. No 3D flow mode can be exited.

Power spectrum of four different signals

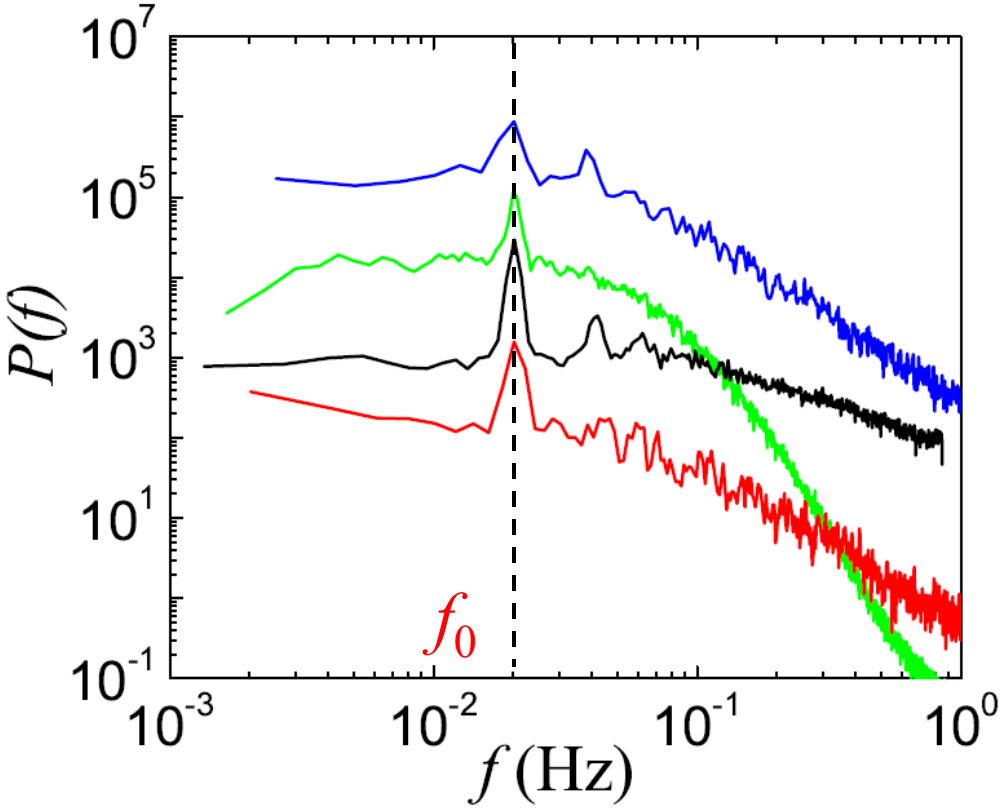

δI_4 plume image

H_0 total heat flux

T_5 local temperature

U_3 local velocity

(2) The coherent oscillations are produced by periodic emission of thermal plumes from the upper and lower boundary layers, which gives rise to a pulsed LSC. The coupling between the two boundary layers can be explained by a new solution of Villermaux's model.

H. Song, E. Villermaux and P. Tong, Phys. Rev. Lett. **106**, 184504 (2011)

(ii) Small-Γ Diagonal Switching (SDS): $0.16 < \Gamma \leq 0.82$

1 cm

30× movie taken at Ra = 7.3×10^9 and Pr ≈ 5 (water).
Floater is located at the center of bottom surface.

Histogram H(θ) of the angular position θ(t) of the LSC rotation plane (2-h-long floater data)

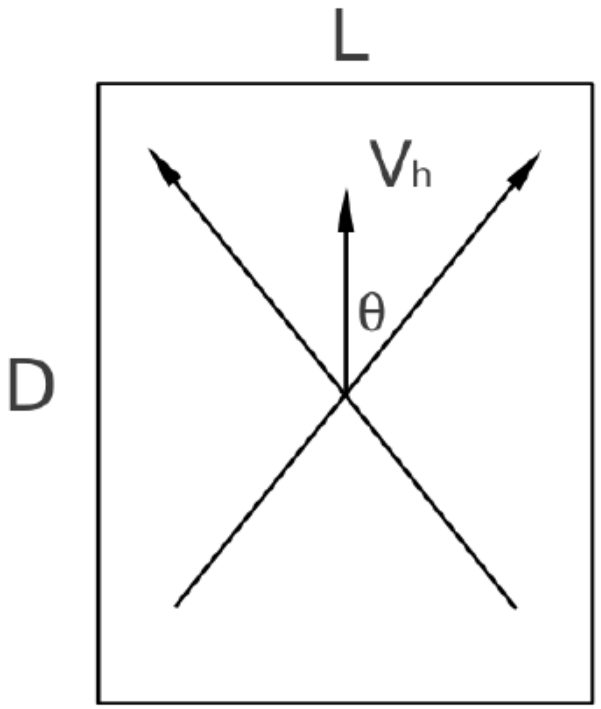

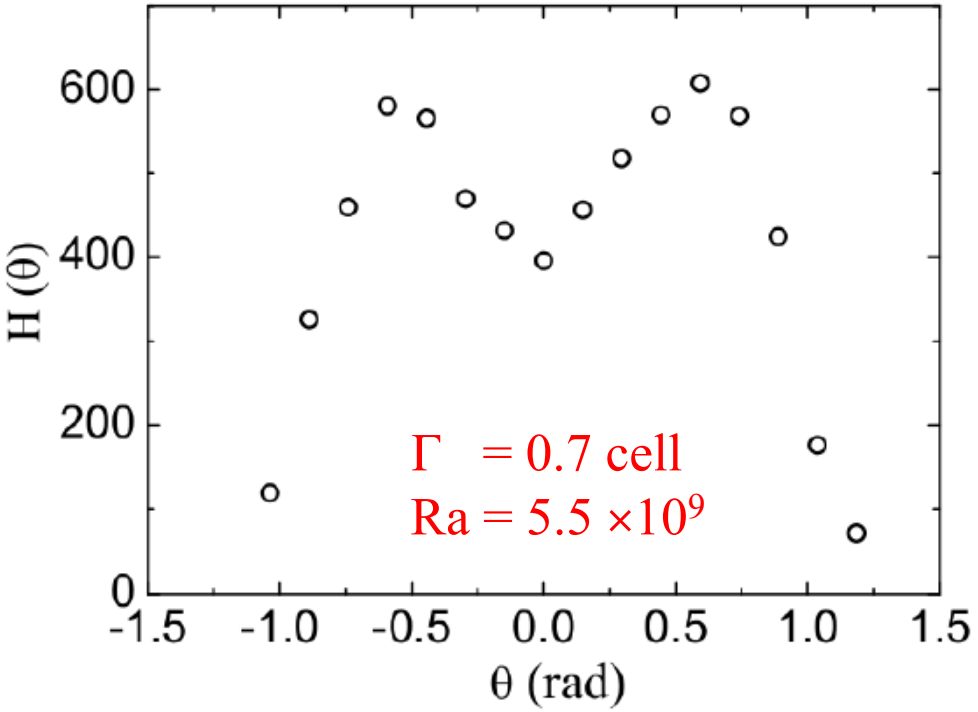

(3) The rotation plane of the LSC is aligned along the longest path of the cell - the diagonal of the cylinder, and switches periodically between the two diagonals, spanning across the curved sidewall.

Correlation function and power spectrum of local velocity fluctuations

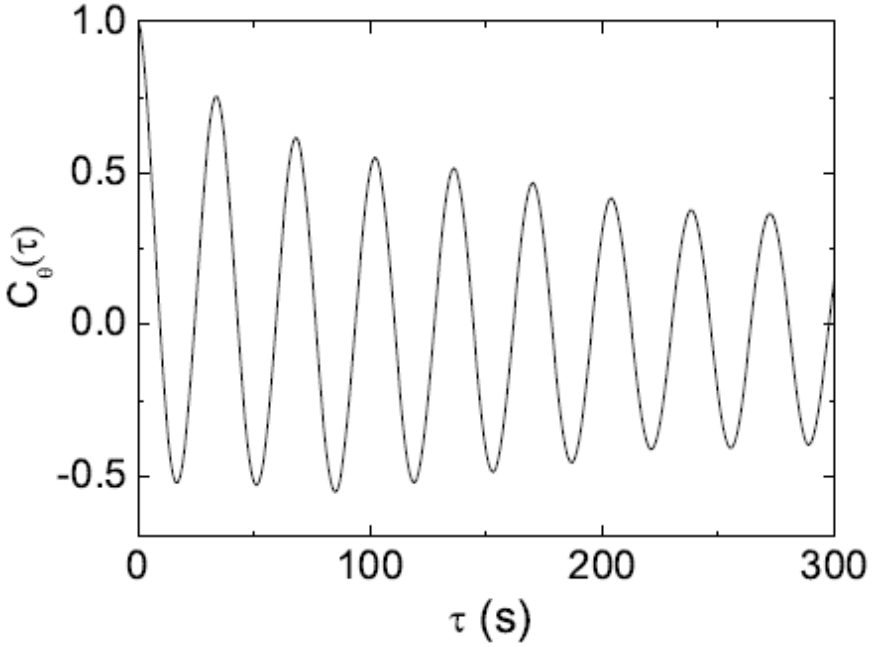

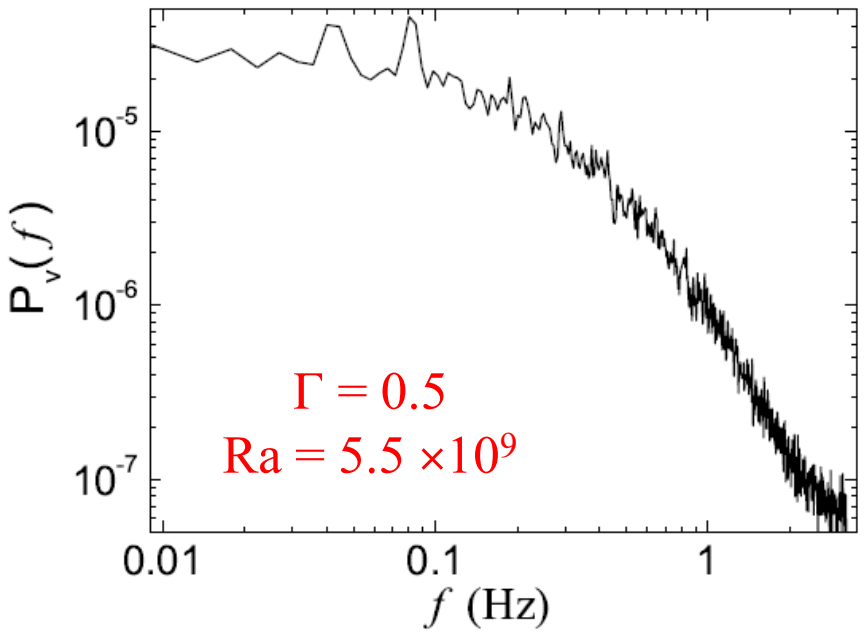

(4) In the SDS phase, the switching period t_0 is found to be approximately equal to the LSC turnover time τ_t.

(iii) Large-Γ Diagonal Switching (LDS): 0.82< Γ ≤ 1.69

Histogram H(θ) of the angular position θ(t) of the LSC rotation plane (2-h-long floater data)

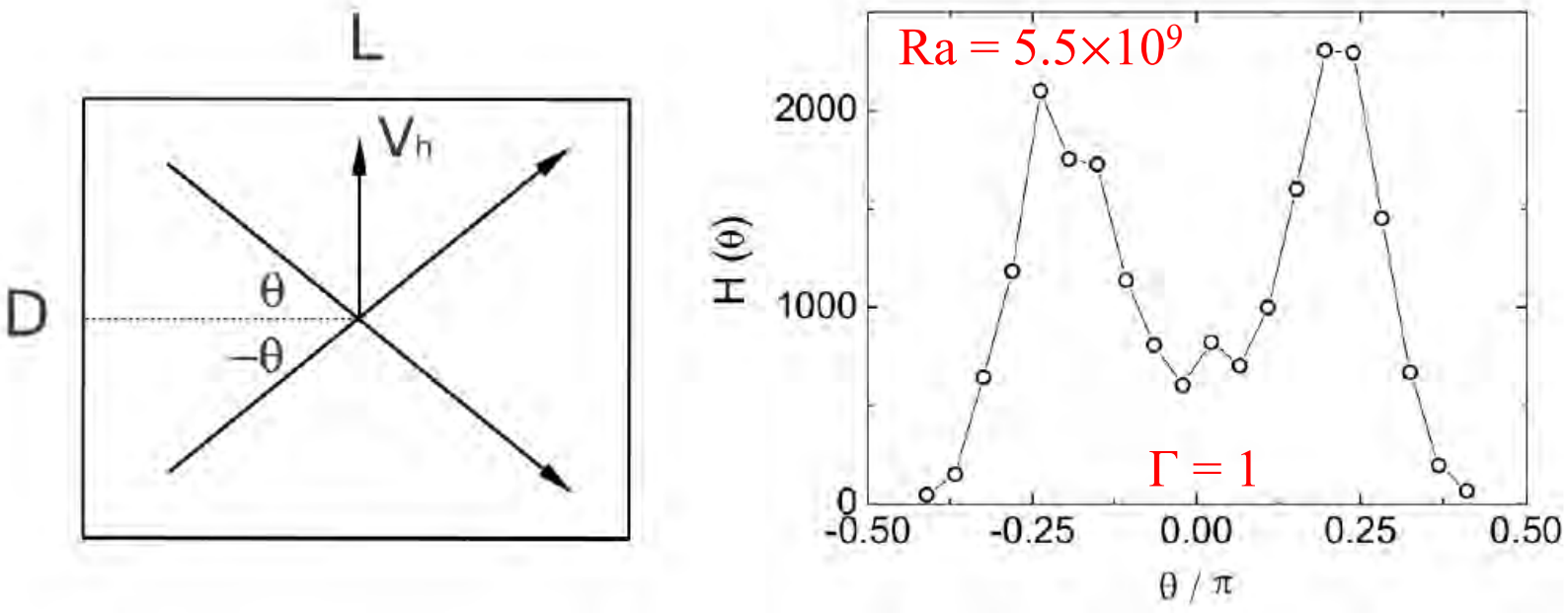

(5) In the LDS phase, the rotation plane of the LSC switches periodically between the two longest diagonals of the cell, spanning across the flat end wall.

Local velocity measurement: $V = \mathrm{U}\sin\theta$

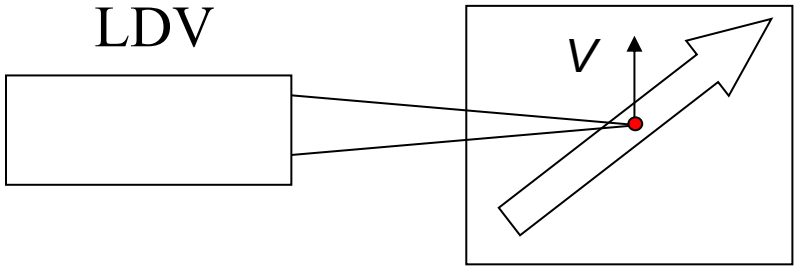

top view

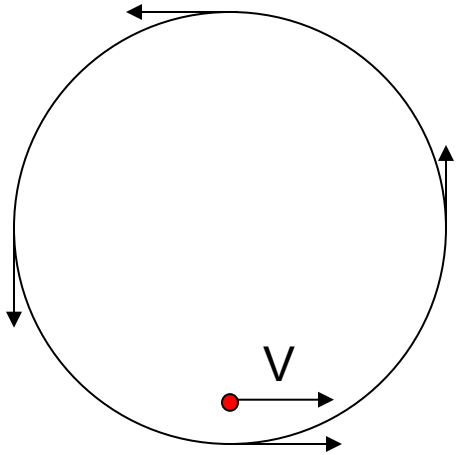

side view

The LSC orientation oscillates between two diagonals of the cell

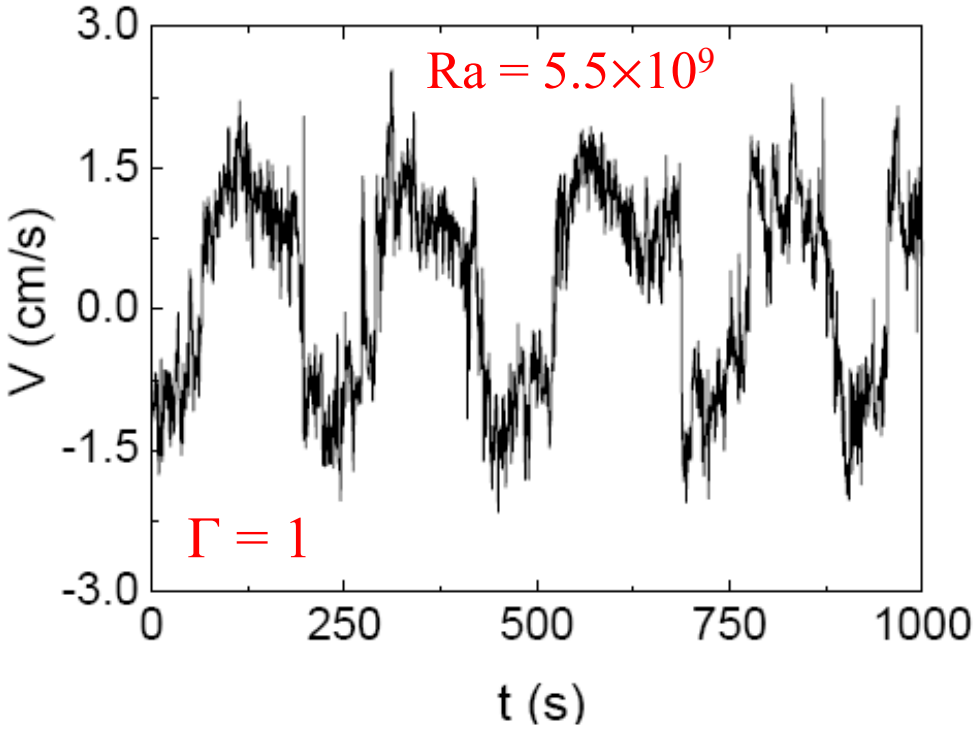

Transition aspect ratio $\Gamma_c \approx 0.82$

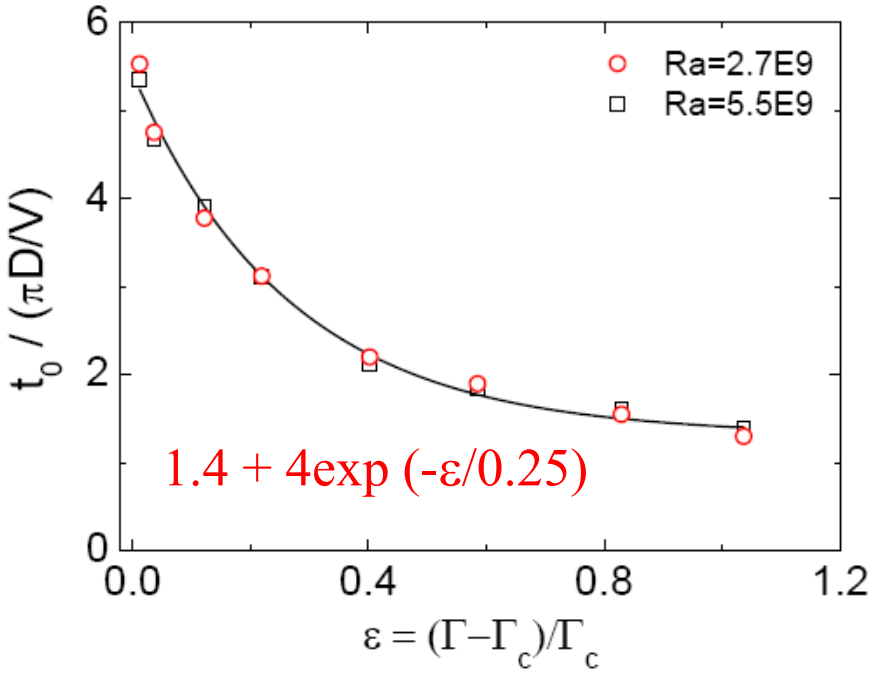

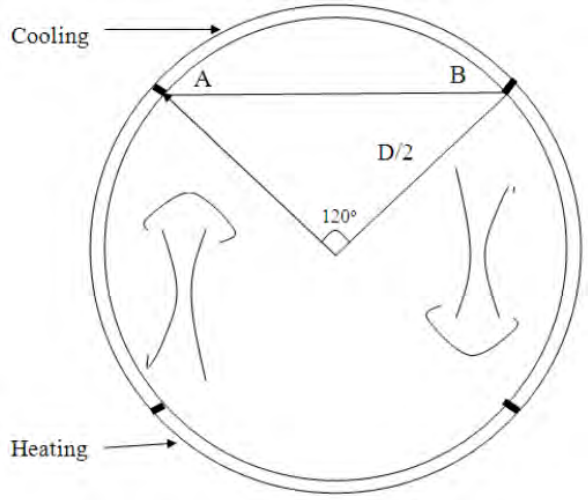

$$\overline{AB} = (\sqrt{3}/2)D \simeq 0.86D \rightleftarrows L$$

(6) The rotation plane of the LSC oscillates between the two diagonals with the shortest span possible (sensitive to the shape of the conducting plates). The normalized switching period $t_0/\ \tau_t$ is exponentially dependent on the aspect ratio Γ (or $\varepsilon = (\Gamma-\Gamma_c)/\Gamma_c$).

Coexist of the switching and wiggling modes in the horizontal cylinder

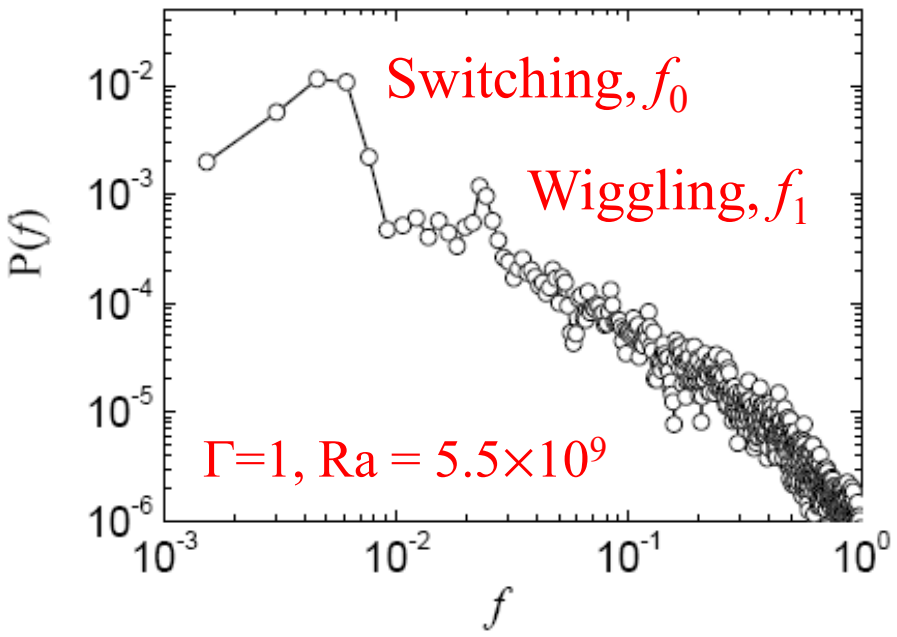

Switching frequency

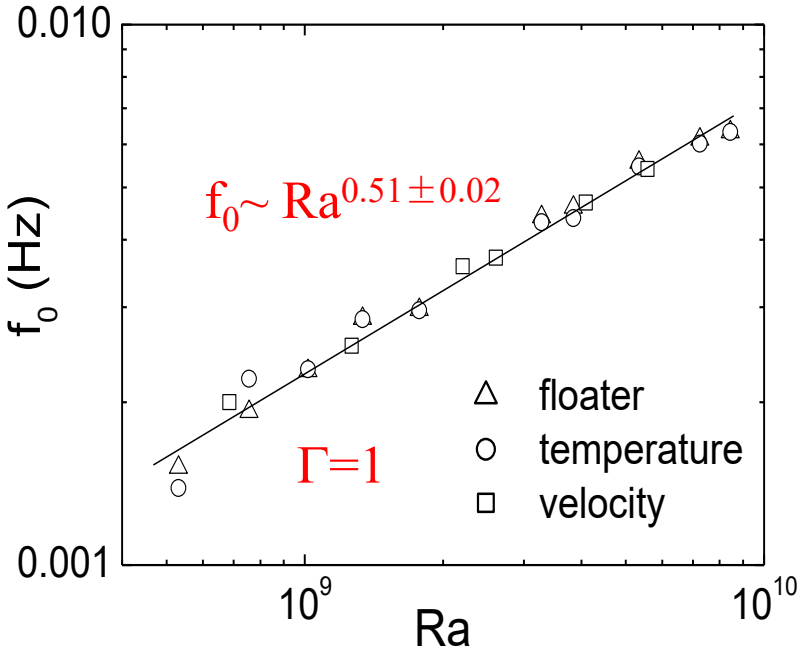

(7) The wiggling mode around the corner of the diagonal plane is explained by the Brown–Ahlers model. The switching mode between the diagonals is a new type of oscillation, which has not been observed in the upright cylinders.

Probability density function (pdf) P(θ) of the LSC orientation θ(t) over varying Γ

Ra = 5.5×10^9

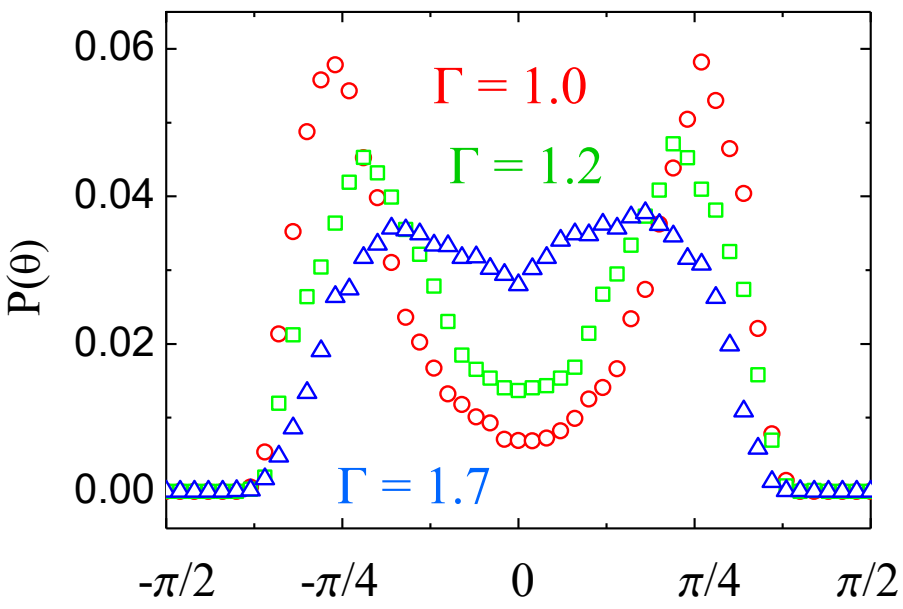

$V(\theta)/V_0 = -\ln[P(\theta)]+\text{const.}$

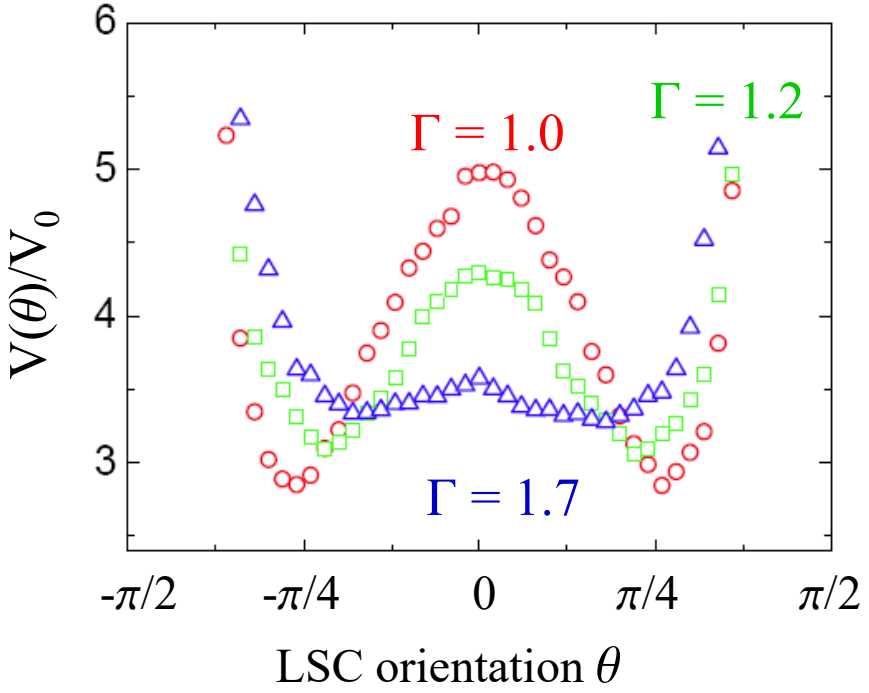

(8) The periodic switching of the LSC orientation between the two diagonals of the cell involves a crossing over an effective energy barrier, $V(\theta)/V_0$, which decreases with Γ.

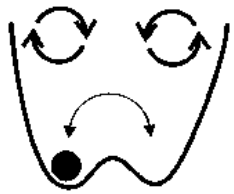

Comparison between the measured potential $V_g(\theta)/V_0$ and the calculation based on the Brown-Ahlers model (which is a low-dimensional model with turbulence noise)

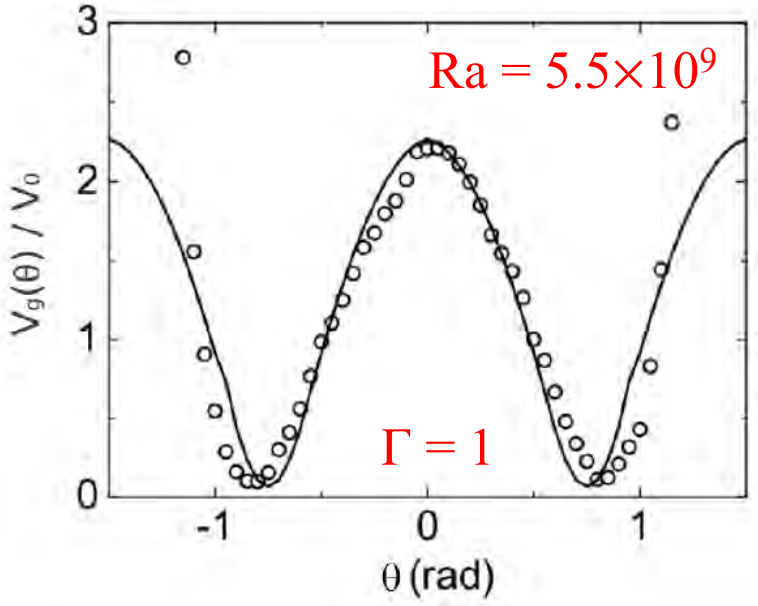

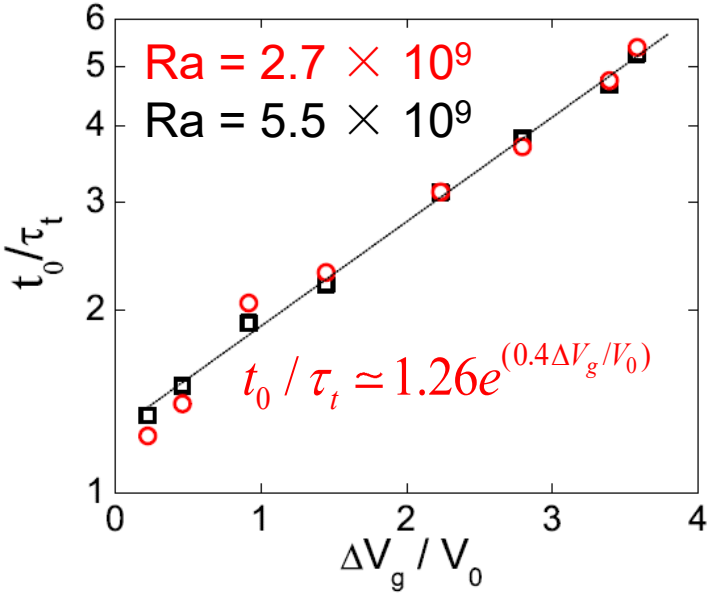

(9) The dynamics of the LSC orientation is adequately described by the Brown-Ahlers model involving a geometry dependent potential $V_g(\theta)$ of double-well shape with a barrier height $\Delta V_g(\theta)$. The normalized switching period t_0/τ_t is linked to $\Delta V_g(\theta)$ via an Arrhenius-Kramers type of equation.

Comparison between the measured pdf P(θ) and the calculation based on the Brown-Ahlers model

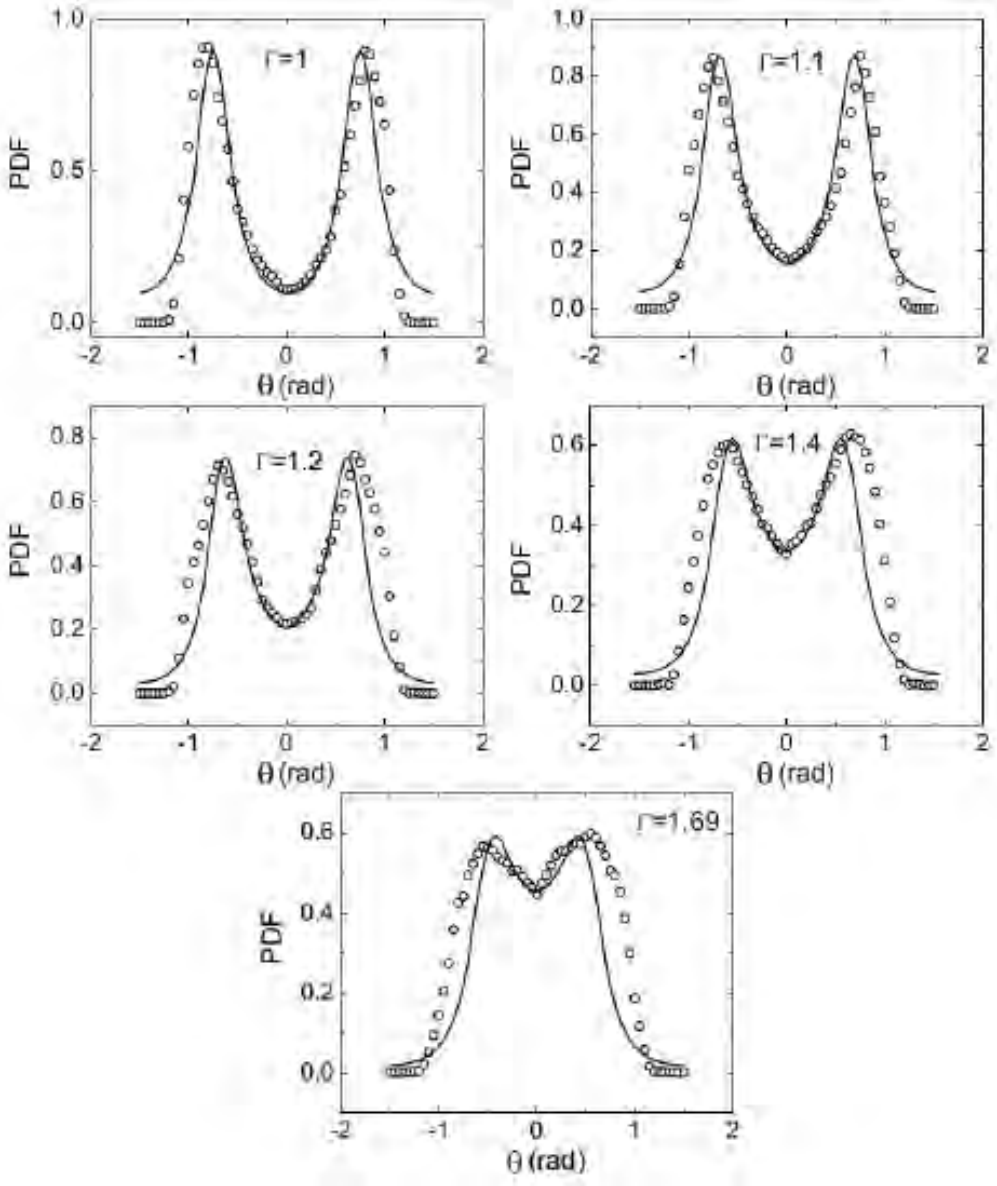

(iv) Periodic Rocking (PR): $1.3 \leq \Gamma \leq 1.69$

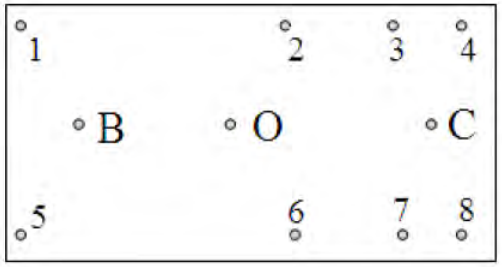

Positions of local temperature measurements near the sidewall

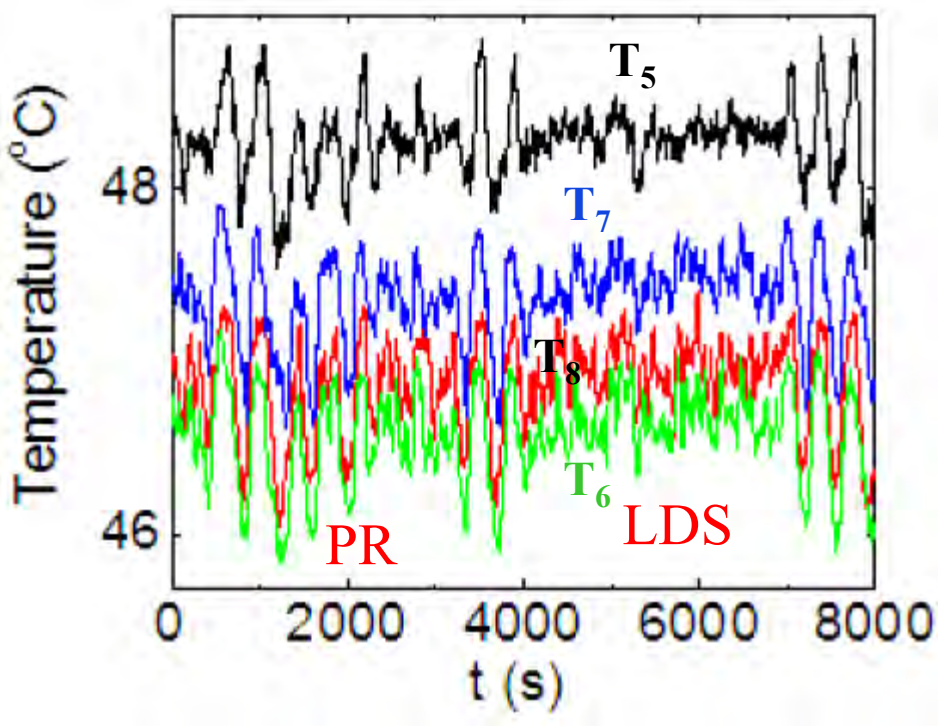

Temperature of the bottom plate

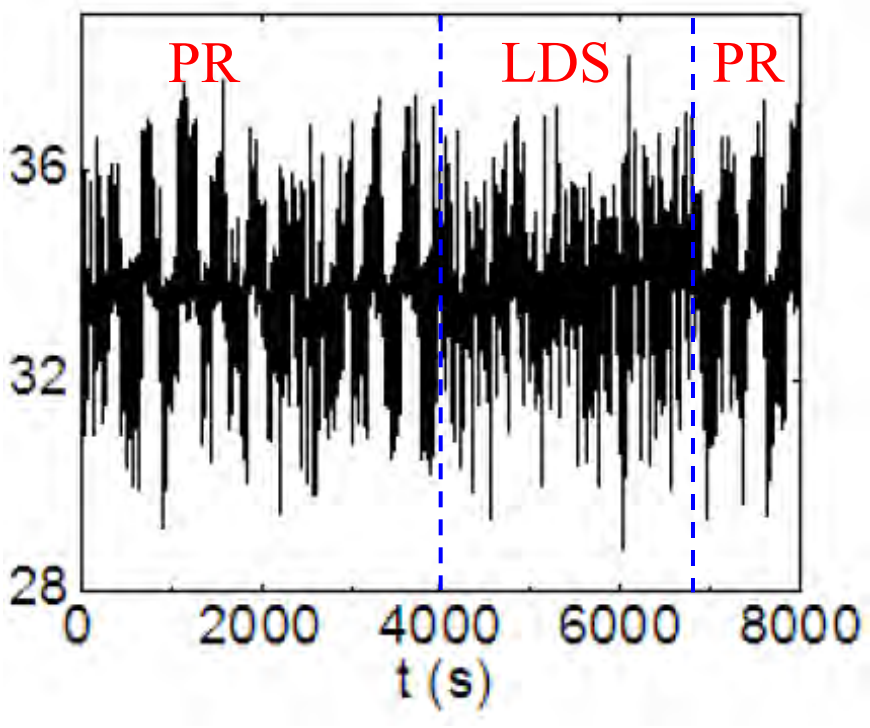

Temperature T_O at position O

Coexistence of the PR and LDS phases

Power spectrum of temperature fluctuations at positions B, O, and C.

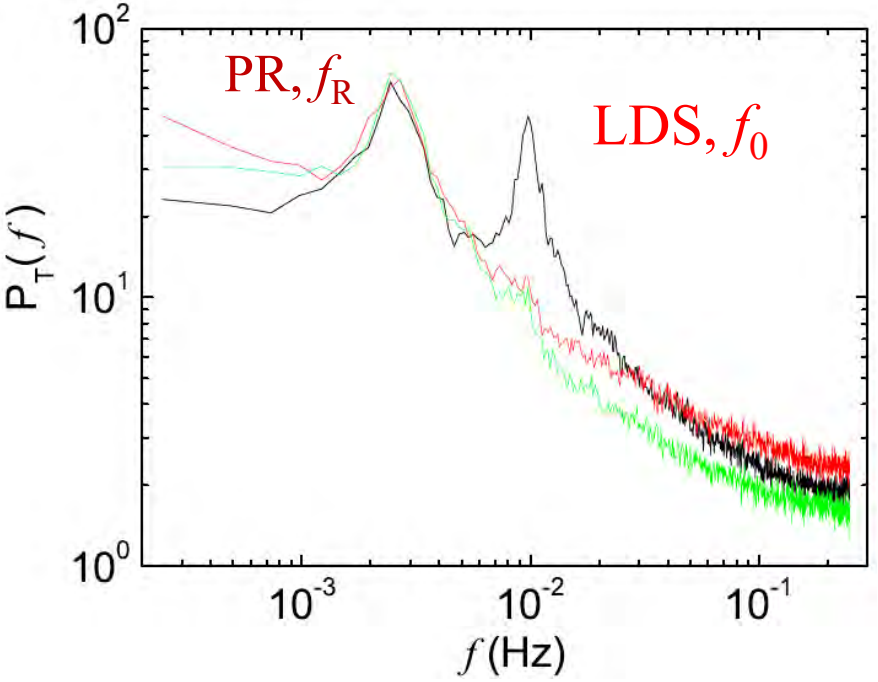

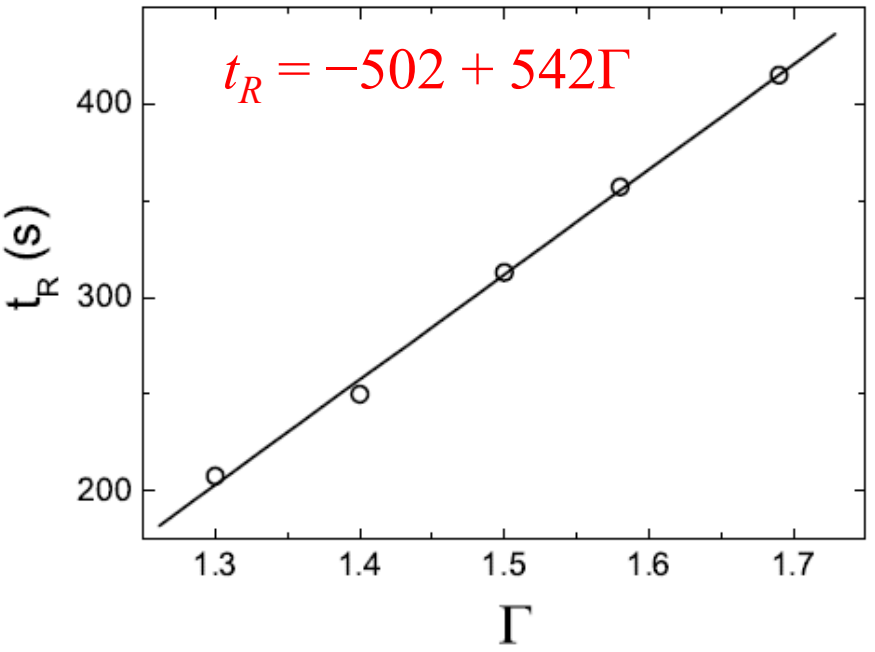

(10) In the PR phase, the bulk fluid rocks back and forth as a whole around the central axis of the horizontal cylinder. The rocking period increases linearly with Γ. The PR phase coexists with the LDS phase, and the two flow modes compete and occupy the cell in a random fashion.

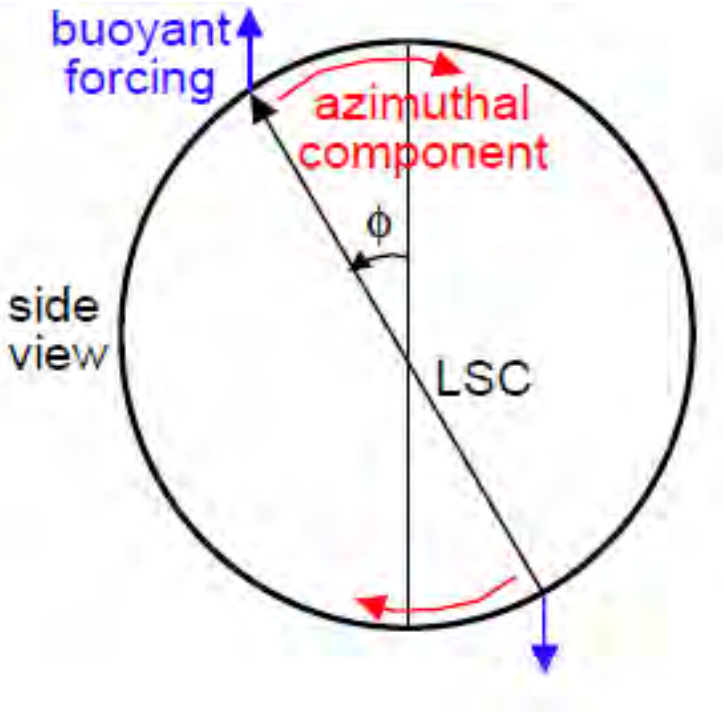

$$\ddot{\phi}_{PR} \approx \frac{2\alpha g\delta}{D}\sin\phi \approx \frac{318R_e^{3/2}\phi\nu^2}{D^4}$$

$$\omega_{PR} \approx \left(\frac{\ddot{\phi}_{PR}}{\phi}\right)^{1/2} \approx \frac{18R_e^{3/4}\nu}{D^2}$$

Four flow modes are identified in the horizontal cylinder with varying Γ, all of them having coherent oscillations associated with LSC.

2DR: $\Gamma \leq 0.16$

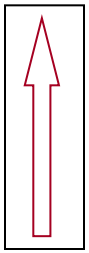

In-plane pulsed rotation,
no 3D switching

SDS: $0.16 < \Gamma \leq 0.82$

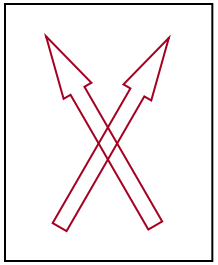

LSC switching across
the curved sidewall

LDS: $0.82 < \Gamma \leq 1.69$

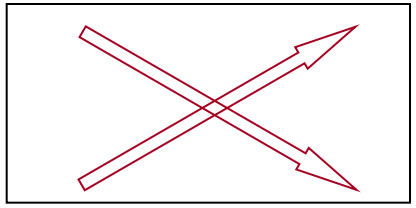

LSC switching across
the flat end wall

PR: $1.3 \leq \Gamma \leq 1.69$

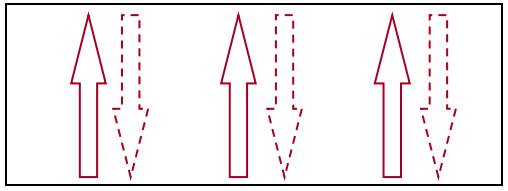

Periodic rocking around
the long axis of the cylinder

5. Summary

- Dynamics in turbulent thermal convection is determined primarily by thermal plumes.

- Thermal plumes organize themselves in a closed cell and generate a large-scale circulation (LSC) across the height of the cell.

- Heat transport is carried out mainly by the thermal plumes. The spatial separation of warm and cold plumes and the resulting LSC provide a fast channel along the cell periphery for the transport of heat.

- Thermal plumes produce strongly correlated temperature and velocity signals, which result in intermittent fluctuations of the local heat flux.

- Structural measurements are essential to the physical understanding of convective turbulence.

5. Summary (cont.)

- Scaling of the Nusselt number remains unchanged. Evidently, the boundary layer dynamics, which determine the heat transport, remain the same under different cell geometry.
- Scaling of the Reynolds number remains the same, insensitive to the geometry change. Buoyancy forces, which drive the large-scale flow, are independent of cell geometry.
- Scaling of the normalized temperature rms changes with the cell shape. Global flow structures affect the scaling of local temperature fluctuations but not much to their PDF.
- Large-scale circulation in the horizontal cylinder shows more interesting dynamics, which is sensitive to cell geometry. Four flow modes are identified in the horizontal cylinder with varying Γ, all of them having coherent oscillations associated with LSC. (Universal?) mechanism for coherent oscillations in turbulent convection remains unsettled.

5. Summary (cont.)

- The oscillations in the thin cell (Γ=0.16) are caused by the in-phase periodic emission of thermal plumes between the upper and lower boundary layers.
- For $0.16 < \Gamma \leq 0.82$, the rotation plane of LSC switches periodically between the two diagonals of the cell, spanning across the curved sidewall.
- For $0.82 < \Gamma \leq 1.69$, the periodic switching spans across the flat end wall. In this phase, the motion of the LSC orientation can be considered as a damped harmonic oscillator moving in a double-well potential, where the two minimum potential positions correspond to the two diagonals of the cell.
- For $1.3 \leq \Gamma \leq 1.69$, the bulk fluid as a whole rotates around the central axis of the horizontal cylinder with periodic reversals.

Large- and Small-scale Dynamics in Turbulent Rayleigh-Bénard Convection II

Penger Tong

Department of Physics

Hong Kong University of Science & Technology

2013 Spring Progress in Mathematical and Computational Studies on Science and Engineering Problems

May 6-8, 2013, National Taiwan University

OUTLINE:

1. Dissipations in Rayleigh-Bénard convection
2. Measurement of the local thermal dissipation rate
3. Scaling behavior of the measured local thermal dissipation rate
   - 3.1 Spatial distribution of the thermal dissipation field
   - 3.2 Ra-dependence of the local thermal dissipation rate
   - 3.3 Scale-dependent statistics of dissipation fluctuations $\epsilon_f(\mathbf{r},t)$
4. Test of the anomalous scaling of passive temperature fluctuations
5. Space-time relation in turbulent Rayleigh-Bénard convection
6. Summary

Collaborators:

Xiao-zhou He (HKUST) and Emily Ching (CUHK)

Work supported by the Hong Kong Research Grants Council

1. Dissipations in Rayleigh-Bénard Convection

For turbulent Rayleigh-Bénard convection, we have

- three local variables, $\mathbf{v}(\mathbf{r},t)$, $T(\mathbf{r},t)$ and $p(\mathbf{r},t)$, and three equations.
- two corresponding dissipation rates, ε_u and ε_T.
- There are two exact relations:

$$\varepsilon_T = \kappa \langle [\partial_i T(\mathbf{r},t)]^2 \rangle_{V,t} = \kappa (\Delta T / H)^2 \, Nu(Ra, \mathrm{Pr})$$

$$\varepsilon_u = \nu \langle [\partial_i \mathbf{v}_j(\mathbf{r},t)]^2 \rangle_{V,t} = (\nu^3 / H^4)(Nu - 1) Ra \, \mathrm{Pr}^{-2}$$

Understanding heat transport, Nu(Ra,Pr), in turbulent convection through spatial decomposition of the dissipation fields ε_u and ε_T

Phenomenology of Grossmann & Lohse (JFM, 2000; PoF, 2004):

boundary *versus* bulk

$$\boxed{\varepsilon_u = \varepsilon_{u,BL} + \varepsilon_{u,bulk}}$$

$$\varepsilon_{u,BL} \sim \nu (u/\lambda_u)^2 (\lambda_u / H)$$

$$\varepsilon_{u,bulk} \sim u^3 / H$$

$$\boxed{\varepsilon_T = \varepsilon_{T,BL} + \varepsilon_{T,bulk}}$$

$$\varepsilon_{T,BL} \sim \kappa (\Delta T/\lambda_T)^2 (\lambda_T / H)$$

$$\varepsilon_{T,bulk} \sim (u\varphi)\Delta T^2 / H$$

Understanding of small-scale properties of turbulence through the statistics of dissipation fluctuations ε_u and ε_T

Kolmogorov refined similarity hypothesis (JFM, 1962)

$$S_u^n(r) = \left\langle \left([\mathbf{u}(x+r,t) - \mathbf{u}(x,t)] \bullet \frac{\mathbf{r}}{r} \right)^n \right\rangle_{x,t} \sim \langle \varepsilon_u(r)^{n/3} \rangle r^{n/3} \sim r^{\zeta_u(n)}$$

$$S_T^n(r) = \left\langle [T(x+r,t) - T(x,t)]^n \right\rangle_{x,t} \sim \langle \varepsilon_u(r)^{-n/6} \rangle \langle \varepsilon_T(r)^{n/2} \rangle r^{n/3} \sim r^{\zeta_T(n)}$$

$$\varepsilon_u(r) = \frac{4\pi}{(4\pi/3)r^3} \int_0^r \varepsilon_u r'^2 \, dr' \qquad \varepsilon_T(r) = \frac{4\pi}{(4\pi/3)r^3} \int_0^r \varepsilon_T r'^2 \, dr'$$

Scale-dependent fluctuations of $\varepsilon_u(r)$ and $\varepsilon_T(r)$ will give rise to anomalous scaling (intermittency) for the velocity and temperature structure functions (SFs).

Our recent work:

- "Measured thermal dissipation field in turbulent Rayleigh-Benard convection," X.-Z. He, P. Tong, and K.-Q. Xia, Phys. Rev. Lett. **98**, 144501 (2007).
- "Measurements of the thermal dissipation field in turbulent Rayleigh-Benard convection," X.-Z. He and P. Tong, Phys. Rev. E **79**, 026306 (2009).
- "Statistics of the locally averaged thermal dissipation rate in turbulent Rayleigh–Benard convection," X.-Z. He, P. Tong and E. Ching, J. of Turbulence, **11**, No. 35, 1-10 (2010).
- "Locally-averaged thermal dissipation rate in turbulent thermal convection: A decomposition into contributions from different temperature gradient components," X.-Z. He, E. Ching, and P. Tong, Phys. Fluids **23**, 025106 (2011).
- "Scaling behavior in turbulent Rayleigh-Benard convection revealed by conditional structure functions," E. Ching, Y.-K. Tsang, T. N. Fok, X.-Z He and P. Tong, Phys. Rev. E **87**, 013005 (2013).

2. Measurement of the local thermal dissipation rate

Instantaneous local viscous dissipation rate:

$$\varepsilon_u(\mathbf{r},t) = \nu \sum_{i,j} \frac{\partial u_i}{\partial x_j} \frac{\partial u_i}{\partial x_j}$$

Instantaneous local thermal dissipation rate:

$$\varepsilon_T(\mathbf{r},t) = \kappa[(\frac{\partial T}{\partial x})^2 + (\frac{\partial T}{\partial y})^2 + (\frac{\partial T}{\partial z})^2]$$

Time-averaged local thermal dissipation rate:

$$\langle \varepsilon_T(\mathbf{r},t) \rangle_t \simeq (\varepsilon_T)_m(\mathbf{r}) + (\varepsilon_T)_f(\mathbf{r}) = \kappa \sum_i \langle (\frac{\partial \bar{T}}{\partial x_i})^2 \rangle_t + \kappa \sum_i \langle (\frac{\partial \tilde{T}}{\partial x_i})^2 \rangle_t$$

Total convective heat flux across the cell:

$$\mathrm{Nu} = \frac{1}{A} \iint \mathrm{J_z}(x,y) dx dy = \frac{1}{\kappa(\Delta T / H)^2} \frac{1}{V} \iiint \langle \varepsilon_T(\mathbf{r},t) \rangle_t d\mathbf{r}$$

Local temperature gradient probe:

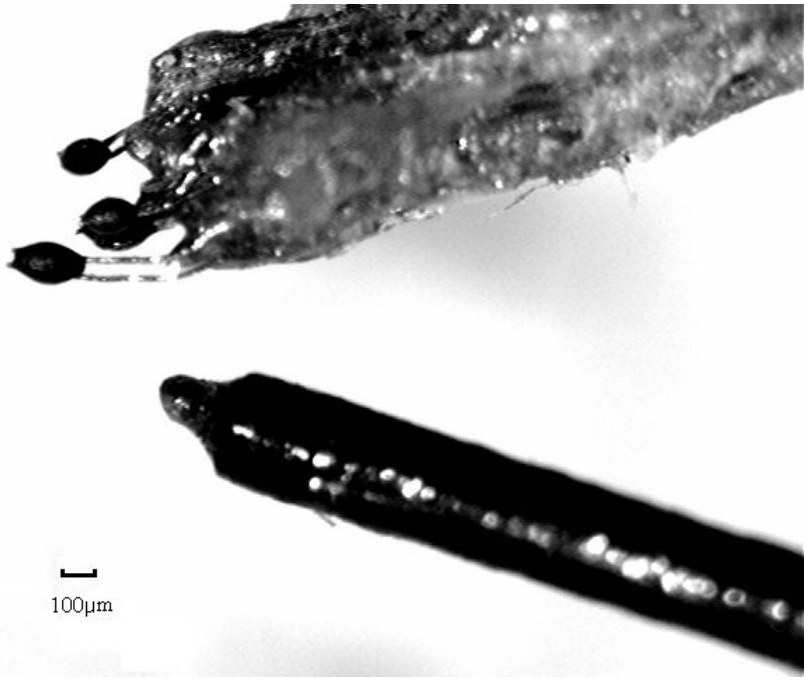

First probe: d = 0.17 mm
$\delta x_i = 0.8$ mm, $\delta T_{min} \approx 5$ mK

Second probe: d = 0.11 mm
$\delta x_i = 0.25$ mm, $\delta T_{min} \approx 5$ mK

$\delta \approx 0.8$ mm at Ra = 3.6×10^9

Rayleigh-Bénard convection cell

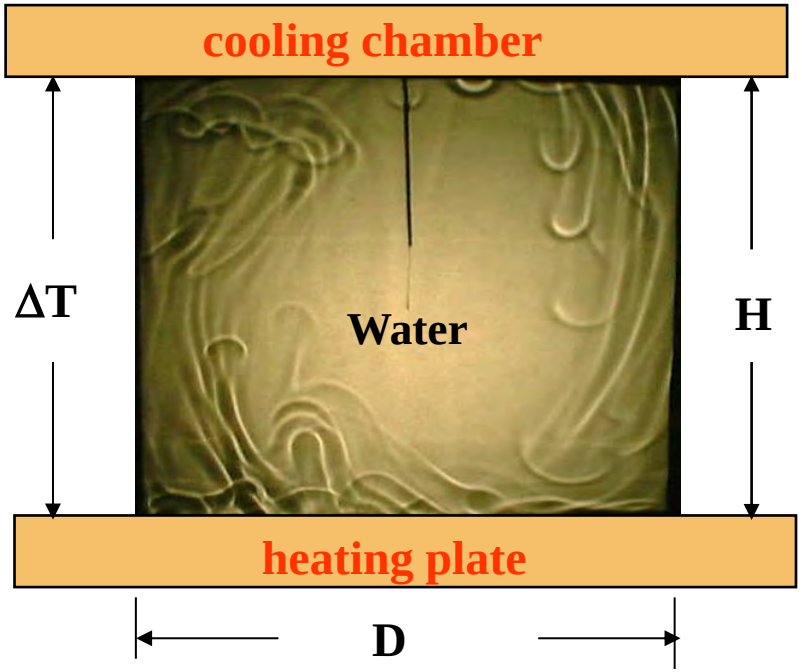

$$Ra = \frac{\alpha g H^3 \Delta T}{\nu \kappa}$$

$$(10^8 \le Ra \le 10^{10})$$

$$\Delta T \simeq 1 \text{ to } 40^{\circ}\text{C}$$

$$\Pr = \frac{\nu}{\kappa} \approx 5.4$$

$$\Gamma = \frac{D}{H} = 1 \text{ and } 0.5$$

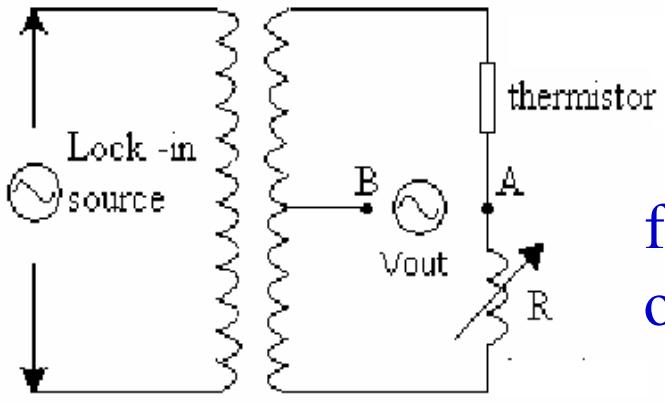

four ac bridges with lock-in amplifiers operated at f ≈ 1 kHz and Δf = 100 Hz

3. Scaling behavior of the local thermal dissipation rate

3.1 Spatial distribution of the thermal dissipation field

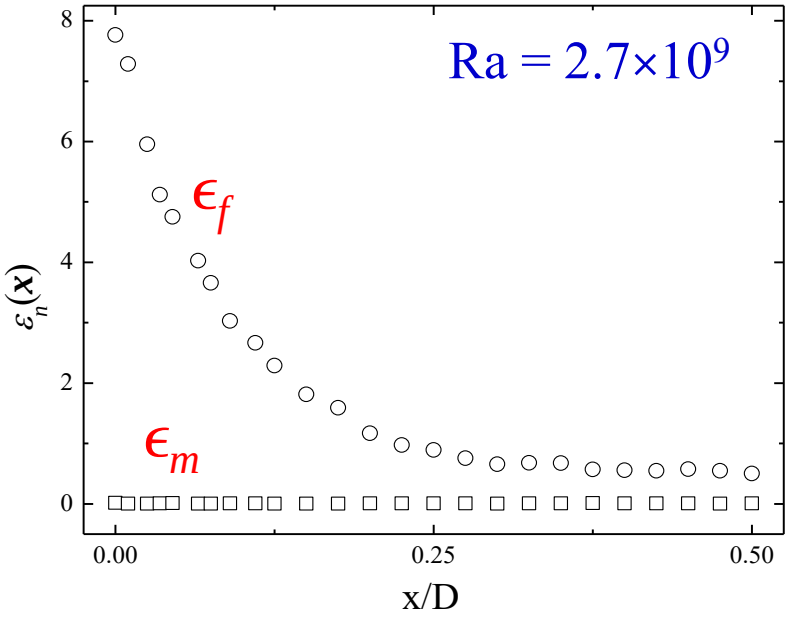

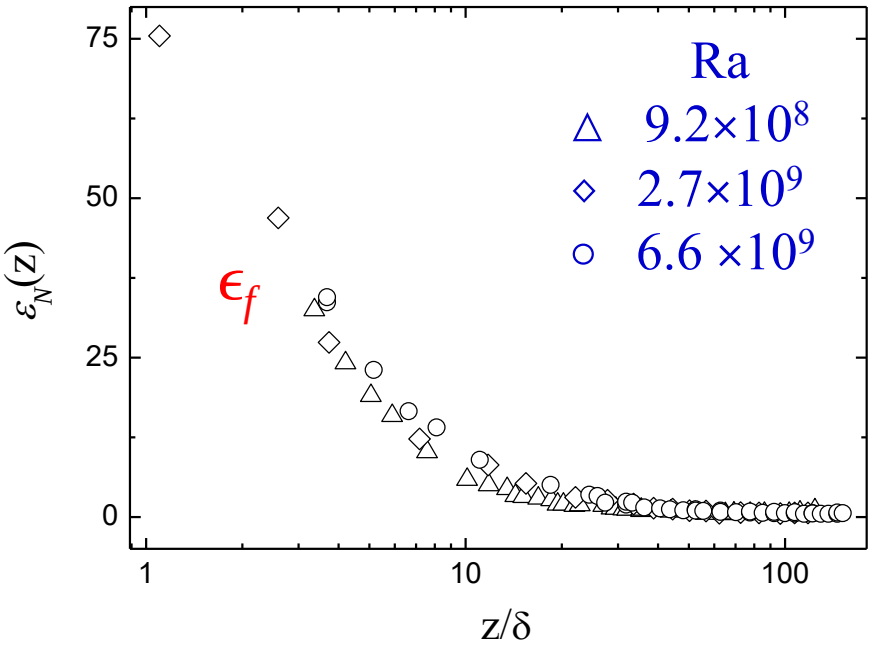

$$\varepsilon_N(\mathbf{r}) = \varepsilon_m(\mathbf{r}) + \varepsilon_f(\mathbf{r})$$

(i) In the bulk region, ϵ_f is dominant and ϵ_m is negligibly small.

(ii) ϵ_f increases rapidly in the $1 \le z/\delta \le 10$ region and is ~140 times larger than that at the cell center.

$Ra = 3.9 \times 10^9$

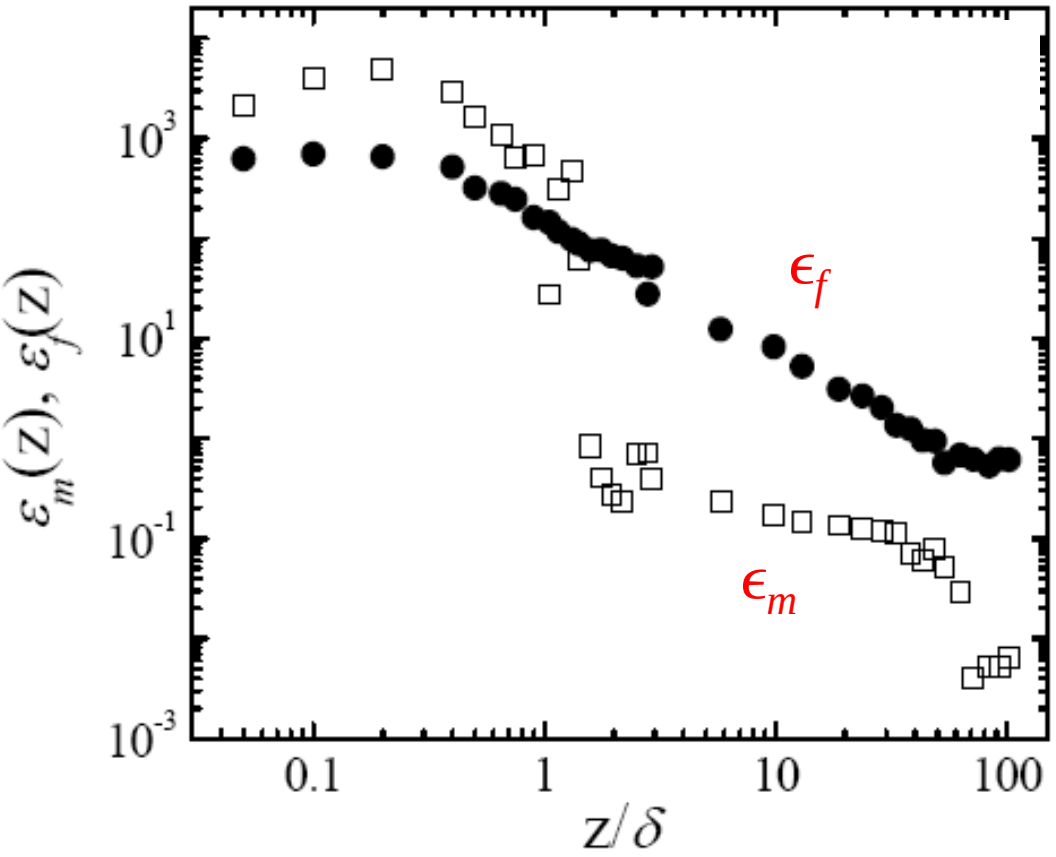

(iii) In the thermal boundary layer, ϵ_m becomes dominant and ϵ_f is smaller.

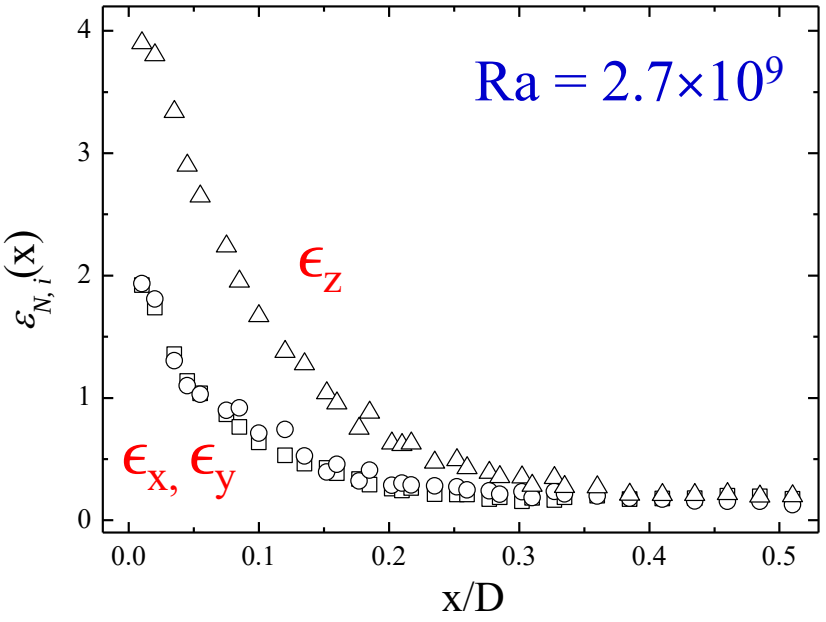

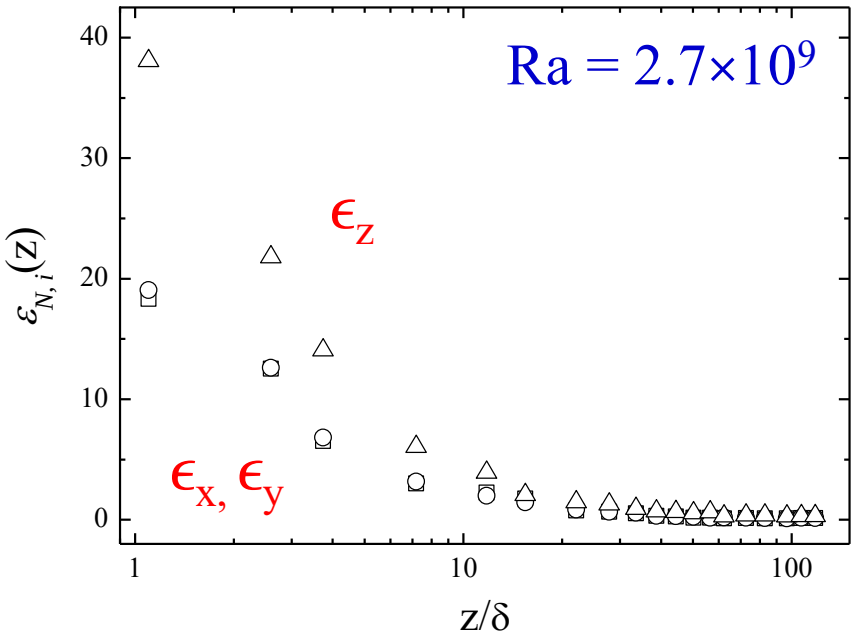

(iv) ϵ_f has three terms, $\epsilon_f = \epsilon_x + \epsilon_y + \epsilon_z$, and the dominant term is ϵ_z, which is twice larger than ϵ_x and ϵ_y.

3.2 Ra-dependence of the local thermal dissipation rate

At the cell center

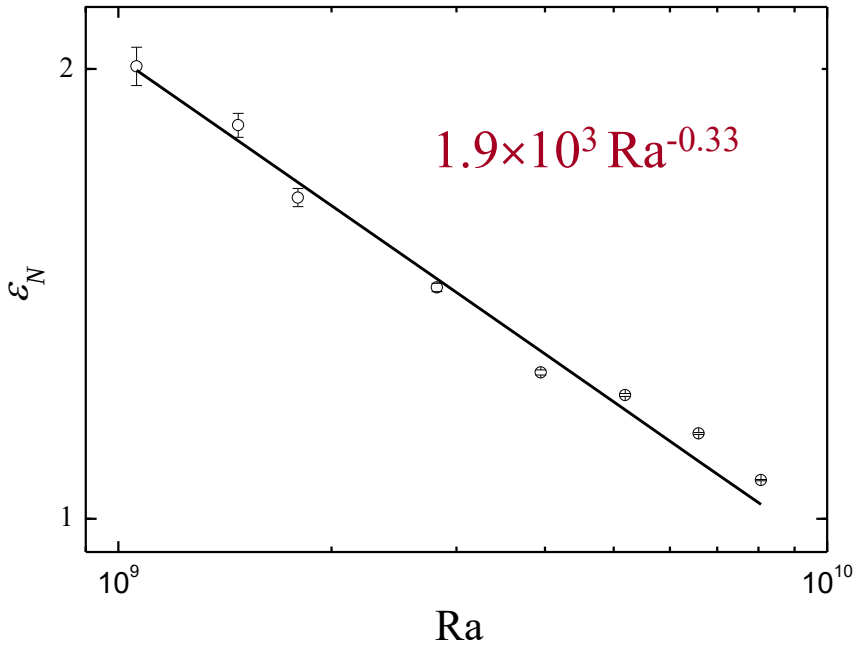

Near the sidewall

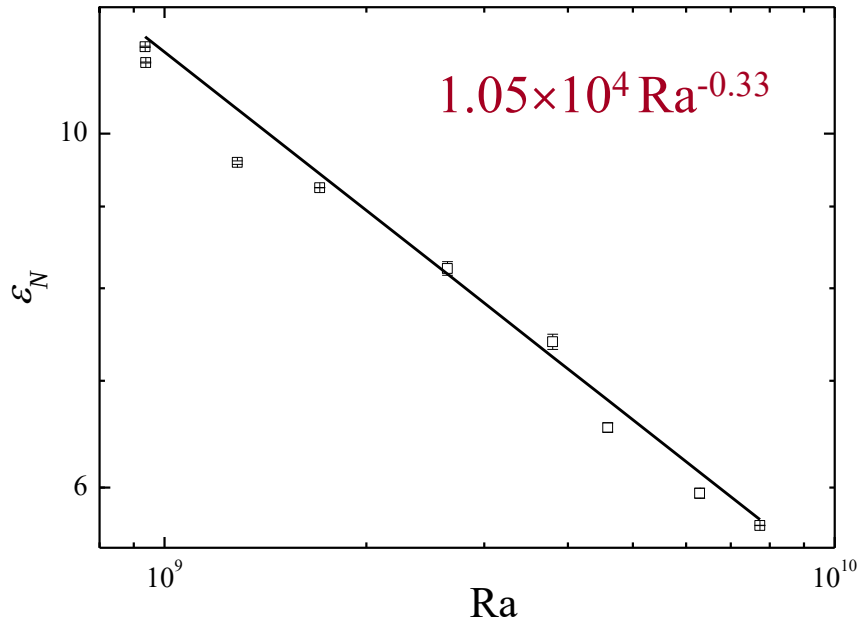

(v) $\epsilon_f \sim Ra^{-\alpha}$ with $\alpha = 0.33 \pm 0.03$ both at the cell center and near the sidewall.

Inside the thermal boundary layer (almost touching the lower surface)

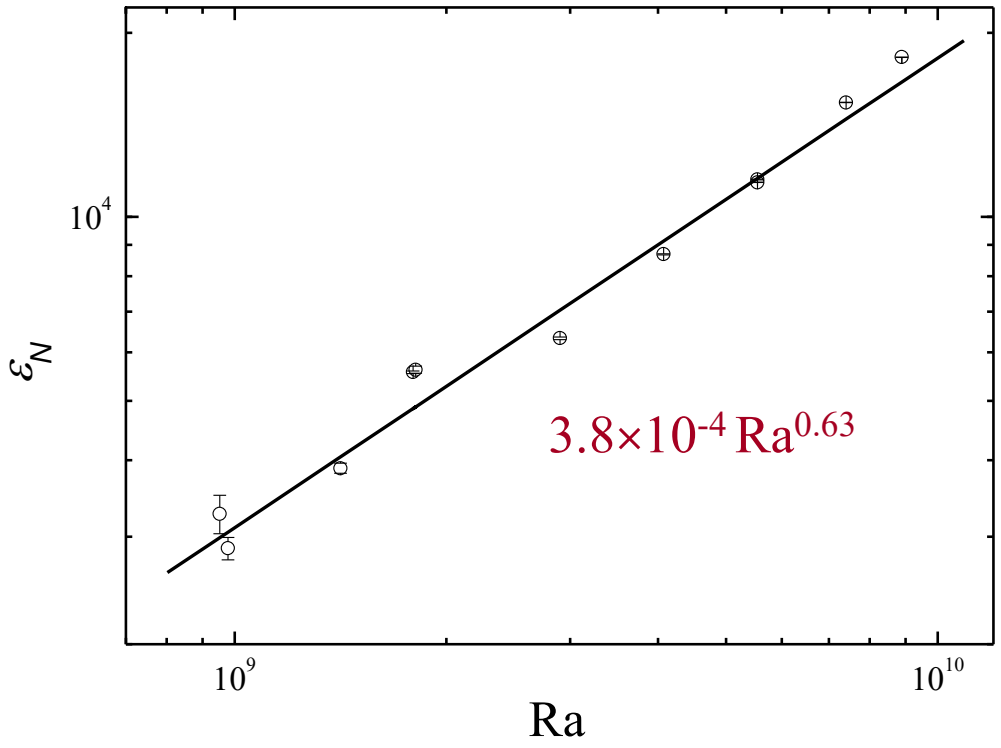

(vi) $\epsilon_m \sim \mathrm{Ra}^{+\beta}$ with $\beta = 0.63 \pm 0.05$ inside the thermal boundary layer.

3.3 Scale-dependent statistics of dissipation fluctuations ϵ_f (r,t)

Near the sidewall at Ra = 3.6×10^9

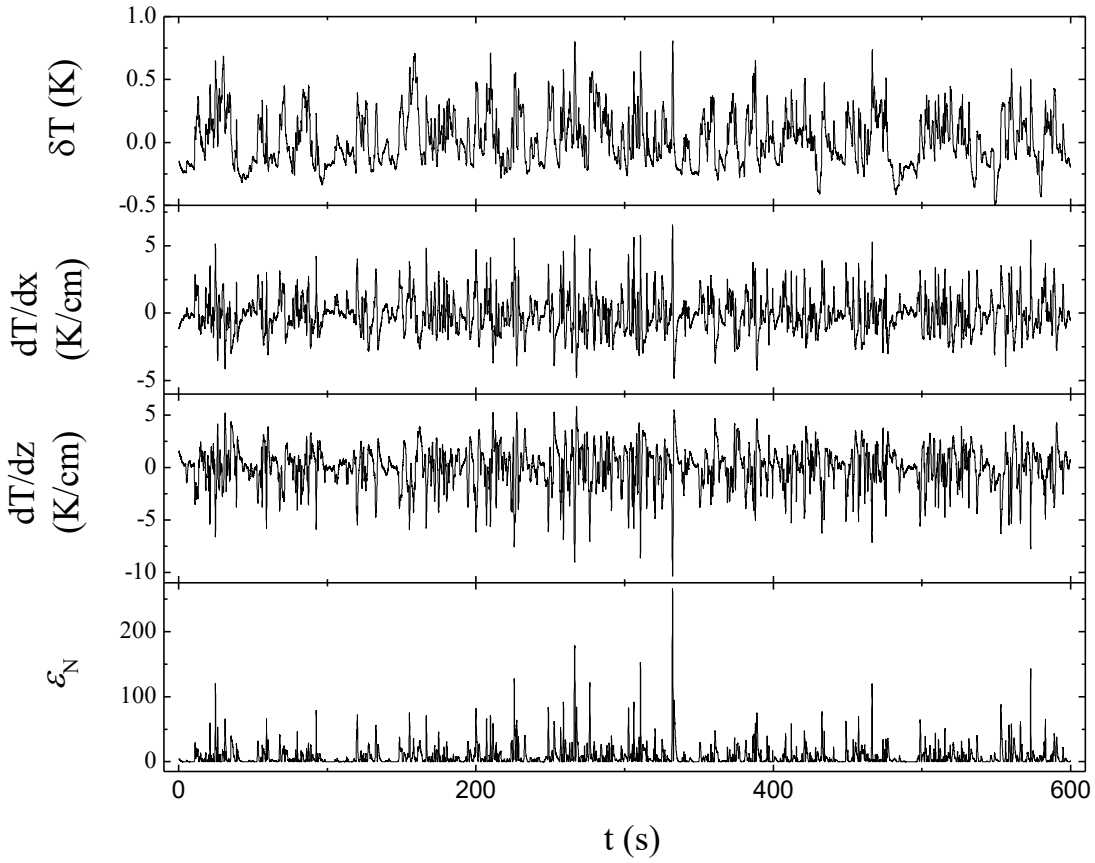

asymmetric

symmetric

slightly asymmetric

asymmetric

Histogram of the three temperature gradient components

At the cell center

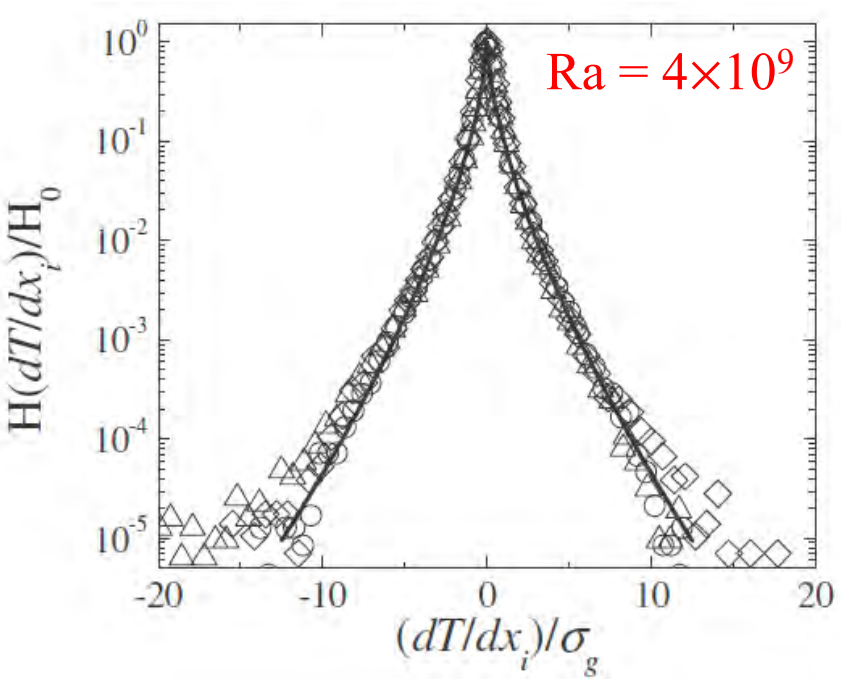

Approximately isotropic

Near the sidewall

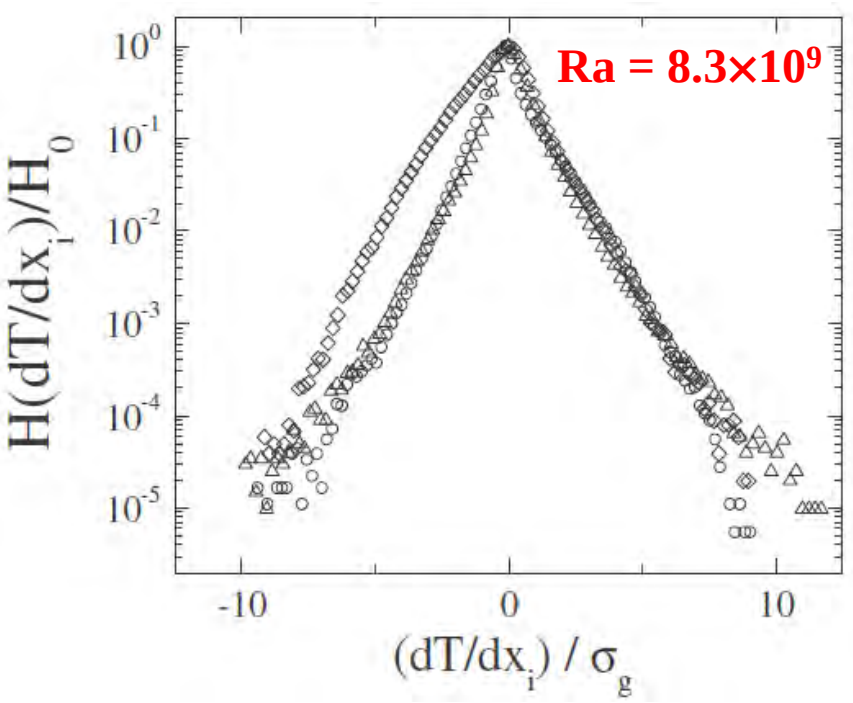

Anisotropic fluctuations

Challenges in identifying anomalous scaling in turbulent convection

- Convective flow in a closed cell is neither homogeneous nor isotropic
  - three representative locations in the cell:
  at the center, near the sidewall and near the lower conducting plate
  - decomposition of the local dissipation rate into contributions
  from three different temperature gradient components.

- Bolgiano length and separation of passive and active scalars within a limited range of length scales

$$L_B \simeq Nu^{1/2}(\mathrm{Pr}\,Ra)^{-1/4} L \simeq 6.3\ mm; \qquad L_B(z) \simeq \varepsilon_u^{5/4}(z)\varepsilon_T^{-3/4}(z)(\alpha g)^{-3/2}$$

- Connection of time-domain results to the theory in spatial domain

Taylor's frozen-flow hypothesis does not hold in turbulent convection

Lohse & Xia, Annu. Rev. Fluid Mech. (2010)

Scale-dependent statistics of the locally averaged $\epsilon_\tau(\mathbf{r},t)$

$$\varepsilon_T(\mathbf{r},t) = \kappa[|\nabla T_m(r)|^2 + 2\nabla T_m(\mathbf{r})\bullet\nabla T_f(\mathbf{r},t) + |\nabla T_f(\mathbf{r},t)|^2]$$

$$\varepsilon_\tau^i(\mathbf{r},t) = \frac{1}{\tau}\int_t^{t+\tau} \kappa[\partial_i T_f(\mathbf{r},t')]^2 dt'$$

$$\langle(\varepsilon_\tau^i)^p\rangle \equiv \langle[\varepsilon_\tau^i(\mathbf{r},t)]^p\rangle_t \sim \tau^{\mu^i(p)}$$

Assuming $\langle(\varepsilon_\tau^i)^p\rangle$ has a hierarchical structure of the She–Leveque form, one finds [Ching & Kwok, PRE **62,** 7587(R) (2000)]

$$\mu^i(p) = c(1-\beta^p) - \lambda p$$

where $c = 3 - D_\epsilon$ is co-dimension of the most dissipative structures, $\lambda = 1 - b$ (for velocity scaling) and

$$0 = c(1-\beta) - \lambda$$

For passive scalars with sheet-like dissipative structures:

$$\lambda = \frac{2}{3}, \quad c = 1 \quad \text{and} \quad \beta = \frac{1}{3}$$

(central region)

For passive scalars with filament-like dissipative structures:

$$\lambda = \frac{2}{3}, \quad c = 2 \quad \text{and} \quad \beta = \frac{2}{3}$$

(vertical exponent in the sidewall region)

For active scalars with sheet-like dissipative structures:

$$\lambda = \frac{2}{5}, \quad c = 1 \quad \text{and} \quad \beta = \frac{3}{5}$$

(inside the thermal boundary layer)

Scaling of $\langle (\varepsilon_\tau^z)^p \rangle$ at the cell center:

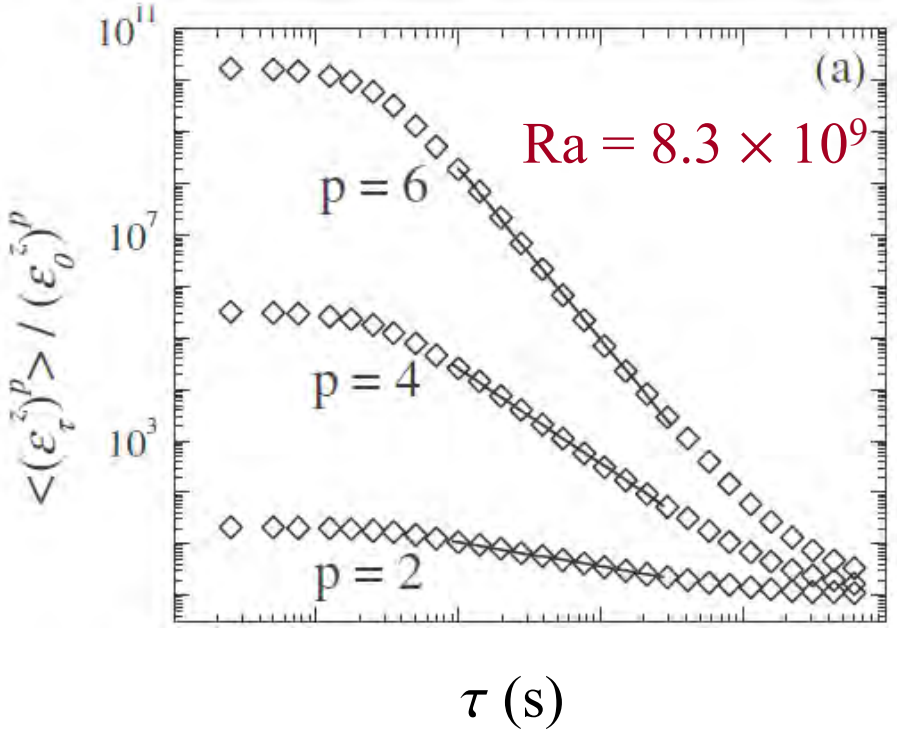

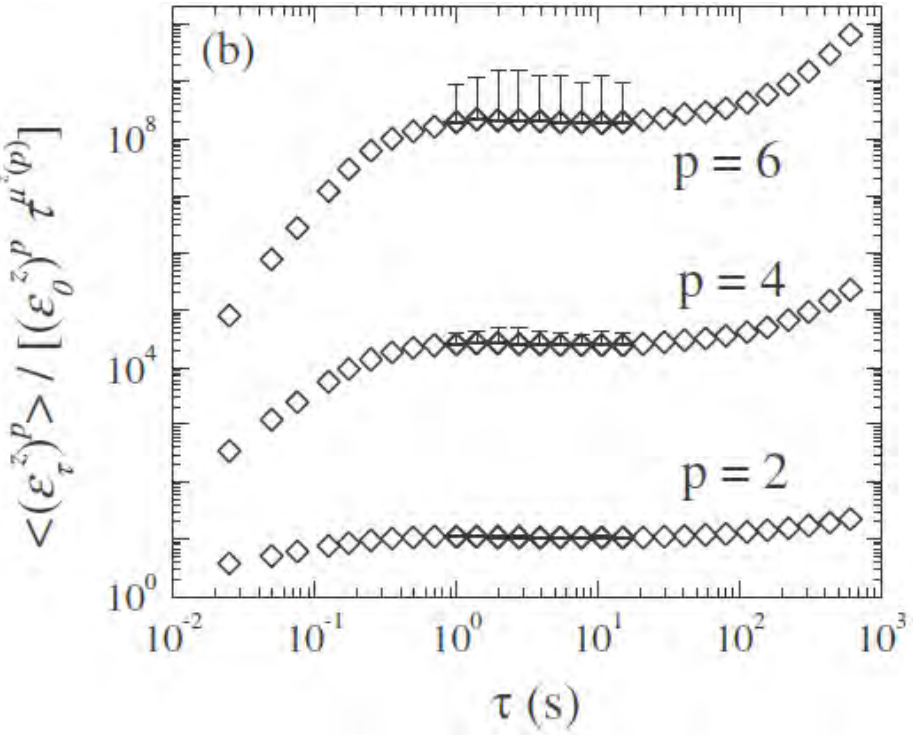

LSC turnover time $\tau_0 \approx 35$ s; local Bolgiano time $\tau_B \approx \tau_0 \, L_B(z)/L \approx 31$ s.

Dissipation time $\tau_d = \tau_0 \, (10\eta)/L \approx 0.8$ s.

Convergence and accuracy of the measured $\langle (\varepsilon_\tau^z)^p \rangle$

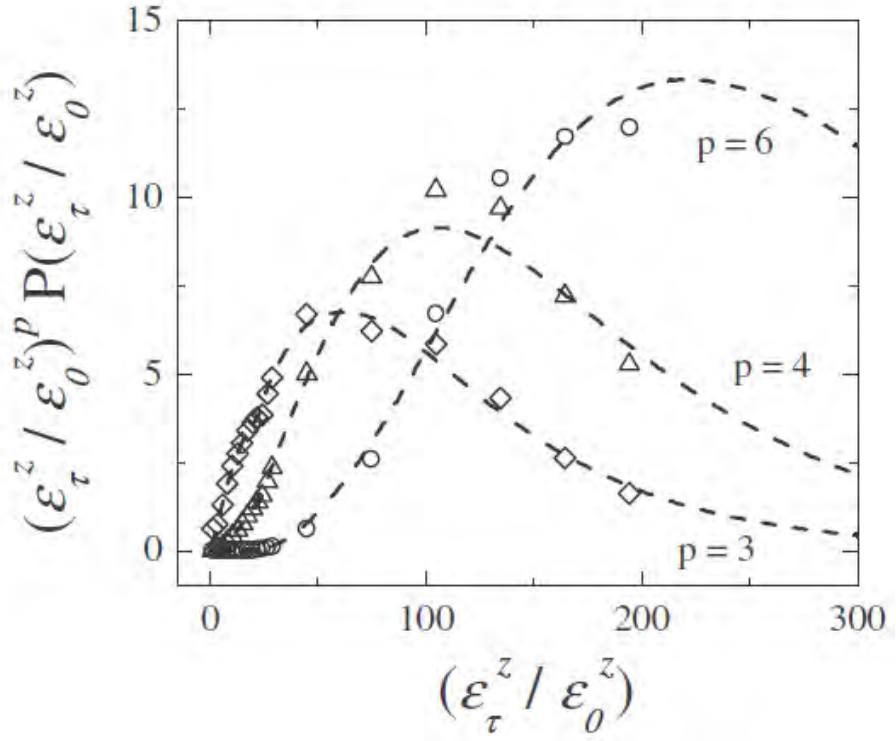

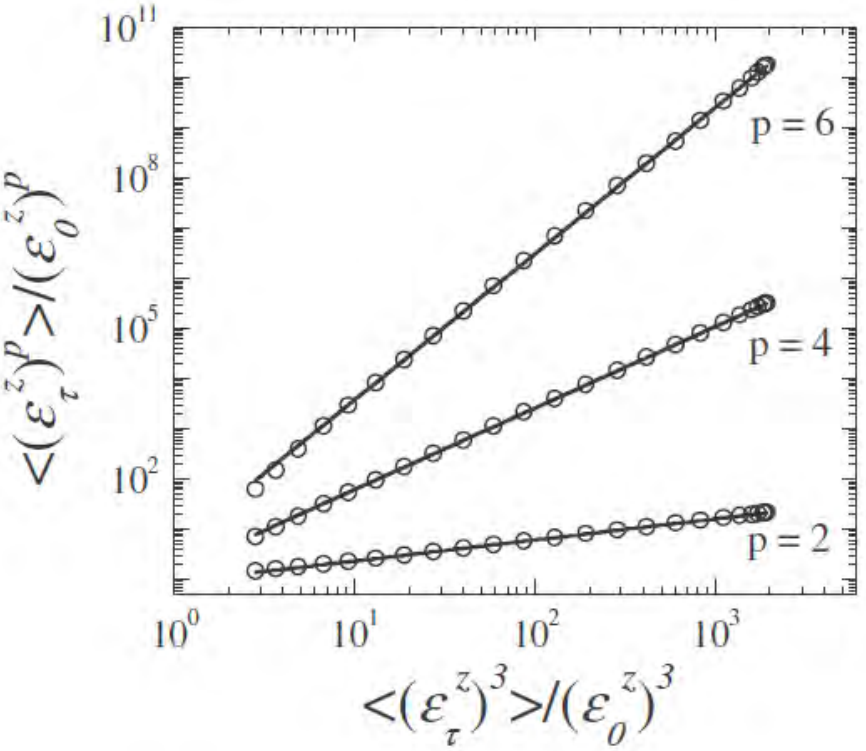

$$\frac{\langle (\varepsilon_\tau^z)^p \rangle}{(\varepsilon_0^z)^p} \simeq \frac{1}{\varepsilon_0^z} \int_0^\infty (\varepsilon_\tau^z / \varepsilon_0^z)^p P(\varepsilon_\tau^z / \varepsilon_0^z) d\varepsilon_\tau^z$$

Extended self-similarity (ESS) plots

Scaling exponent μ^z(p) at the cell center:

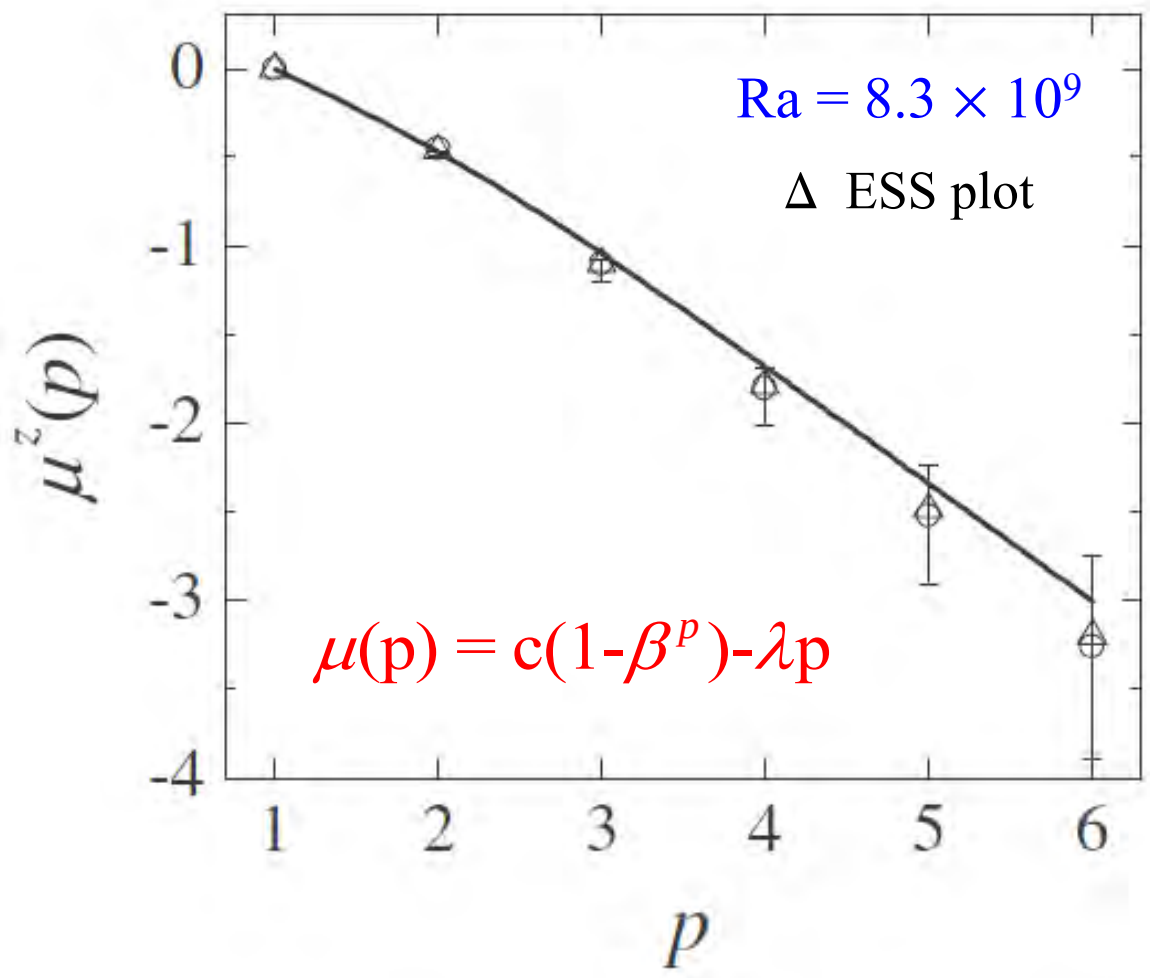

Central: c = 1 (sheet-like), β = 1/3 and λ = 2/3 (passive)

Scaling of $\langle (\varepsilon_\tau^x)^p \rangle$ and $\langle (\varepsilon_\tau^y)^p \rangle$ at the cell center:

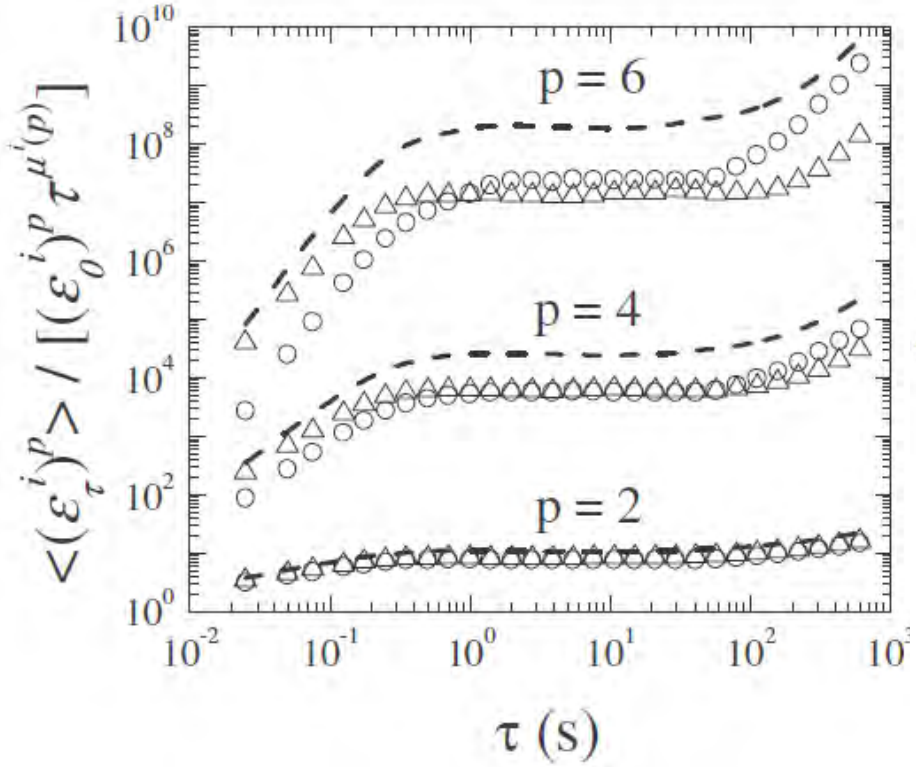

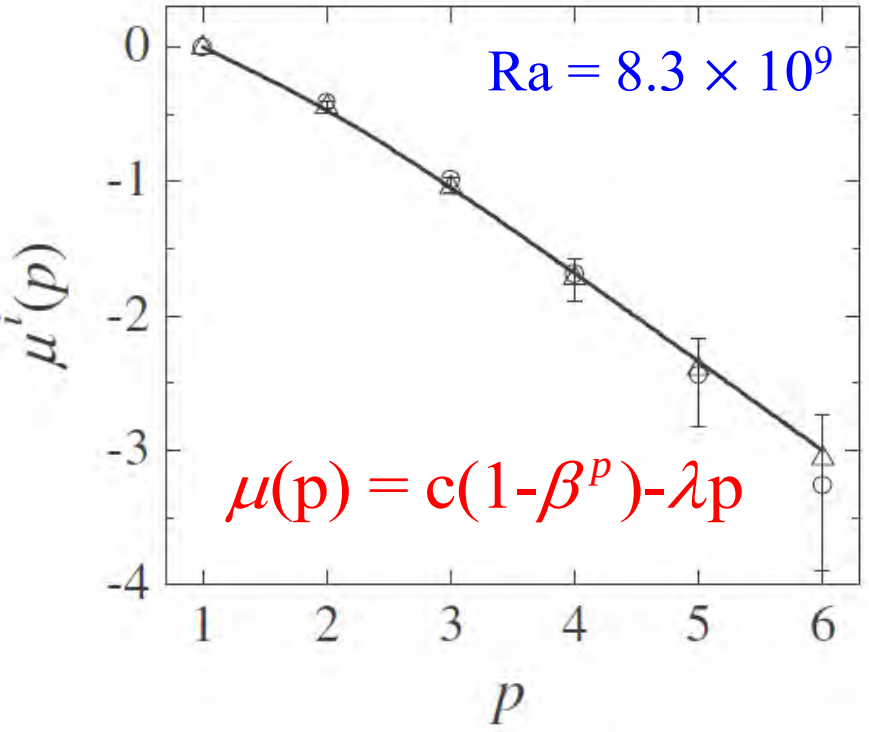

In the central region, $\mu^x(p)$ and $\mu^y(p)$ are the same as $\mu^z(p)$:

c = 1 (sheet-like), β = 1/3 and λ = 2/3 (passive)

Scaling of $\langle (\varepsilon_\tau^i)^p \rangle$ near the sidewall:

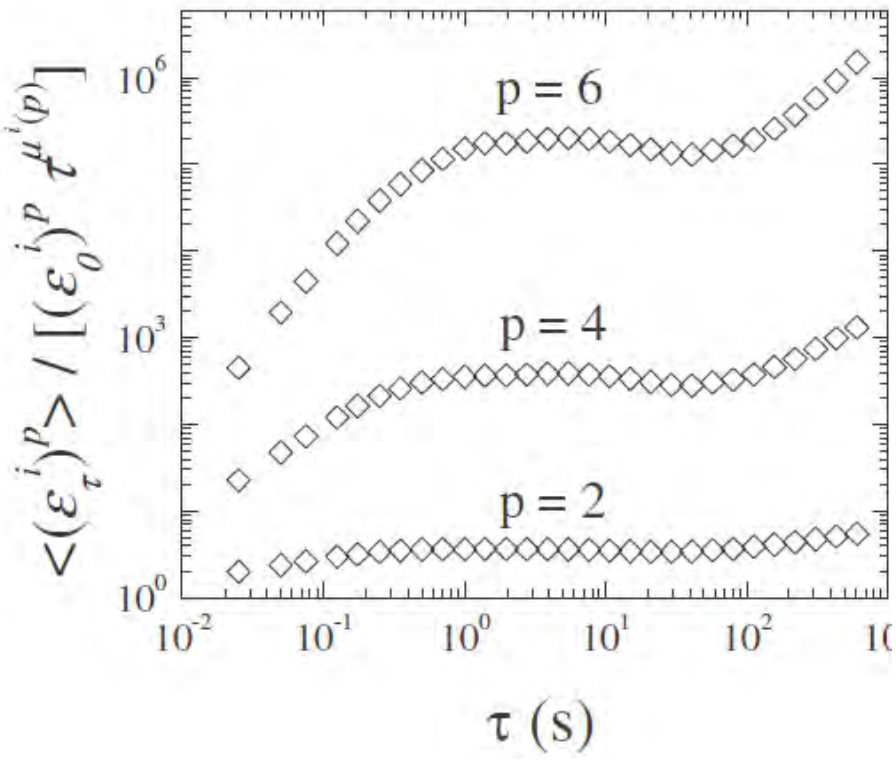

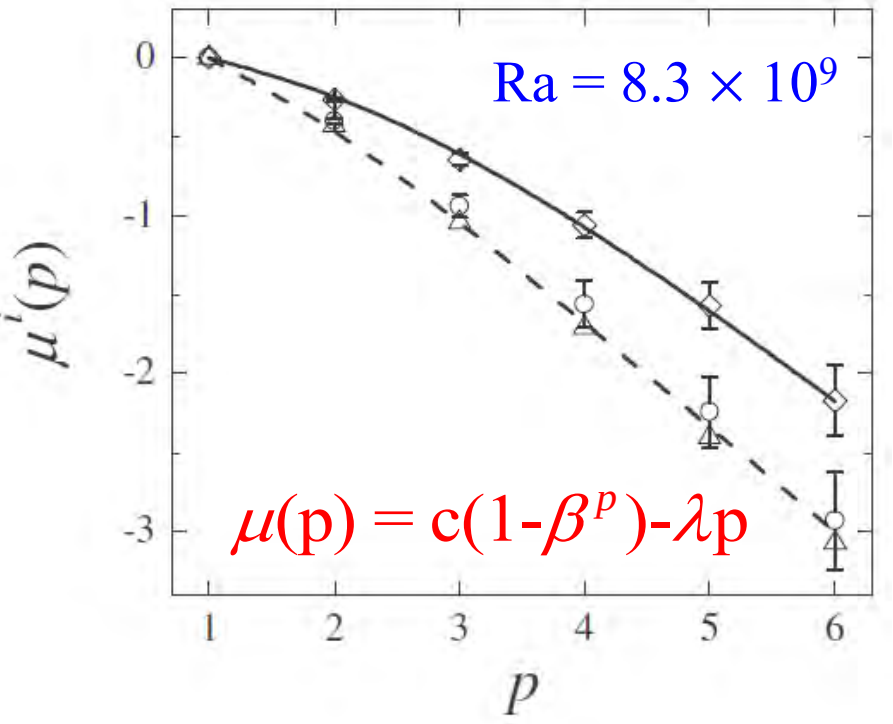

x and y components: c = 1 (sheet-like), β = 1/3 and λ = 2/3 (passive)

z-component: c = 2 (filament-like), β = 2/3 and λ = 2/3 (passive)

Temperature profile and histogram of the temperature gradient components near the thermal boundary layer

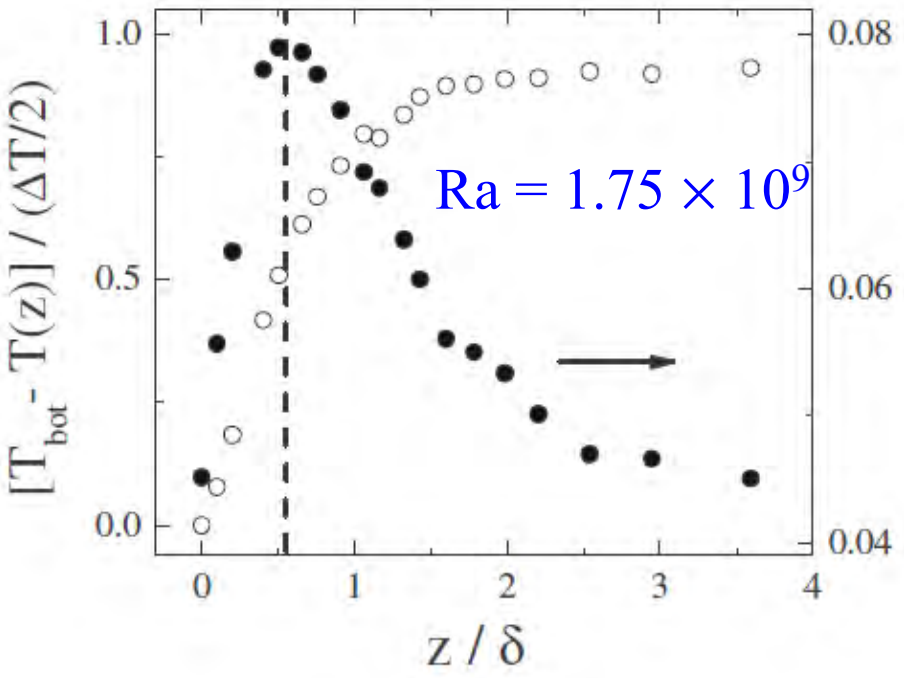

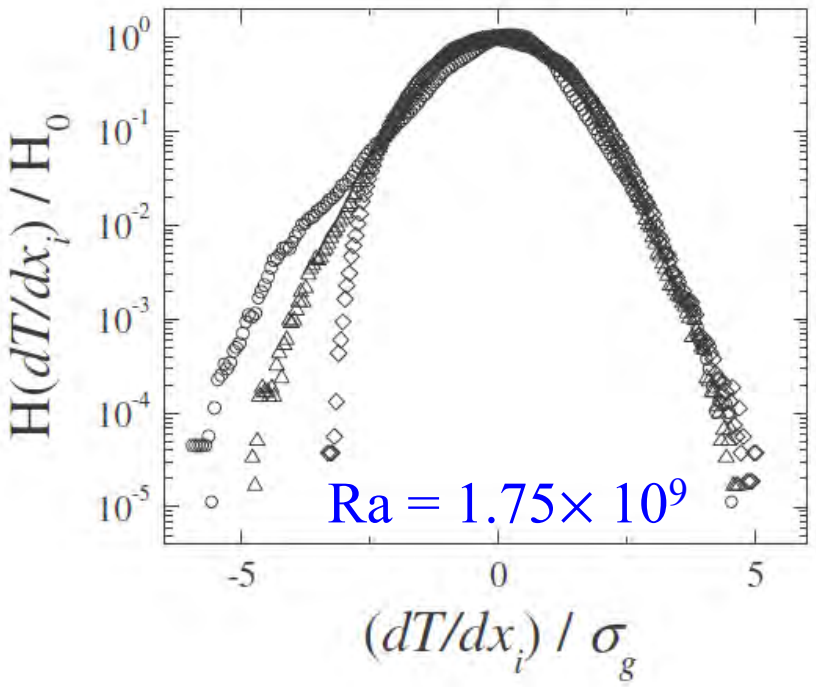

Temperature fluctuations near the lower conducting plate are governed by the thermal boundary layer thickness, δ, which decreases with increasing Ra. Measurements were made in the peak region ($0.5 \leq z/\delta \leq 0.9$).

Scaling of $\langle (\varepsilon_\tau^i)^p \rangle$ near the lower conducting plate:

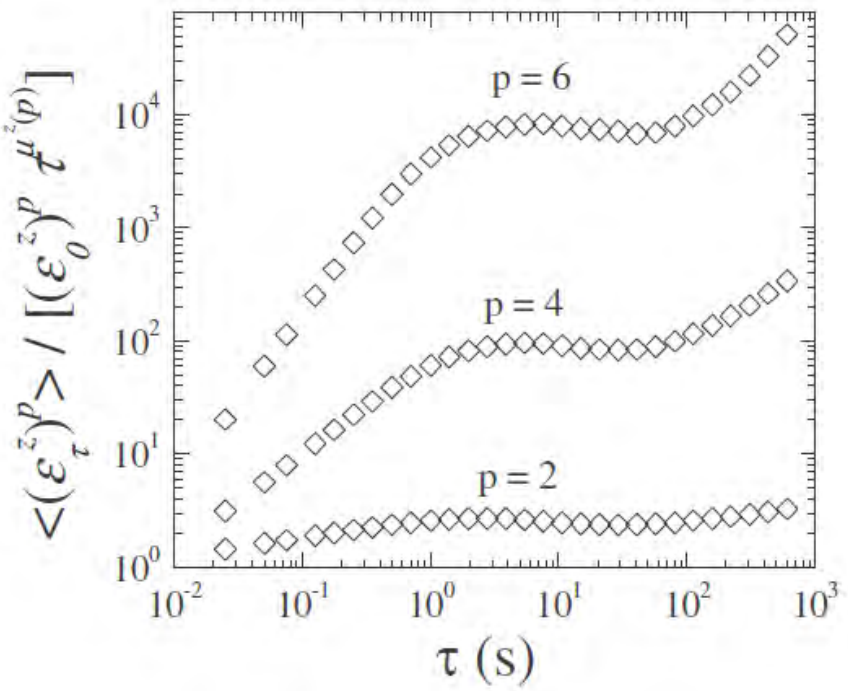

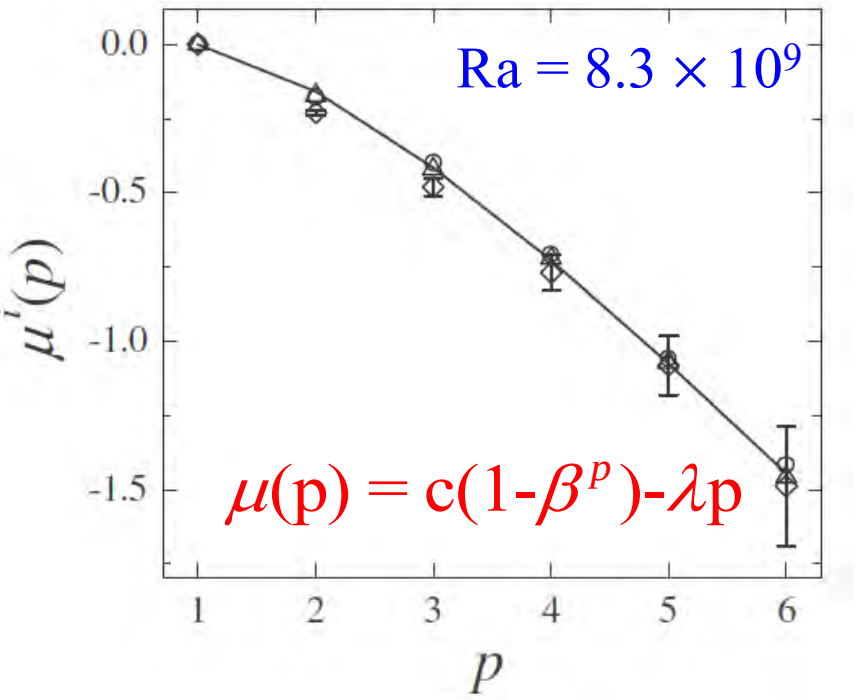

Local Bolgiano time $\tau_B \approx \tau_0 \, L_B(0)/L \approx 3.5$ s.

Inside the thermal boundary layer (all components):

c = 1 (sheet-like), $\beta = 3/5$ and $\lambda = 2/5$ (active)

Scaling exponent μ(p) of the total dissipation:

$Ra = 8.3 \times 10^9$

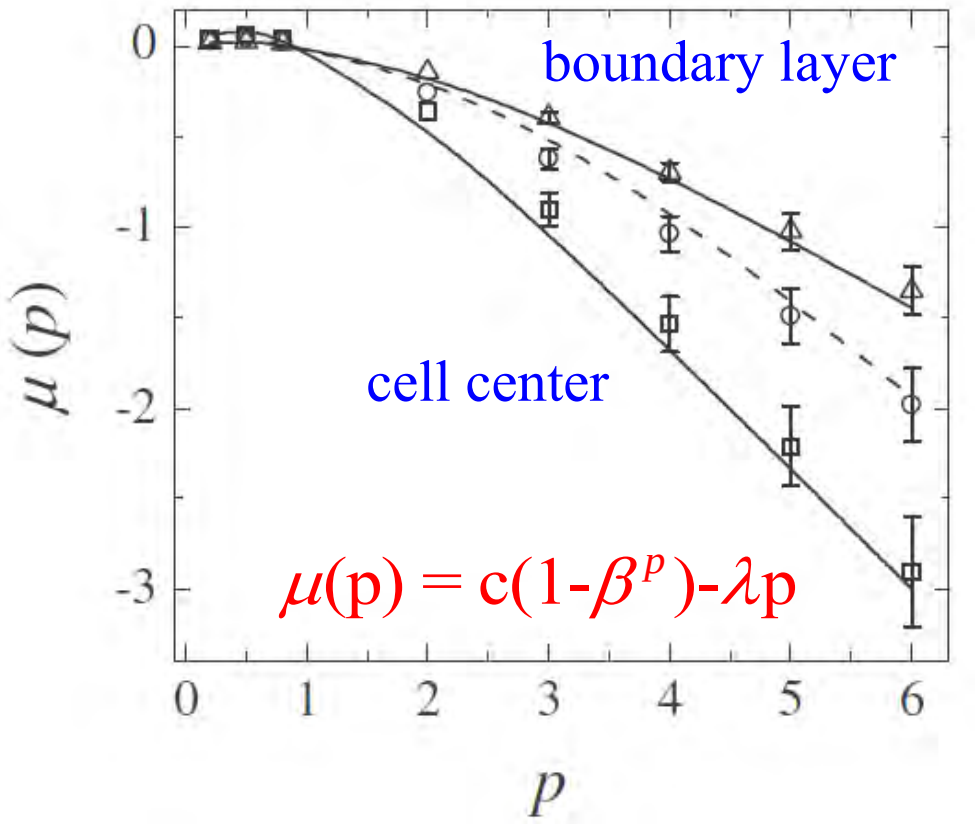

Sidewall: c = 2.4 (sheet-like), $\beta = 0.72$ and $\lambda = 2/3$ (passive)

Evolution of μ(p) along the central axis

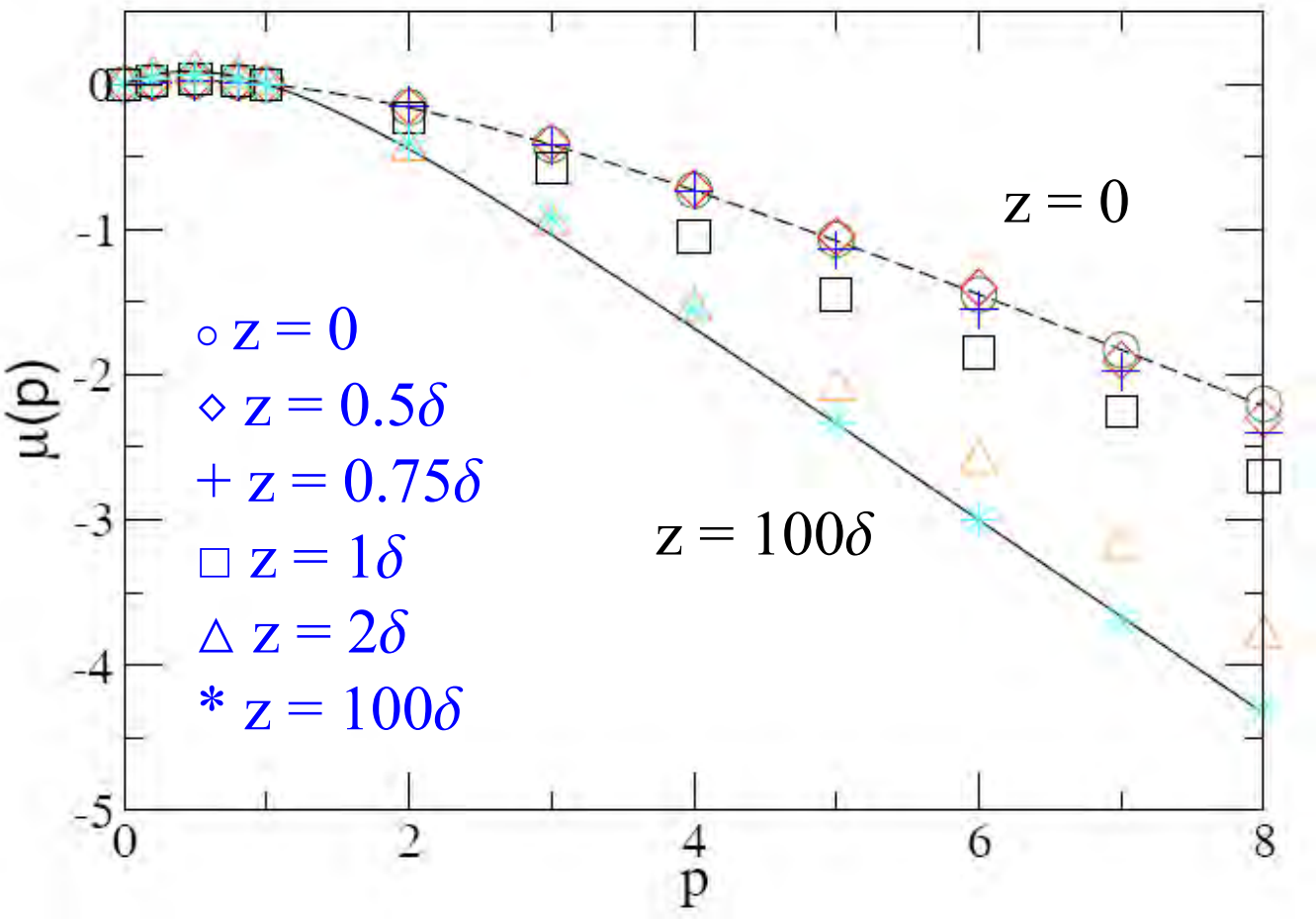

$$\mu(p) = c(1-\beta^p) - \lambda p = 1-[1-\lambda(z)]^p - \lambda(z)\,p$$

4. Test of the anomalous scaling of passive temperature fluctuations

- While the intermittency problem of passive scalars is understood in the Kraichnan model, direct experimental verification was made only partially by measuring the velocity and temperature SFs.
- The interpretation of early measurements of SFs in turbulent convection was complicated by other effects, such as flow anisotropy and buoyancy effect at the Bolgiano scale.
- Recently, the space-resolved velocity and temperature SFs were obtained by PIV and multiple temperature probes (Sun et al., Phys. Rev. Lett., 2006).
- DNS studies (Calzavarini et al., Phys. Rev. E, 2002; Kunnen et al., Phys. Rev. E, 2008) identified the active and passive regions in the convection cell.
- More recently, we measured the instantaneous $\varepsilon_T(\mathbf{x},t)$ and studied its spatial distribution (He et al., Phys. Rev. Lett., 2007; Phys. Rev. E 2009) and statistics (He et al., J. Turbulence, 2010; Phys. Fluids, 2011).

- To test the refined similarity ideas for anomalous scaling, one needs to check the r-scaling of both the SFs and $\varepsilon_u(r)$ and $\varepsilon_T(r)$.

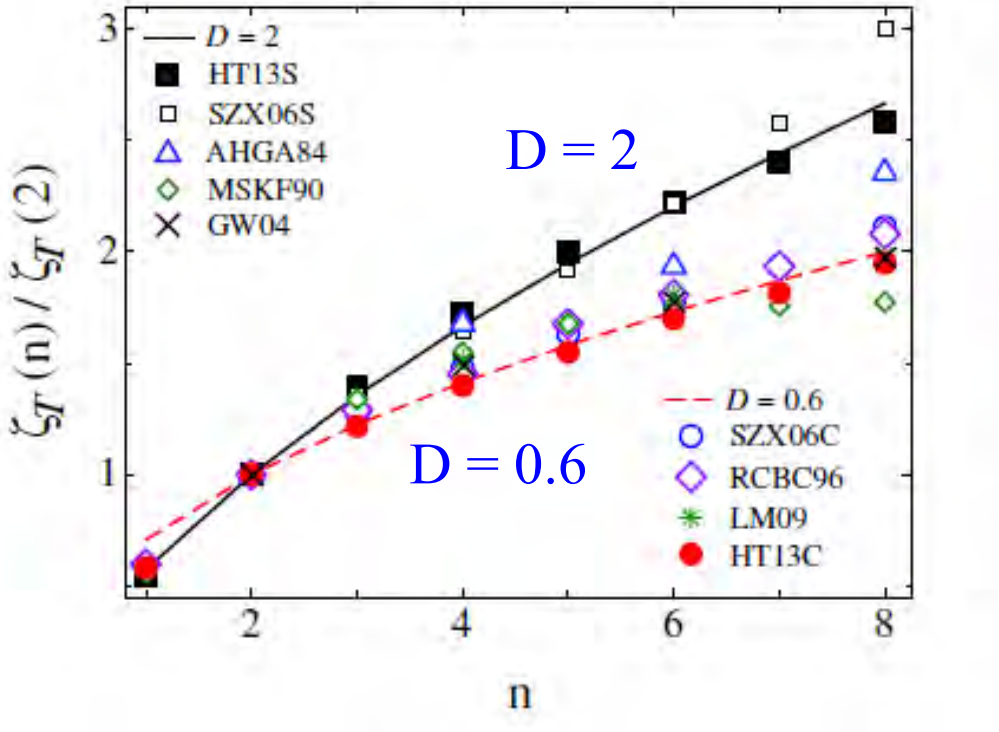

HST13S (black solid squares, present work, RBC near sidewall);SZX06S (black open squares, RBC near sidewall);AHGA84 (Blue triangles, heated jet);MSKF90 (Green diamonds, heated wake);GW04 (black crosses, grid turbulence);SZX06C (blue circles, RBC at cell center);RCBC96 (purple diamonds, heated wake);LM09 (green flakes, grid turbulence);HST13C (red solid circles, present work, RBC at cell center).

$$\frac{\varsigma_T(n)}{\varsigma_T(2)} = \frac{1}{2}[2nx + (x-1)^2]^{1/2} - \frac{1}{2}(x-1); \quad x = \frac{D}{\varsigma_T(2)}$$

5. Space-time relation in turbulent Rayleigh-Bénard convection

Equal-time velocity correlation function:

$$C_u(r,0) = \frac{\langle u(x,t)\ u(x+r,t)\rangle_t}{(\sigma_u)_1 (\sigma_u)_2}$$

or energy spectrum

$$E_u(k) = \int_{-\infty}^{\infty} C_u(r,0)\, e^{-ikr}\, dr$$

Velocity structure functions:

$$S_u^{(p)}(r) = \left\langle ([\mathbf{u}(x+r,t) - \mathbf{u}(x,t)] \bullet \frac{\mathbf{r}}{r})^p \right\rangle_t$$

Single-point time series measurements (LDV, hot wire, …):

(i) Temporal velocity correlation function:

$$C_u(0,\tau) = \frac{\langle u(x,t)u(x,t+\tau)\rangle_t}{(\sigma_u)_1(\sigma_u)_2}$$

or frequency power spectrum:

$$E_u(f) = \int_{-\infty}^{\infty} C_u(0,\tau)\, e^{-i2\pi f\tau} d\tau$$

(ii) Temporal velocity structure functions:

$$S_u^{(p)}(\tau) = \left\langle [u(x,t+\tau) - u(x,t)]^p \right\rangle_t$$

Two-point time series measurements (PIV or two local probes):

Velocity space-time cross-correlation function:

$$C_u(r,\tau) = \frac{\langle u(x,t)u(x+r,t+\tau)\rangle_t}{(\sigma_u)_1(\sigma_u)_2}$$

Taylor's frozen flow hypothesis:

$$u(x,t) \rightleftharpoons u(x+U_0\tau, t+\tau)$$

Then we have

$$C_u(r,\tau) = \frac{\langle u(x+U_0\tau,t+\tau)\ u(x+r,t+\tau)\rangle_t}{(\sigma_u)_1(\sigma_u)_2} = C_u(r_T,0)$$

with $r_T = r - U_0\tau$

Requirement for Taylor's hypothesis: $U_0 >> (\sigma_u)_i$

Elliptic model of He and Zhang (Phys. Rev. E, 2006)

$$C_u(r,\tau) = C_u(0,0) + \cancel{\frac{\partial C_u(0,0)}{\partial r}} r + \cancel{\frac{\partial C_u(0,0)}{\partial \tau}} \tau + \frac{\partial^2 C_u(0,0)}{\partial r \partial \tau} r\tau + \frac{1}{2}\left[\frac{\partial^2 C_u(0,0)}{\partial r^2} r^2 + \frac{\partial^2 C_u(0,0)}{\partial \tau^2} \tau^2\right]$$

$$= C_u(0,0) + \frac{1}{2}\frac{\partial^2 C_u(0,0)}{\partial r^2} r_E^2 = C_u(0,0) - \left(\frac{r_E}{\lambda_u}\right)^2 = C_u(r_E, 0)$$

$$r_E^2 = (r - U\tau)^2 + V^2\tau^2$$

$$U = -\frac{\partial^2 C_u(0,0)}{\partial r \partial \tau}\left[\frac{\partial^2 C_u(0,0)}{\partial r^2}\right]^{-1} = U_0$$

$$V^2 = \frac{\partial^2 C_u(0,0)}{\partial \tau^2}\left[\frac{\partial^2 C_u(0,0)}{\partial r^2}\right]^{-1} - U^2 = (s\lambda_u)^2 + \sigma_u^2$$

$$\lambda_u = \left[-\frac{1}{2}\frac{\partial^2 C_u(0,0)}{\partial r^2}\right]^{-1/2}$$

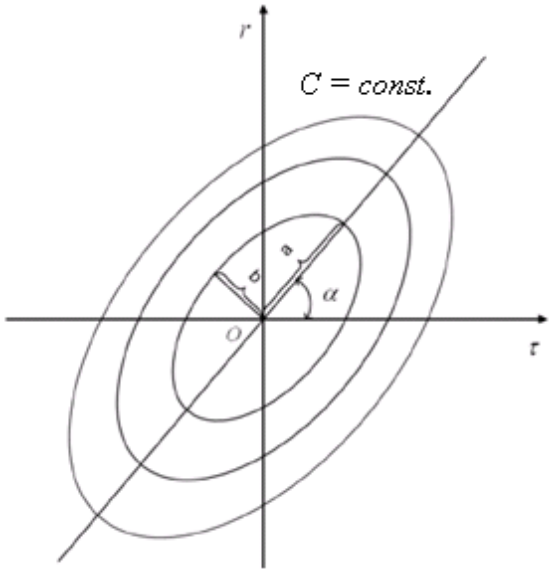

iso-correlation contours

Two-point temperature measurements over varying distance r

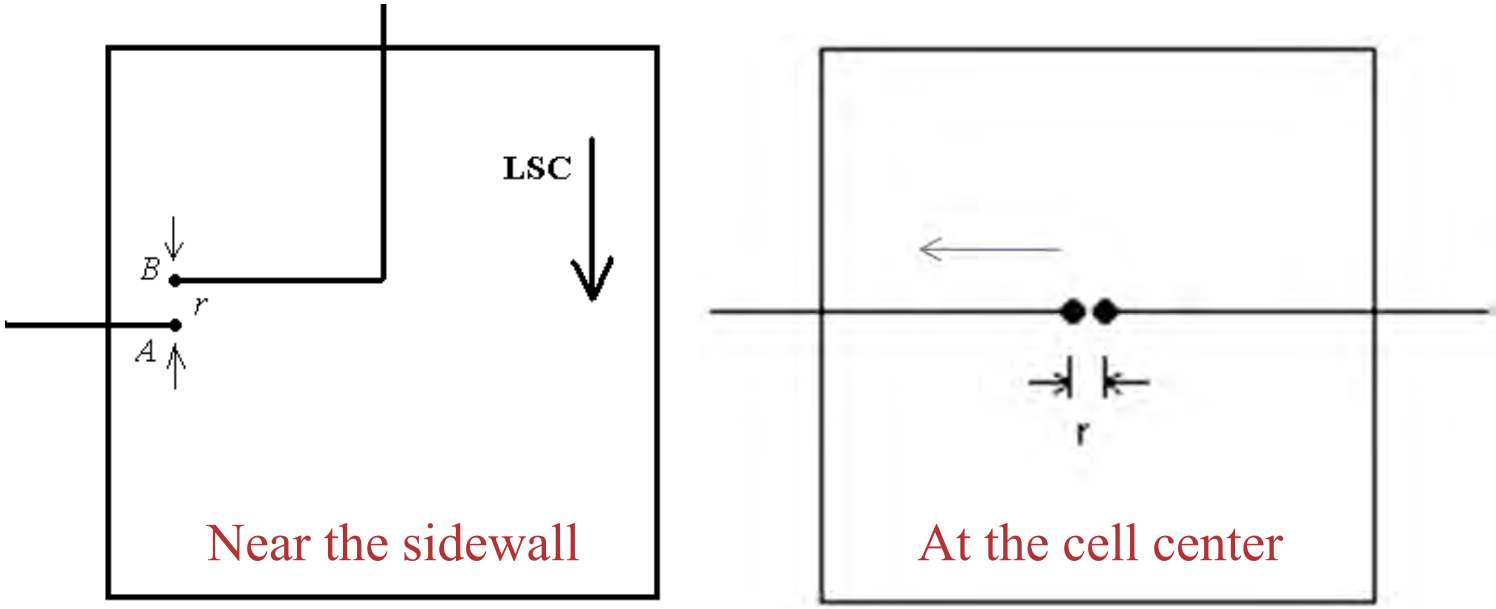

Temperature space-time cross-correlation function:

$$C_T(r,\tau) = \frac{\langle T(x,t)\ T(x+r,t+\tau)\rangle_t}{(\sigma_T)_1(\sigma_T)_2}$$

Temperature is a passive scalar in the bulk region, and thus $C_T(r,\tau)$ is expected to have the same scaling form as $C_u(r,\tau)$ does.

Experimental results near the sidewall

3-D plot of the measured $C_T(r,\tau)$

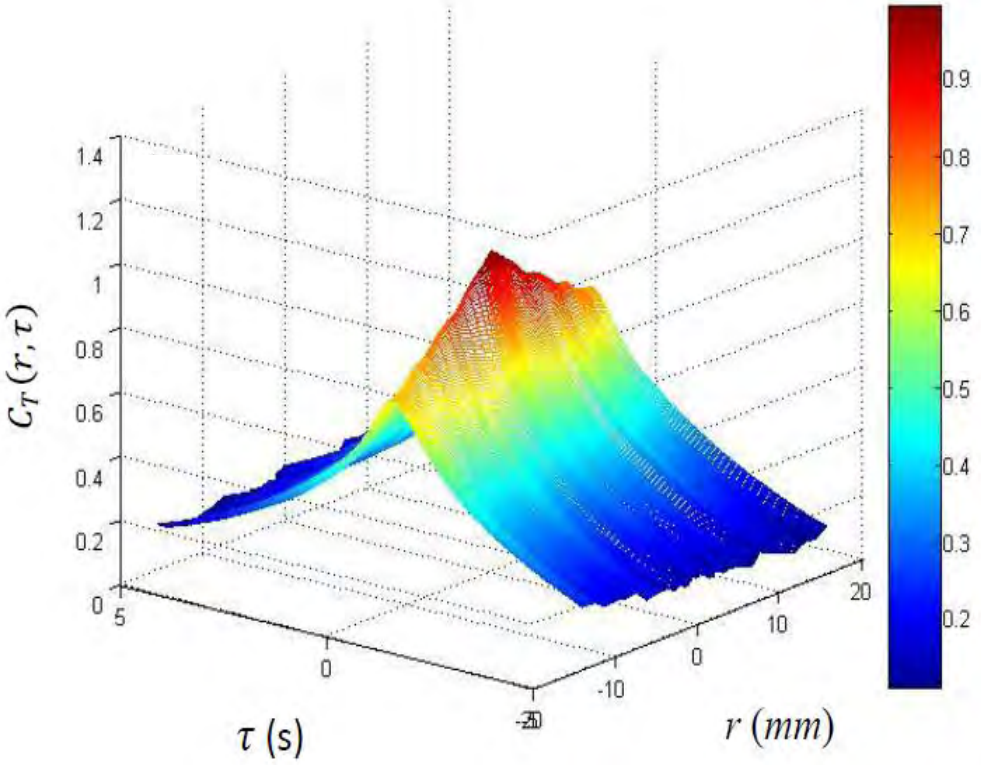

2-D plot of iso-correlation contours

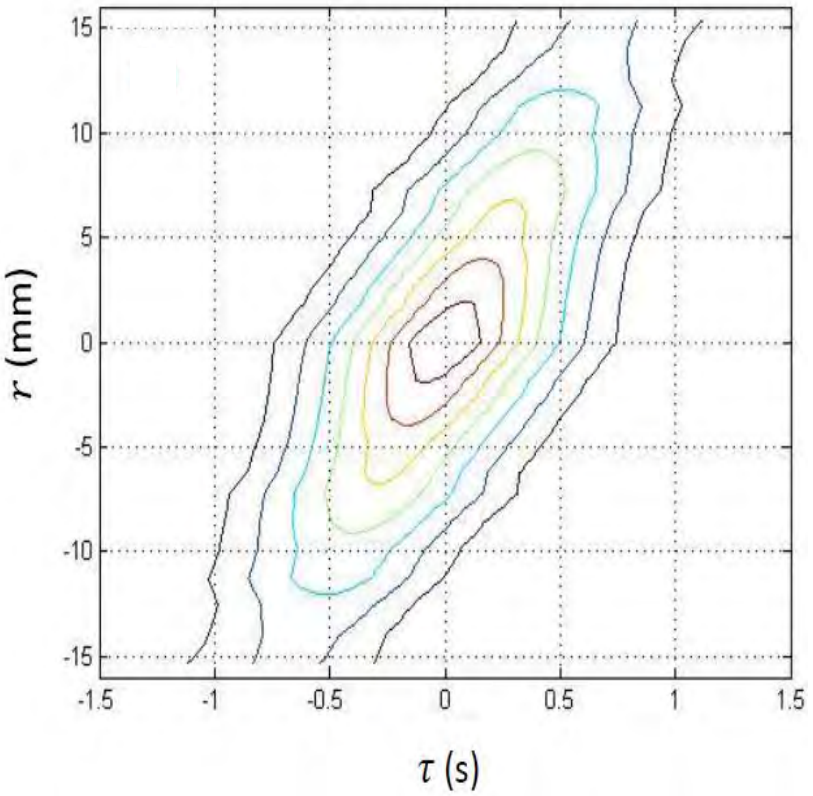

Experiment confirms the elliptic model:

$$C_T(r,\tau) = C_T(r_E,0)$$

$$r_E^2 = (r - U\tau)^2 + V^2\tau^2$$

He, He and Tong, Phys. Rev. E, **81**, 065303(R), 2010.

Elliptic model

Taylor's hypothesis

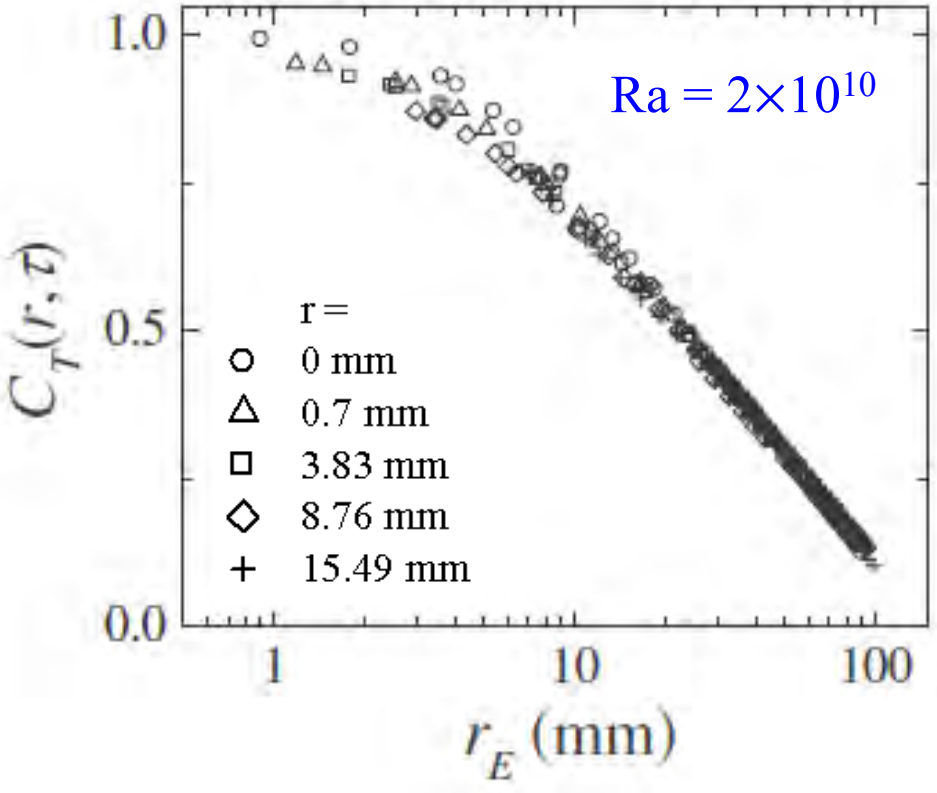

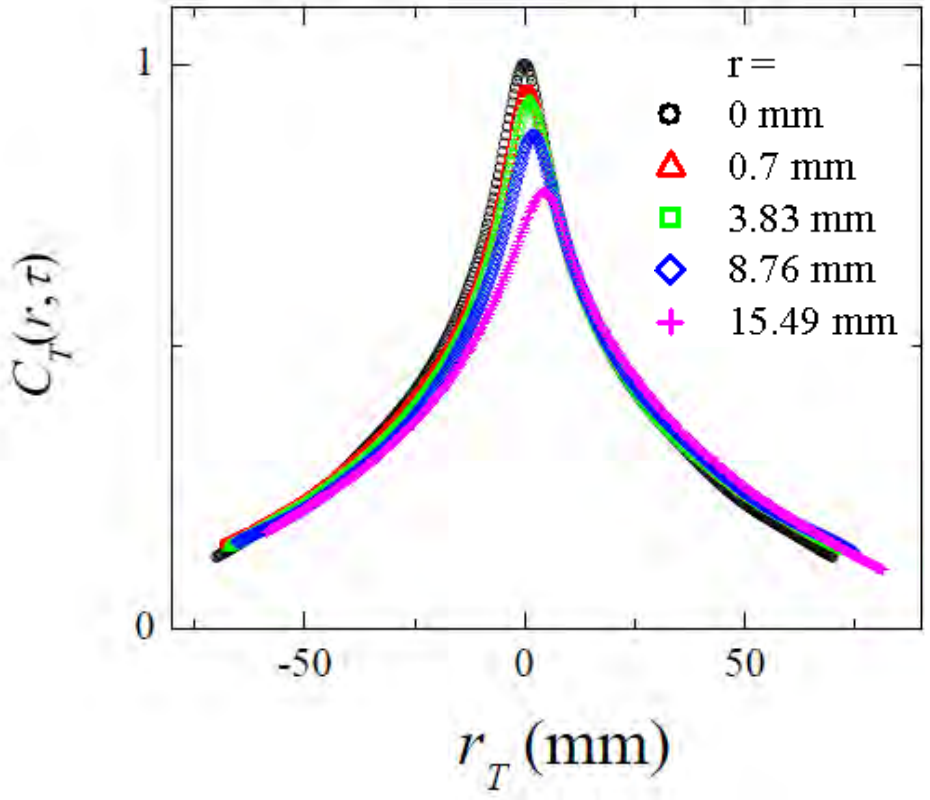

$$r_E^2 = (r - U\tau)^2 + V^2\tau^2$$

$$C(r,\tau) = C(r_E, 0)$$

$$r_T = r - U\tau$$

$$C(r,\tau) = C(r_T, 0)$$

Taylor's hypothesis does not hold

Single-point temperature measurement ($r = 0$): $C_T(0,\tau) = C_T(r_E, 0)$

$r_E = \sqrt{U^2 + V^2}\,\tau$ Power spectrum: $E_T(f) = \int_{-\infty}^{\infty} C_T(0,\tau) e^{-2\pi i f \tau} d\tau$

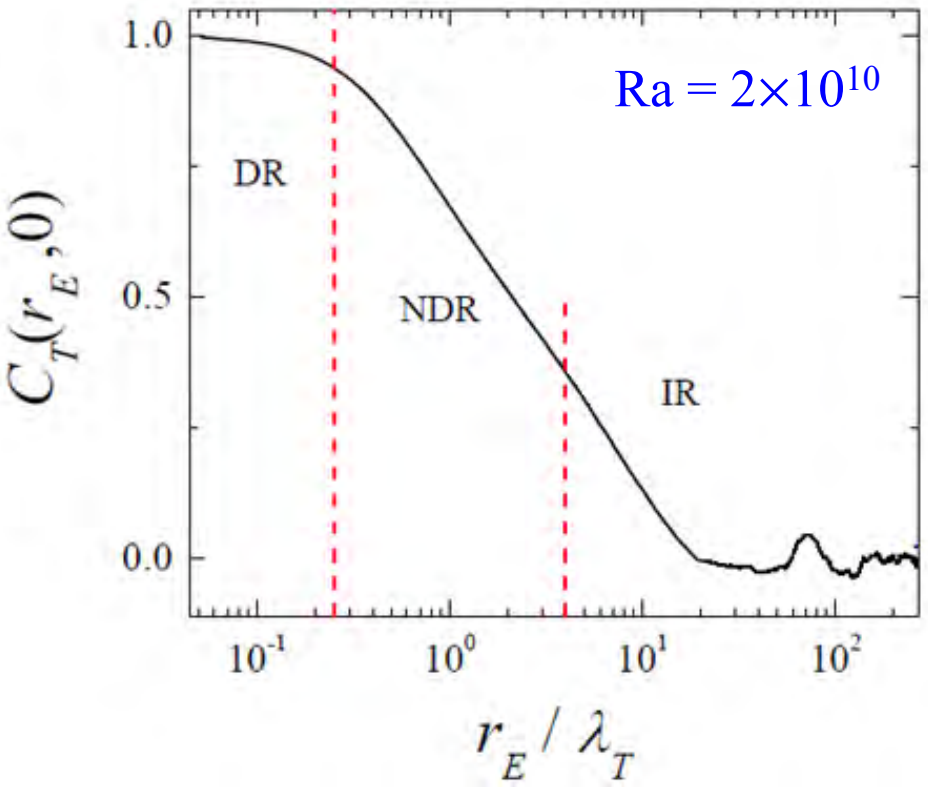

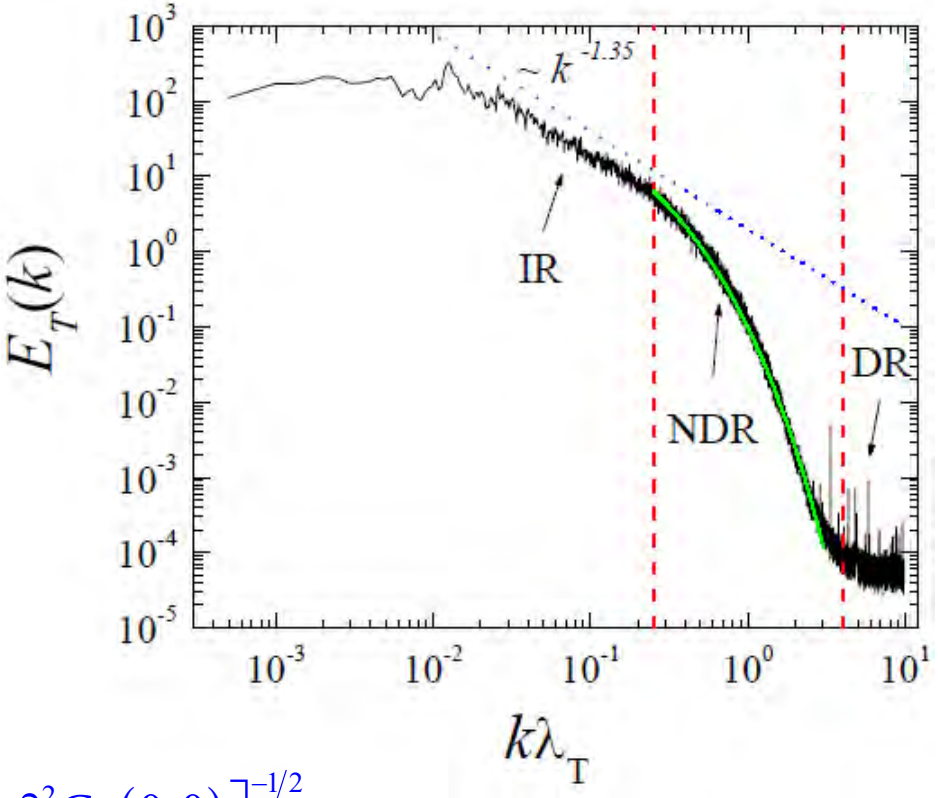

Taylor's micro-scale: $\lambda_T = \left[-\frac{1}{2} \frac{\partial^2 C_T(0,0)}{\partial r^2} \right]^{-1/2} = 8.53 \text{ mm}$

Reynolds number: $\text{Re}_{\lambda_T} \approx \left(U^2 + V^2\right)^{1/2} \lambda_T / \nu \approx 240$

Experimental results at the cell center

3-D plot of the measured $C_T(r,\tau)$

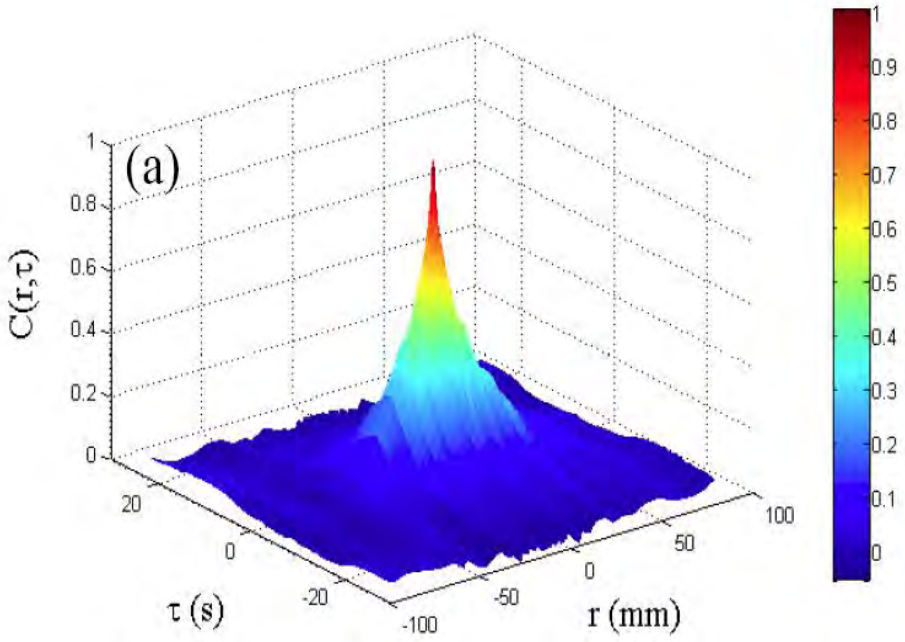

2-D plot of iso-correlation contours

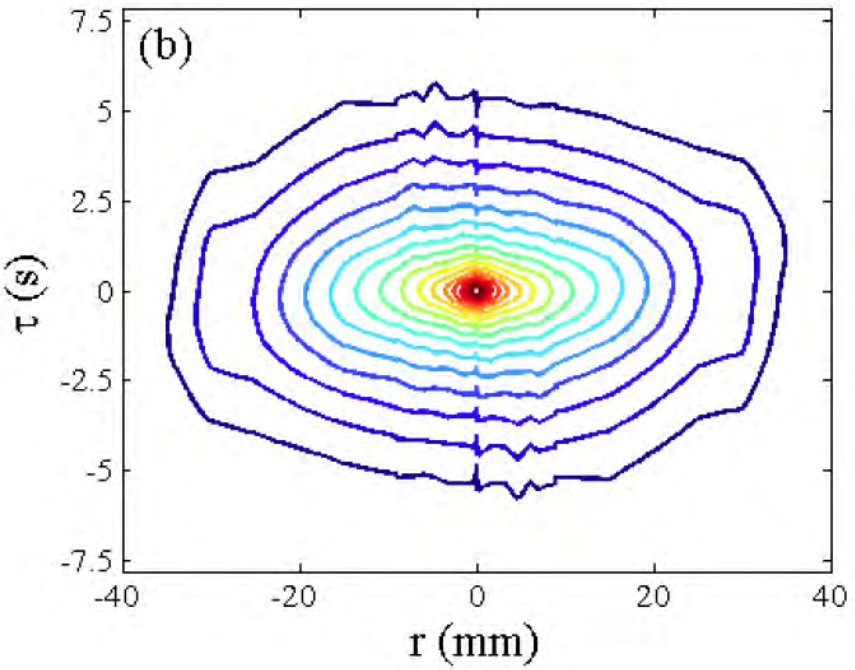

Experiment confirms the elliptic model:

$$C_T(r,\tau) = C_T(r_K,0) \quad \text{with} \quad r_K^2 = r^2 + V^2\tau^2 \quad \text{or} \quad \frac{r^2}{a^2} + \frac{\tau^2}{b^2} = 1$$

He and Tong, Phys. Rev. E, **83**, 037302 (2011).

Scaling behavior of $C_T(r,\tau)$ in the central region of the cell

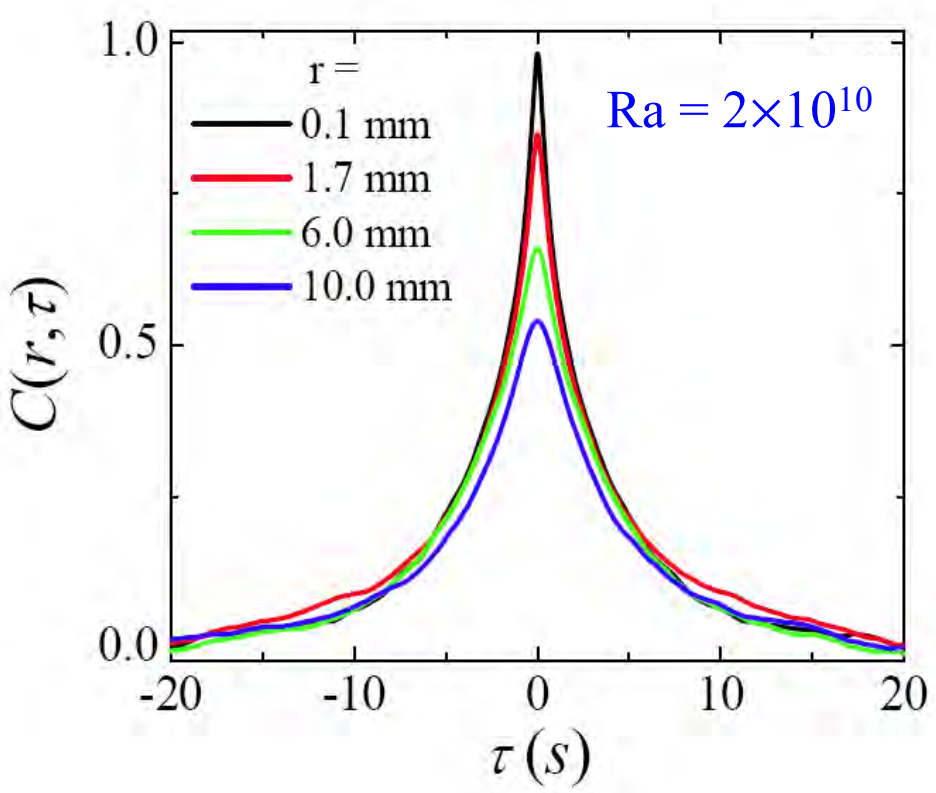

Measured mean velocity:

$U_0 = 0$

and rms velocity:

$\sigma_u = 8$ mm/s

Symmetric shape with $\tau_p = \dfrac{U}{U^2 + V^2} r \;\rightarrow\; U = 0$ and $V = 8.5$ mm/s

Kraichnan's random sweeping hypothesis is valid in the inner region.

Comparison between $C_T(r_E,0)$ and $C_T(r,0)$ in the bulk region

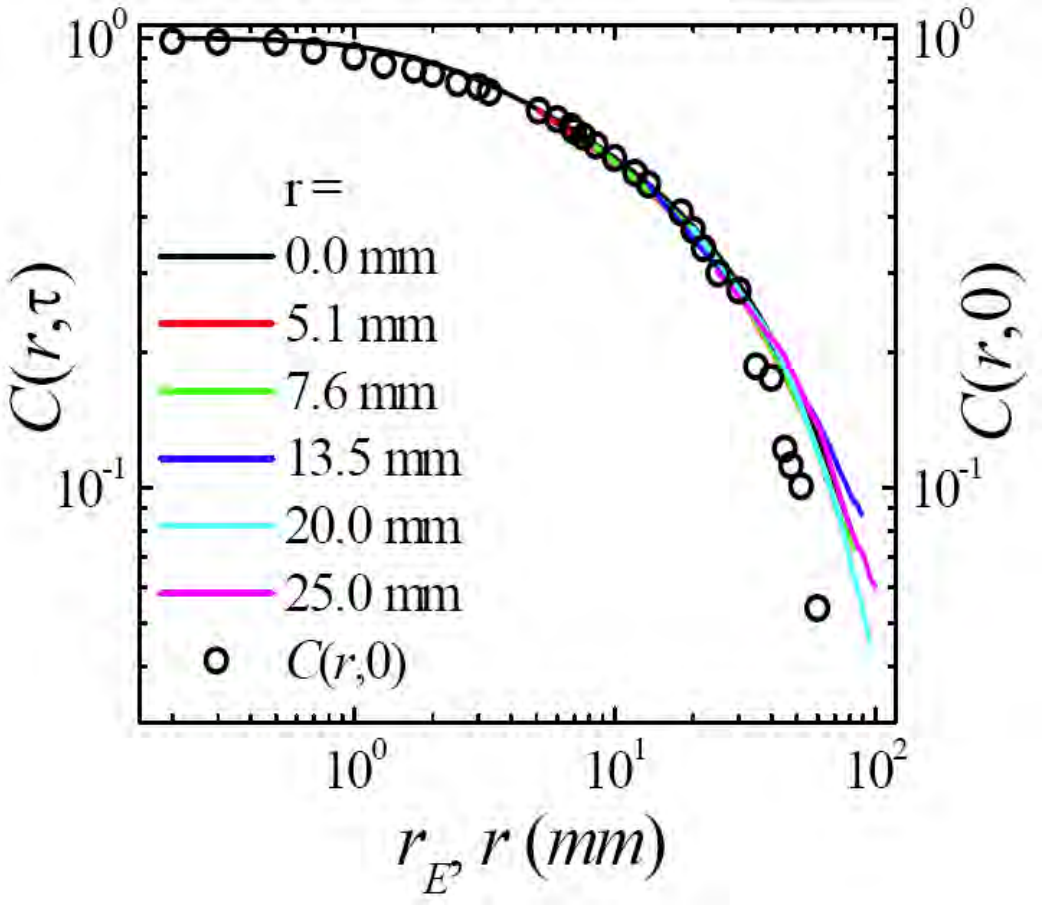

Ra = 2×10^{10}

$$r_E^2 = \left(r - U(r)\tau\right)^2 + V^2(r)\tau^2$$

Connection of time-domain results to the theory in spatial domain

Show that

$$\varepsilon_\tau^i(\mathbf{r},t) = \frac{1}{\tau}\int_t^{t+\tau} \kappa[\partial_i T_f(\mathbf{r},t')]^2 dt' \cong \varepsilon_r^i(\mathbf{x},t) = \frac{1}{\frac{4\pi}{3}r^3}\int_0^r \kappa[\partial_i T_f(\mathbf{r}',t)]^2 dr'$$

Given that $C_T(r,\tau) = C_T(r_E,0)$ with $r_E^2 = (r-U\tau)^2 + V^2\tau^2$

- At the cell center, we have $r_E = V\tau$ (r = 0) and the average over $d\tau$ (or dt) is equivalent to the average over dr_E (average over a sphere of radius $r_E = Vt$).

- Near the sidewall, we have $r_E = (U^2+V^2)^{1/2}\,\tau$ (r = 0) and the average over $d\tau$ (or dt) is equivalent to the average over dr_E (average over a ellipsoid of major axis $r_E = (U^2+V^2)^{1/2}\,\tau$ and minor axis $r_E = Vt$).

6. Summary

- Measured thermal dissipation field has the form $\epsilon_T(\mathbf{r}) = \epsilon_m(\mathbf{r}) + \epsilon_f(\mathbf{r})$, with $\epsilon_m(\mathbf{r})$ concentrating in the thermal boundary layers and $\epsilon_f(\mathbf{r})$ occupying mainly in the plume-dominated bulk region.

- Measured $\epsilon_f(\mathbf{r}) \sim \mathrm{Ra}^{-0.33}$ in the bulk region and $\epsilon_m(\mathbf{r}) \sim \mathrm{Ra}^{+0.63}$ inside the thermal boundary layer.

- Measured moments have the power-law form $\langle (\varepsilon_\tau^i)^p \rangle \sim \tau^{\mu^i(p)}$ with $\mu^i(\mathrm{p}) = \mathrm{c}(1\text{-}\beta^p)\text{-}\lambda\mathrm{p}$ for all three temperature gradient components and for all values of p up to 6 and are observed at three representative locations in the cell.

- Scaling of $\langle (\varepsilon_\tau^i)^p \rangle$ contains two contributions: (i) the horizontal exponents $\mu^i(p)$ ($i = x,y$) have the same parameters in the bulk region: $c = 1$ (sheet-like) and $\lambda = 2/3$ (passive scalar) but become $c = 1$ (sheet-like) and $\lambda = 2/5$ (active scalar) in the thermal boundary layer.

- (ii) Superimposed on this background is the vertical exponent $\mu^z(p)$, which varies with the position. At the cell center and inside the thermal boundary layer, $\mu^z(p)$ remains the same as the two horizontal exponents, whereas near the sidewall, $\mu^z(p)$ becomes different from $\mu^i(p)$ ($i = x,y$) with the parameters $c = 2$ (filament-like) and $\lambda = 2/3$ (passive scalar).

- Measured temperature space-time cross-correlation function $C_T(r,\tau)$ has the scaling form $C_T(r_E,0)$ with $r_E^2 = (r\text{-}U\tau)^2 + V^2\tau^2$. This equation goes beyond Taylor's frozen flow hypothesis and gives a linear relationship between r_E and τ when $r = 0$.

- A good agreement between the temperature-velocity CSF exponents and the dissipation exponent is observed. The experiment reveals that the anomalous scaling of passive temperature fluctuations is indeed caused by the spatial intermittency of the dissipation field. The experiment also demonstrates that the functional form of the SF and CSF exponents changes with the geometry of the most dissipative structures in the flow.